

ADVANCED FEATURE EXTRACTION ALGORITHMS FOR AUTOMATIC FINGERPRINT RECOGNITION SYSTEMS

By

Chaohong Wu

April 2007

A DISSERTATION SUBMITTED TO THE
FACULTY OF THE GRADUATE SCHOOL OF STATE
UNIVERSITY OF NEW YORK AT BUFFALO
IN PARTIAL FULFILLMENT OF THE REQUIREMENTS
FOR THE DEGREE OF
DOCTOR OF PHILOSOPHY

© Copyright 2007

by

Chaohong Wu

Abstract

In this thesis we have developed an improved framework for advanced feature detection algorithms in automatic fingerprint recognition systems. We have studied the factors relating to obtaining high performance feature points detection algorithm, such as image quality, segmentation, image enhancement, feature detection, feature verification and filtering.

Fingerprint image quality is an important factor in the performance of automatic fingerprint identification systems(AFIS). Commonly used features for fingerprint image quality are Fourier spectrum energy, Gabor filter energy, local orientation certainty level. However, no systematic method to combine texture features in the frequency domain and spatial domain has been reported in the literature. We propose composite metrics which combine band-limited ring-wedge spectral metrics in the frequency domain and complementary local statistical texture features (called inhomogeneity) in the spatial domain to classify images based on quality and select appropriate pre-processing and enhancement parameters.

Accurate segmentation of fingerprint ridges from noisy background are necessary for efficiency and accuracy of subsequent enhancement and feature extraction algorithms.

There are two types of fingerprint segmentation algorithms: unsupervised and supervised. Unsupervised algorithms extract blockwise features such as local histogram of ridge direction, gray-level variance, magnitude of the gradient in each image block, and Gabor features. Supervised methods usually first extract features such as coherence, average gray level, variance and Gabor response. In practice, the presence of noise, low contrast area, and inconsistent contact of a fingerprint tip with the sensor may result in loss of minutiae or produce of false minutiae. Supervised methods are time consuming, and possibly has an overfitting problem. Technically, it is difficult to find the optimal threshold value for boundary blocks (for block level feature based unsupervised methods), because it is uncertain what percentage of pixels in the boundary block belong to either foreground versus background. We observe that the strength of Harris points in the foreground is generally higher than in the background. Therefore the boundary ridge endings usually render stronger Harris corner points. Some Harris points in noisy blobs might have higher strength, but they can be filtered as outliers using the corresponding Gabor response. Our experiments show that the efficiency and accuracy of the new method are significantly higher than those of previously described methods.

Most fingerprint enhancement algorithms rely heavily on local orientation of ridge flows. However, significant orientation changes also occur around the delta and core points in fingerprint images, posing a challenge to the enhancement of ridge flows in high-curvature regions. Instead of first identifying the singular points, we compute the orientation coherence map and determine the minimum coherence regions as high-curvature areas. We adaptively choose the Gaussian filter window sizes to smooth the local orientation map. Because the smoothing operation is applied to local ridge shape structures, it efficiently joins broken ridges without destroying the essential singularities and enforces continuity of directional fields even in creases. Coherence

has not previously been used to estimate ridge curvature, and curvature has not been used to select filter scale in this field. Experimental results demonstrate the effectiveness of our innovative method.

Traditional minutiae detection methods are usually composed of five steps: image segmentation, image enhancement, binarization, thinning and extraction. Aberrations and irregularities adversely affect the fingerprint thinning procedure, so a relatively large number of spurious minutiae are introduced by the thinning operations. Two new thinning-free minutiae detection algorithms have been developed in this thesis to improve detection efficiency and accuracy. Experimental results show that our algorithms achieve higher accuracy than the method described by NIST.

We have proposed an improved framework for extracting high accuracy minutiae set, by integrating a robust point-based unsupervised segmentation algorithm, topological pattern adaptive fingerprint enhancement algorithm with singularity preservation, a thinning-free minutiae detection algorithm and new feature filtering, and verification algorithms.

Contents

Abstract	iii
1 Introduction	1
1.1 Basic Definitions	5
1.1.1 System Error Rates	5
1.1.2 Fingerprint Features	11
1.1.3 Global Ridge Pattern	11
1.1.4 Local Ridge Detail	12
1.1.5 Intra-ridge Detail	16
1.1.6 Texture Features: Gabor Feature and FFT phase-only feature	17
1.2 Technical Problems	18
1.2.1 Segmentation	18

1.2.2	Image Quality Assessment	18
1.2.3	Enhancement	18
1.2.4	Feature Detection Accuracy	19
1.3	Outline	19
1.4	Benchmarks	20
2	Matching and Performance Evaluation Framework	22
2.1	Correlation-based Matching Algorithm	22
2.1.1	Minutiae Triplet	23
2.1.2	Multi-path Matching Algorithm	25
2.1.3	Localized Size-specific Matching Algorithm	28
3	Objective Fingerprint Image Quality Modeling	37
3.1	Background	37
3.2	Proposed Quality Classification Features	39
3.2.1	Global Quality Measure: Limited Ring-Wedge Spectral Energy	39
3.2.2	Local Quality Measure: Inhomogeneity and directional contrast	43
3.3	Adaptive Preprocessing Method	44

3.4	Experiments	46
3.5	Summary	48
4	Robust Fingerprint Segmentation	49
4.1	Features for Fingerprint Segmentation	50
4.2	Unsupervised Methods	54
4.3	Supervised Methods	55
4.4	Evaluation Metrics	55
4.5	Proposed Segmentation Methods	56
4.5.1	Strength of Harris-corner points of a Fingerprint Image	58
4.6	Summary	62
5	Adaptive Fingerprint Image Enhancement	68
5.1	Introduction	68
5.2	Local ridge orientation field Estimation	69
5.3	Review of fingerprint image enhancement methods	71
5.3.1	Spatial Domain	72
5.3.2	Frequency Domain	72

5.4	New Noise Model	74
5.4.1	Anisotropic Filter	75
5.4.2	Orientation estimation	81
5.5	Singularity preserving fingerprint adaptive filtering	86
5.5.1	Computation of Ridge Orientation and High-Curvature Map	87
5.5.2	Experiments	88
6	Feature Detection	92
6.1	Introduction	92
6.2	Previous Methods	93
6.2.1	Skeletonization-based Minutiae Extraction	93
6.2.2	Gray-Level Minutiae Extraction	99
6.2.3	Binary-image based Minutiae Extraction	101
6.2.4	Machine Learning	104
6.3	Proposed Chain-code Contour Tracing Algorithm	106
6.4	Proposed Run-length Scanning Algorithm	109
6.4.1	Definitions	109

6.4.2	One-pass embedding labeling run-length-wise thinning and minutiae detection algorithm	112
6.5	Minutiae Verification and Filtering	115
6.5.1	Structural Methods	115
6.5.2	Learning Methods	117
6.5.3	Minutiae verification and filtering rules for chain-coded contour tracing method	117
6.6	Experiments	119
7	Conclusions	122

Chapter 1

Introduction

Today, we can obtain routine information from dedicated websites, retrieve easily information via search engines, manage our bank accounts and credit information, shop online and bid for products. To access the internet safely, high-security authentication systems are essentials. According to 2002 the NTA Monitor Password Survey, heavy web users have an average of 21 passwords, 81% of users choose a common password and 30% write their passwords down or store them in a file. Most passwords can be guessed easily because users tend to pick easily-remembered passwords which usually contain personal information such as pet name, home address. Due to the vulnerability of conventional authentication systems, cybercrime has increased in the past few years. According to the 2006 October special report in USA today, FBI estimates annual U.S. businesses lost \$67.2 billion because of computer-related crimes. Identity authentication, which is based on biometric feature such as face, iris, voice, hand geometry, retina, handwriting, fingerprint etc., can significantly decrease the fraud. Among biometrics, fingerprint systems have been one of most widely researched and deployed because of their easy access, low price of fingerprint sensors,

non-intrusive scanning, and relatively good performance[51].

In recent years, significant performance improvements have been achieved in commercial automatic fingerprint recognition systems. However the state-of-the-art system reported at the Fingerprint Verification Competition(FVC)2004 has total error rate of 4% with 2% False Reject Rate (FRR) and False Accept Rate (FAR) [16]. The Fingerprint Vendor Technology Evaluation (FpVTE) 2003, which was conducted by the National Institute of Standards & Technology (NIST) on behalf of the Justice Management Division (JMD) of the U.S. Department of Justice, reported the lowest FRR of 0.1% at the FAR of 1%. Therefore, it is imperative to continue research on improving the reliability, stability, performance and security of fingerprint recognition systems. Low quality fingerprint image, distortion, the partial image problems, large fingerprint databases [16] are all major areas of research needed to improve the accuracy of current systems.

Major causes for degradation of fingerprint image quality include the physiological condition of fingers friction ridge skin and other physiological state of the fingers, performance of the capture devices (device reliability, consistency, degradation of sensing elements, image resolution, signal-to-noise ratio, etc.), acquisition environment (external light, temperature and humidity weather conditions), user/device interaction, cleanliness of device surface, acquisition pressure, and contact area of the finger with the scanner. Thus, current fingerprint recognition technologies are vulnerable to poor quality images. According to recent report by the U.S. National Institute of Standards and Technology(NIST), 16% of the images collected are of sufficiently poor quality to cause a significant deterioration of the overall system performance [46].

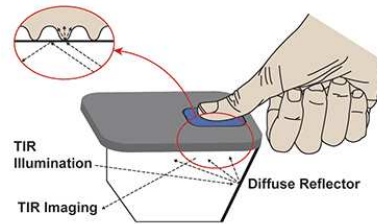
Many researchers in both academics and industry are working on improving the overall fingerprint recognition performance. Hardware efforts are focused on improving

the acquisition device capability for obtaining high quality images. Lumidigm (New Mexico, U.S.) has designed and developed an innovative high-performance fingerprint biometric imaging system, which incorporates a conventional fingerprint optical sensor with a multispectral imager during each instance of image capture [74]. A typical optical sensor is illustrated in Figure 1.0.1(a). It is based on total internal reflectance (TIR). The inset in the upperleft of the Figure shows the intersection of the optical mechanism that occurs at the fingerprint ridges and valleys. Fingerprint ridges allow light to cross the platen interface so that the corresponding regions in the collected image are dark. Fingerprint valleys permit TIR to occur so that the regions corresponding to the valley in the collected image appears bright. The general architecture for a multispectral imager is shown in Figure 1.0.1(b). The system obtains the “subsurface internal fingerprint”, which is a complex pattern of collagen and blood vessels that mirror the surface ridge pattern. Because of the different chemical compositions of the living human skin, it exhibits varied absorbance properties and scattering effects. Therefore, different wavelengths of light can cause the sensor to not only acquire high quality images, but also provide capability for the automatic liveness detection. Latent prints on the fingerprint image can pose a challenge to segmentation procedure. Deformation in touch-based sensing technology also causes problem due to contact between the elastic skin of the finger and a rigid surface. TBS [63] designed an innovative touchless device (surround Imager) to address the limitations of touch-based sensing devices. It combines five specially designed cameras, and avoids the tedious, uncomfortable and error-prone rolling procedure required by current capture technologies.

Software related efforts research are focused on feature detection, and matching algorithms. This thesis will focus on robust feature detection algorithms. This first

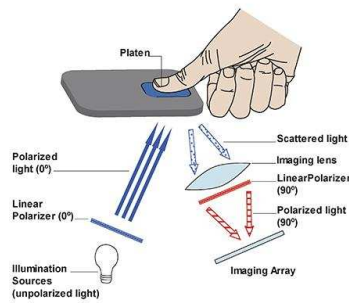
chapter is organized as follows. Section 1.1 discusses basic terms for fingerprint recognition systems. Section 1.2 will outline the technical problems. The road map of this dissertation will be sketched in Section 1.3. Finally, the experiment databases are discussed in Section 1.4.

TIR Imager



(a)

Multispectral Imager



(b)

Figure 1.0.1: (a) Layout of a typical optical fingerprint sensor based on total internal reflectance (TIR); (b) schematic diagrams of a multispectral fingerprint imager (adopted from [74]).

1.1 Basic Definitions

In order to understand the structure of fingerprints and how the recognition system works, we will introduce the terminology to facilitate discussion.

1.1.1 System Error Rates

Fingerprint authentication is a pattern recognition system that recognizes a person via the individual information extracted from the raw scanned fingerprint image. A typical fingerprint authentication system is shown in 1.1.1 as a schematic diagram. The term *fingerprint recognition* can be either in the identification mode or in the verification mode depending on the application. For both modalities, user's fingerprint image information (raw image or feature template or both) must be first registered correctly and its quality assessed. This important step is called *Enrollment* and is usually conducted under supervision of trained personnel. The two modalities of fingerprint recognition systems differ based on the relationship type (cardinality constraint) of the query fingerprint and the reference fingerprint(s). If the query fingerprint is processed with the claimed identity, which is subsequently used to retrieve the reference fingerprint from the system database, the cardinality ratio is 1 : 1 and refers to the verification modality. If the cardinality ratio is 1 : N , it implies that the query fingerprint is matched against the template of all the users in the system database. This modality is referred to as identification system. The authentication results are either positive (confirmed identity) or negative (denied user). Because identification of one user in a large database (like US-VISIT) is extremely time-consuming, advanced indexing and classification methods are utilized to reduce the number of related templates which are fully matched against the query fingerprint.

Fingerprint patterns can be classified into five classes according to *Henry* classes[31] for the purpose of pruning the database.

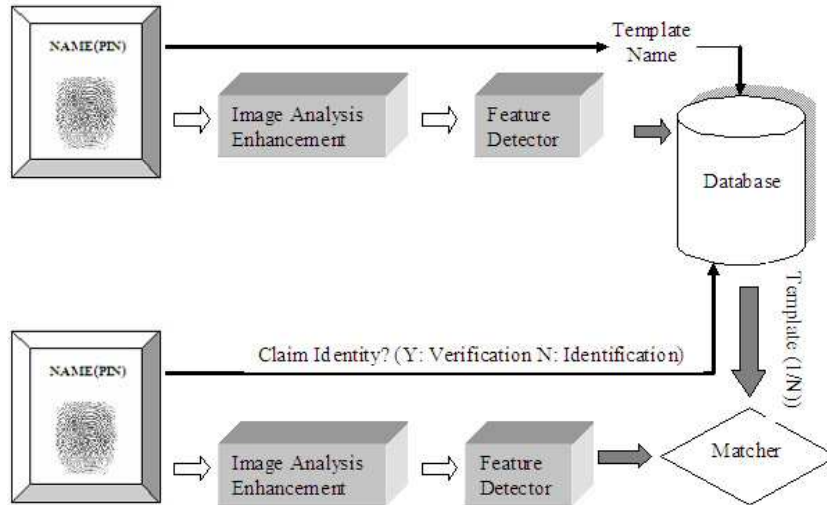


Figure 1.1.1: Schematic diagram of Fingerprint recognition Systems.

Due to the variations present on each instance of fingerprint capture no recognition system can give an absolute answer about the individual’s identity; instead it provides the individual’s identity information with a certain *confidence level* based on a similarity score. This is different from traditional authentication systems (such as passwords) where the match is exact and an absolute “yes” or “no” answer is returned. The validation procedure in such cases is based on whether the user can prove the exclusive possessions(cards) or the secret knowledge (password or PIN number). The biometric signal variations of an individual are usually referred to as *intra-class variations* (Figure1.1.2); whereas variations between different individuals are referred to as *interclass variations*.

A fingerprint matcher takes two fingerprint, F_I and F_J , and produces a similarity measurement $S(F_I^T, F_J^T)$, which is normalized in the interval $[0, 1]$. If $S(F_I^T, F_J^T)$ is



Figure 1.1.2: Examples of intraclass variation. These are eight different fingerprint impressions (biometric signals) of the same finger (individual). Note that huge differences of image contrasts, locations, rotations, sizes, and qualities, exist among them.

close to 1, the matcher has greater confidence that both fingerprints come from the same individual. In the terminology of the field, the identity of a queried fingerprint is either a *genuine type* or an *imposter type*; hence, there are two statistical distributions of similarity scores, which are called genuine distribution and imposter distribution (Figure 1.1.3). Each type of input identity has one of the two possible results, “match” or “non-match”, from a fingerprint matcher. Consequently, there are four possible scenarios:

1. a genuine individual is accepted;
2. a genuine individual is rejected;
3. an imposter individual is accepted;
4. an imposter individual is rejected.

An ideal fingerprint authentication system may produce only the first and fourth

outcomes. Because of image quality and other intraclass variations in the fingerprint capture devices, and the limitations of fingerprint image analysis systems, enhancement methods, feature detection algorithms and matching algorithms, realistically, a genuine individual could be mistakenly recognized as an imposter. This scenario is referred to as “false reject” and the corresponding error rate is called the false reject rate (FAR); An imposter individual could be also mistakenly recognized as genuine. This scenario is referred to as “false accept” and the corresponding error rate is called the false reject rate (FRR). FAR and FRR are widely used measurements in today’s commercial environment. The distributions of the similarity score of genuine attempts and imposter attempts cannot be separated completely (Figure 1.1.3) by a single carefully chosen threshold. FRR and FAR are indicated in the corresponding areas given the selected threshold, and can be computed as follows:

$$(1.1.1) \quad FAR(T) = \int_{th}^1 p_i(x)dx$$

$$(1.1.2) \quad FRR(T) = \int_0^{th} p_g(x)dx$$

Both FAR and FRR are actually functions of a threshold t . When t decreases, the system would have more tolerance to intraclass variations and noise, however the FAR will increase. Similarly, if t is lower, the system would be more secure and the FRR decreases. Depending on the nature of the application, the biometric system can operate at low FAR configuration (for example, login process in ATMs), which requires high security, or to operate at low FRR configuration (for example, the access control system for a library), which provides easy access. A system designer may have no prior knowledge about the nature of the application in which the biometric system is to be applied, thus it is helpful to report the system performance at all possible operating parameter settings. A *Receiver Operating Characteristic* (ROC) curve is obtained by plotting FAR(x-axis) versus $1 - FRR$ (y-axis) at all thresholds. The

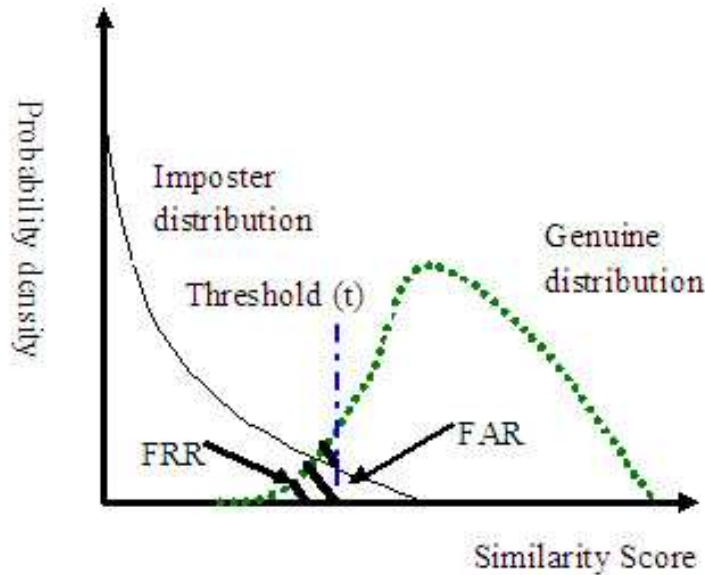


Figure 1.1.3: Example of genuine and imposter distributions.

threshold t of the related authentication system can be tuned to meet the requirement of application. Figure 1.1.4 illustrates the typical curves of FAR, FRR, and ROC.

Other useful performance measurements which are sometimes used are:

- **Equal Error Rate (EER):** the error rate where FAR equals FRR (Figure 1.1.4(a)). In practice, the operating point corresponding to EER is rarely adopted in the fingerprint recognition system, and the threshold t is tailored to the security needs of the application.
- **ZeroFNMR:** the lowest FAR at which no false reject occurs.
- **ZeroFMR:** the lowest FRR at which no false accept occurs.
- **Failure To Capture Rate:** the rate at which the biometric acquisition device fails to automatically capture the biometric signal. A high failure to capture rate makes the biometric system hard to use.

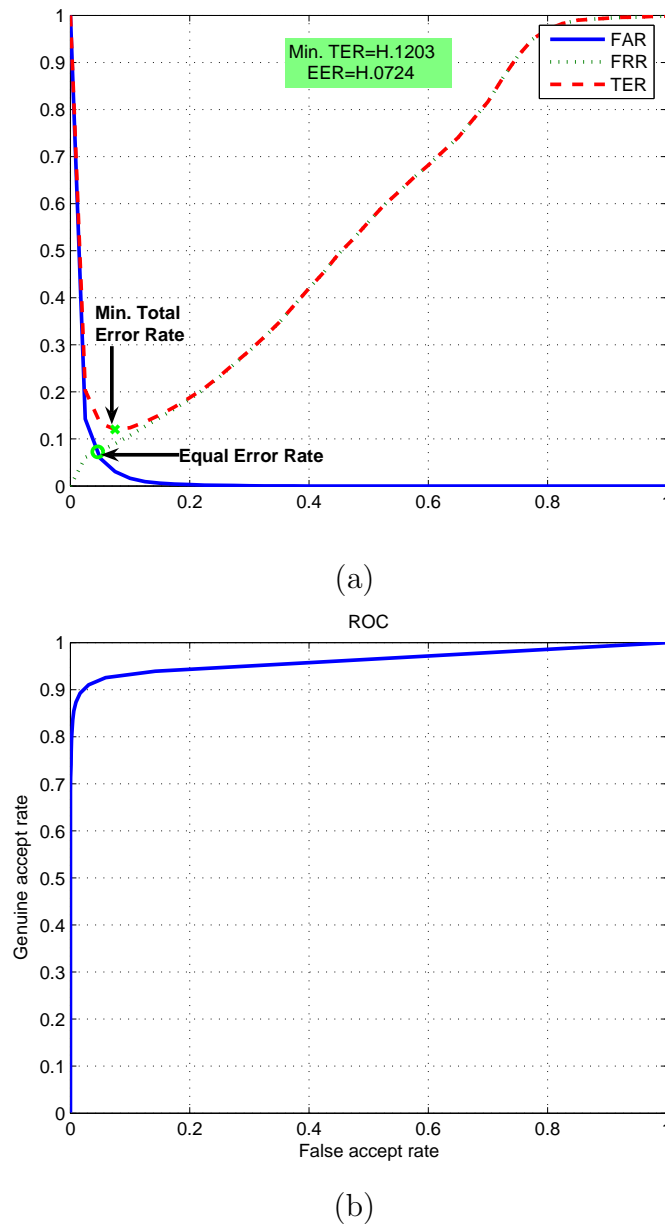


Figure 1.1.4: Examples of (a) FAR and FRR curves; (b) ROC curve.

- **Failure To Enroll Rate:** the rate at which users are not able to enroll in the system. This error mainly occurs when the biometric signal is rejected due to its poor quality.
- **Failure To Match Rate:** occurs when the biometric system fails to convert the input biometric signal into a machine readable/understandable biometric template. Unlike FRR, a failure to match the error occurs at a stage prior to the decision making stage in a biometric system.

1.1.2 Fingerprint Features

In [35], fingerprint features are classified into three classes. Level 1 features show macro details of the ridge flow shape, Level 2 features (minutiae point) are discriminative enough for recognition, and Level 3 features (pores) complement the uniqueness of Level 2 features.

1.1.3 Global Ridge Pattern

A fingerprint is a pattern of alternating convex skin called ridges and concave skin called valleys with a spiral-curve-like line shape (Figure 1.1.5). There are two types of ridge flows: the pseudo-parallel ridge flows and high-curvature ridge flows which are located around the core point and/or delta point(s). This representation relies on the ridge structure, global landmarks and ridge pattern characteristics. The commonly used global fingerprint features are:

- *singular points* – discontinuities in the orientation field. There are two types of singular points. A core is the uppermost of the innermost curving ridge [31],

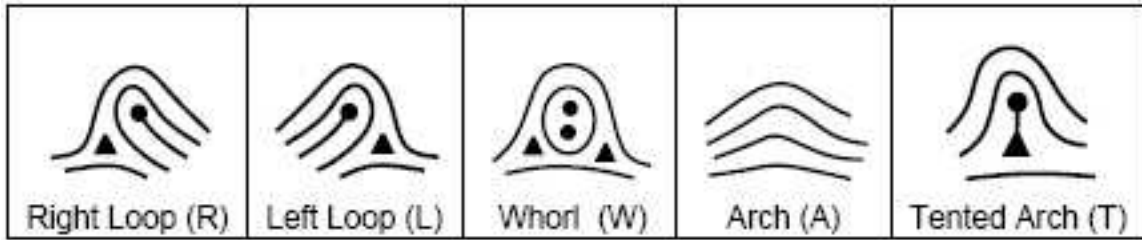


Figure 1.1.5: Global Fingerprint Ridge Flow Patterns.

and a delta point is the junction point where three ridge flows meet. They are usually used for fingerprint registration, fingerprint classification.

- *ridge orientation map* – local direction of the ridge-valley structure. It is commonly utilized for classification, image enhancement, minutia feature verification and filtering.
- *ridge frequency map* – the reciprocal of the ridge distance in the direction perpendicular to local ridge orientation. It is formally defined in [32] and is extensively utilized for contextual filtering of fingerprint images.

This representation is sensitive to the quality of the fingerprint images [36]. However, the discriminative abilities of this representation are limited due to absence of singular points.

1.1.4 Local Ridge Detail

This is the most widely used and studied fingerprint representation. Local ridge details are the discontinuities of local ridge structure referred to as *minutiae*. Sir Francis Galton (1822-1922) was the first person who observed the structures and permanence of minutiae. Therefore, minutiae are also called “Galton details”. They

are used by forensic experts to match two fingerprints.

There are about 150 different types of minutiae [36] categorized based on their configuration. Among these minutia types, “ridge ending” and “ridge bifurcation” are the most commonly used, since all the other types of minutiae can be seen as combinations of “ridge endings” and “ridge bifurcations”. Some minutiae are illustrated in Figure 1.1.6.

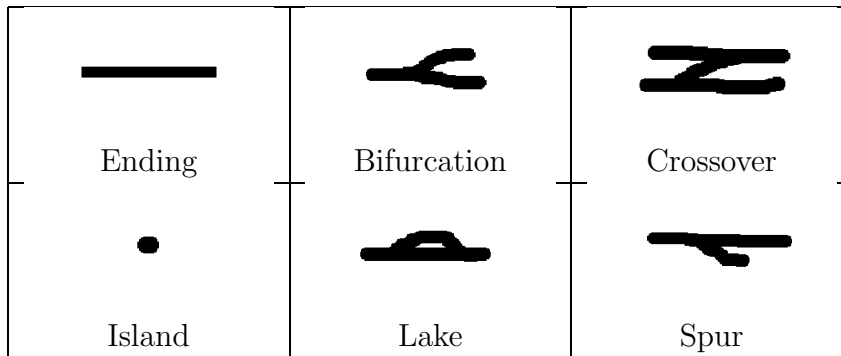


Figure 1.1.6: Some of the common minutiae types.

The American National Standards Institute-National Institute of Standard and Technology (ANSI-NIST) proposed a minutiae-based fingerprint representation. It includes minutiae location and orientation[7]. Minutia orientation is defined as the direction of the underlying ridge at the minutia location (Figure1.1.7). Minutiae-based fingerprint representation can also assist privacy issues since one cannot reconstruct the original image from using only minutiae information. Actually, minutiae are sufficient to establish fingerprint individuality [62].

The minutiae are relatively stable and robust to contrast, image resolutions, and global distortion when compared to other representations. However, to extract the minutiae from a poor quality image is not an easy task. Although most of the automatic fingerprint recognition systems are designed to use minutiae as their fingerprint

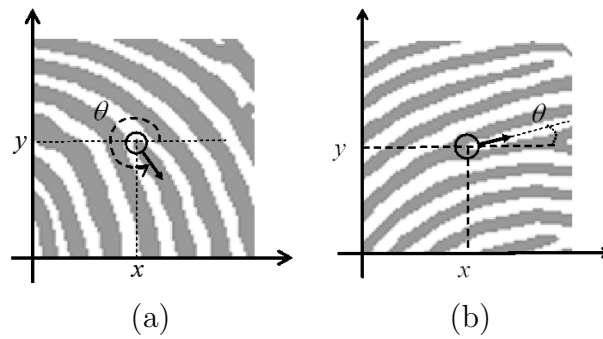


Figure 1.1.7: (a) A ridge ending minutia: (x,y) are the minutia coordinates; θ is the minutia's orientation; (b) A ridge bifurcation minutia: (x,y) are the minutia coordinates; θ is the minutia's orientation.

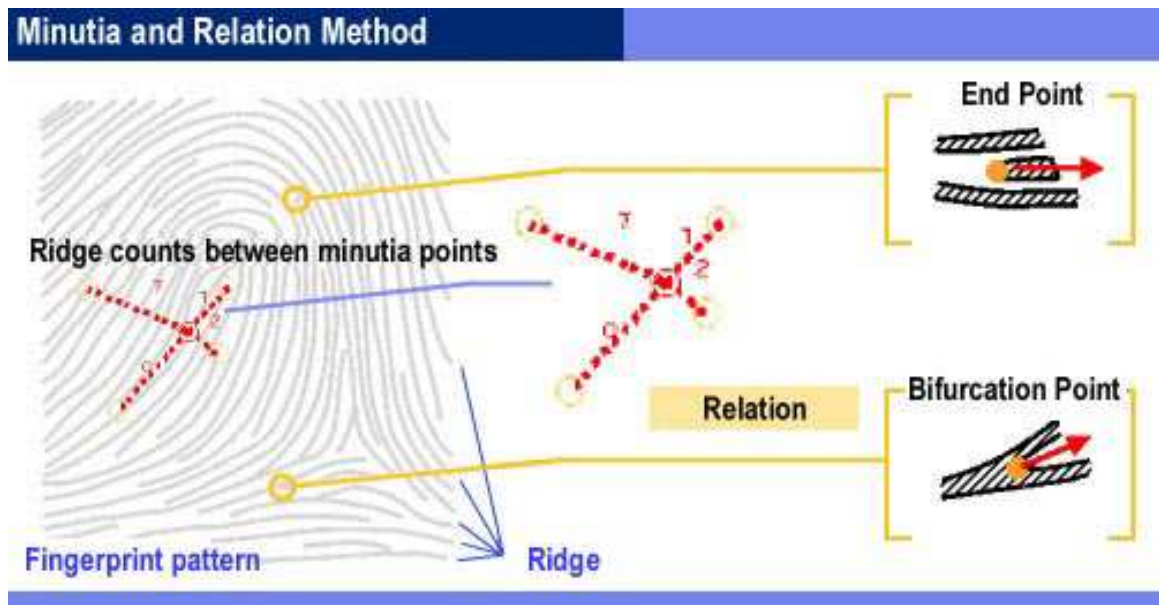


Figure 1.1.8: Minutiae relation model for NEC.

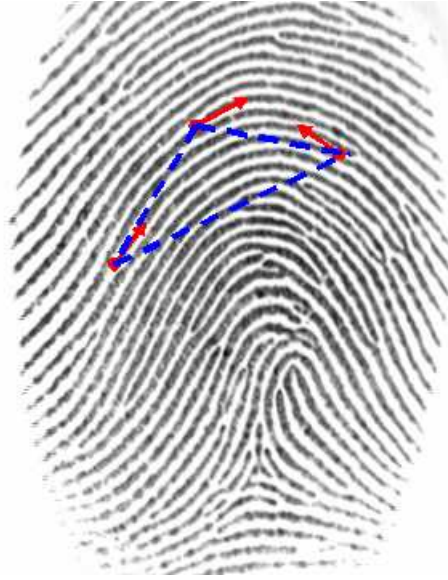


Figure 1.1.9: Minutiae Triplet on a raw fingerprint with the minutiae angles shown.

representations, the location information and the direction of a minutia point alone are not sufficient for achieving high performance because of the variations caused by the flexibility and elasticity of fingerprint skins. Therefore, ridge counts between minutiae points (Figure 1.1.8) are often extracted to increase the discriminating power of minutia features. Because a single minutia feature vector is dependent on the rotation and translation of the fingerprint, and inconsistencies caused by contact pressure and skin elasticity, minutiae-derived secondary features (called *triplets*) are used [26, 13, 94]. In a triplet, the relative distance and radial angle are reasonably invariant with respect to the rotation and translation of the fingerprint (Figure 2.1.1).

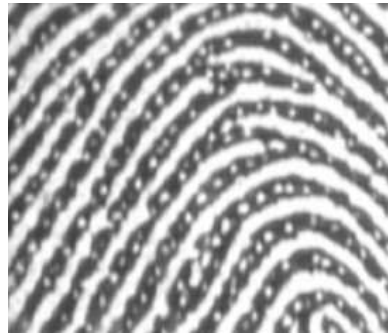


Figure 1.1.10: A portion of a fingerprint where sweat pores (white dots on ridges) are visible.

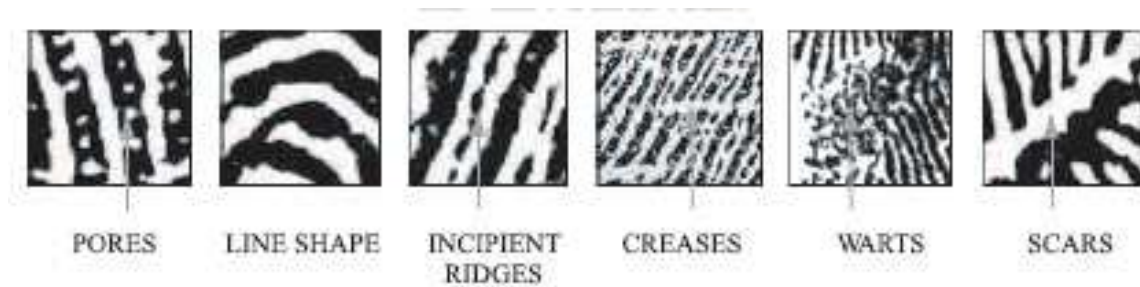


Figure 1.1.11: Global Fingerprint Ridge Flow Patterns (adopted from [35]).

1.1.5 Intra-ridge Detail

On every ridge of the finger epidermis, there are many tiny sweat pores (Figure 1.1.10) and other permanent details (Figure 1.1.11). Pores are considered to be highly distinctive in terms of their number, position, and shape. However, extracting pores is feasible only in high-resolution fingerprint images (for example 1000 DPI) and with very high image quality. Therefore, this kind of representation is not adopted by currently deployed automatic fingerprint identification systems [35].

If the sensing area of a finger is relatively small, or the placement of a finger on the fingerprint sensor is deviated from normal central contact, it is possible that there is not enough discriminating power for identification purpose. This could be because

either most discriminative regions do not get included in the image, or because the number of detected minutiae is not enough. Level 3 features can increase discriminating capacity of Level 2 features. Experiments [35] demonstrate that a relative 20% reduction of EER is achieved if Level 3 features are integrated into the current Level 1 and Level 2 features-based fingerprint recognition systems.

1.1.6 Texture Features: Gabor Feature and FFT phase-only feature

Texture features have been extensively explored in fingerprint processing, and have been applied to fingerprint classification, segmentation and matching [38, 73, 69, 34]. The fingerprint is tessellated into 16×16 cells [73], a bank of 8 directions Gabor filters are used to convolve with each cell, and the variance of the energies of the 8 Gabor filter responses in each cell is used as a feature vector. Because phase information in the frequency domain is not affected by image translation and illumination changes, it is also robust against noise. The only phase information that has been successfully used thus far for low quality fingerprint recognition has been described in [34].

1.2 Technical Problems

1.2.1 Segmentation

The segmentation process needs to separate foreground from background with high accuracy. Inclusion of noisy background can pose problems to the following enhancement, feature extraction and matching performance. Exclusion of foreground decreases the matching performance especially partial in fingerprint images.

1.2.2 Image Quality Assessment

Objective estimation of fingerprint image quality is a nontrivial technical problem. The commonly used features for fingerprint image quality are Fourier spectrum energy, Gabor filter energy, and local orientation certainty level. However, there is no systematic method to combine the texture features in the frequency domain and spatial domain. Combining the metrics in the frequency domain and the spatial domain is a classification problem, which must be solved to select appropriate preprocessing and enhancement parameters.

1.2.3 Enhancement

For good quality fingerprint images, most AFISs can accurately extract minutiae points in the well defined ridge-valley regions of a fingerprint image where the ridge orientation changes slowly, but can not get satisfactory results in the high-curvature regions. Gabor filter has been used extensively to enhance fingerprint images, and

local ridge orientation and ridge frequency are critical parameters for high performance. However, researchers have only used a single low-pass filter with the size of 5×5 with the assumption that there is slow orientation change in local ridges. Noisy regions like creases can not be smoothed successfully with a gaussian kernel of that size. The inherent relationship between ridge topology and filter window size must be studied.

1.2.4 Feature Detection Accuracy

Although there are several methods available for detecting minutiae, the technical problems related to the improvement of feature extraction are still active fields of research. All existing minutiae extraction methods need their corresponding feature verification and filtering procedure. We propose a chain-coded contour tracing method for minutiae detection, and explore several heuristic rules for spurious minutiae filtering associated with this thinning-free method.

1.3 Outline

In the second chapter we will summarize the-state-of-art matching algorithms, the matching algorithms proposed by Jea in [39] will be discussed in detail because we utilize Jea's method for final performance evaluation.

In the third chapter we discuss features for fingerprint image quality estimation, introduce new metrics in the frequency domain and the spatial domain, describe the method for composite metrics and the application for image preprocessing and enhancement.

The fourth chapter first discusses the types of fingerprint segmentation and the relative use of texture features. The reason for using point features is discussed, following a review of the Harris corner point detection method. Finally we present a novel Harris corner point based fingerprint segmentation algorithm with heuristic outliers filtering method using Gabor filter.

Orientation smoothing and singularity-preserving image enhancement algorithms are discussed in Chapter five. We investigate the ridge topological pattern, and propose simple and efficient gradient-based localization and classification method. A new noise model is also proposed in this chapter.

Chapter six will review available minutiae extraction methods, and compare their advantages and disadvantages. Two thinning-free feature extraction methods: chain-code contour tracing and two-pass run-length code scanning are presented in this chapter. The corresponding feature filtering rules are discussed, and innovative boundary minutiae filtering method is proposed.

Finally, chapter seven contains the summary of our work and contributions made.

1.4 Benchmarks

To compare our segmentation algorithm, enhancement algorithm and feature detection methods with published methods, publicly available fingerprint databases for Fingerprint Verification Competition(FVC) in 2000, 2002 and 2004 [24] have been chosen. Among them, only databases which are acquired by fingerprint sensors are considered. Each database contains 880 fingerprints, originated from 110 different fingers of untrained volunteers. The same finger is needed to give 8 impressions. The

Database Name	Sensor Type	Image Size	Resolution(dpi)
2000 DB1	Low-cost Optical Sensor	300×300	500
2000 DB2	Low-cost Capacitive Sensor	256×364	500
2000 DB3	Optical Sensor	448×478	500
2002 DB1	Optical Sensor	388×374	500
2002 DB2	Optical Sensor	296×560	569
2002 DB2	Capacitive Sensor	300×300	500
2004 DB1	Optical Sensor	640×480	500
2004 DB2	Optical Sensor	328×364	500
2004 DB3	Thermal Sweeping Sensor	300×480	500

Table 1.4.1: Parameters of the chosen databases

image properties for all the selected databases are shown in Table1.4.1.

Chapter 2

Matching and Performance Evaluation Framework

2.1 Correlation-based Matching Algorithm

To verify the efficiency and accuracy of our proposed segmentation method, image quality modeling, image enhancement strategy and feature detection algorithms, the matching algorithm developed at CUBS [39] has been adopted. In Jea's Dissertation [39], two matching methods, multi-path and localized size-specific matching algorithm, were proposed. In the following sections, minutiae derived secondary feature called Triplet is discussed in detail, and then a simple sketch of multi-path matching scheme is presented. This is followed by a detailed explanation of localized size-specific fingerprint matching algorithm for completeness.

2.1.1 Minutiae Triplet

The minutiae-derived feature called Triplet was first proposed by Germain et al. [26]. They found that redundant combinations of three minutiae points not only form new features which provide more discriminative information than does a single minutia point, but also reduce deformation effects due to skin elasticity and inconsistent contact pressure. Furthermore, side length constraints were used to guarantee a relatively constant number of triplets, and an appropriate binning mechanism was used to allow dynamic tolerance for irreproducible minutiae positions.

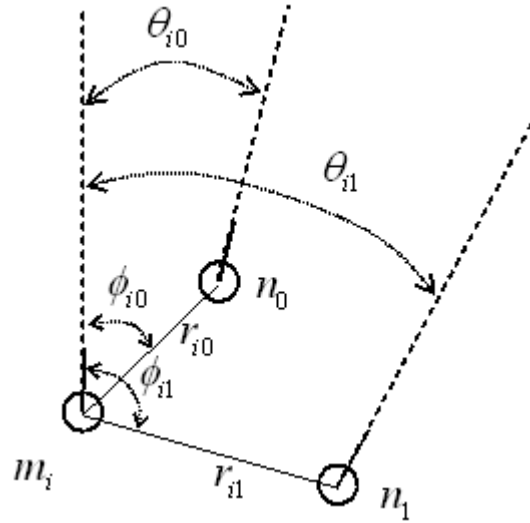


Figure 2.1.1: Modified minutiae triplet structure.

Figure 2.1.1 shows the local structure information of a minutiae triplet used by Jiang and Yau [94]. For each central minutia $m_i(x_i, y_i, \theta_i)$ and its two neighboring minutiae $n_0(x_{n0}, y_{n0}, \theta_{n0})$ and $n_1(x_{n1}, y_{n1}, \theta_{n1})$, the modified triplet minutiae feature vector is given by:

$$Trp_i = (r_{i0}, r_{i1}, \theta_{i0}, \theta_{i1}, \phi_{i0}, \phi_{i1}, n_{i0}, n_{i1}, t_i, t_0, t_1)^T \quad (2.1.1)$$

where r_{i0} and r_{i1} are the Euclidean distances between the central minutia m_i and its neighbors n_0 and n_i , respectively. θ_{i0} and θ_{i1} are the relative angles between the central minutia m_i and its neighbors n_0 and n_i , and ϕ_{i0} and ϕ_{i1} are the relative angles formed by line segments $\overline{m_i n_0}$ and $\overline{m_i n_1}$ with respect to θ_i , respectively. n_{i0} and n_{i1} are the ridge counts between the central minutia m_i and its neighbors n_0 and n_i , respectively, and t_i, t_0, t_1 represent the corresponding minutia type. Apparently, this minutia-derived feature is invariant to the rotation and translation of the fingerprint, and to some extent invariant to deformation. In [26], three minutiae points are ordered consistently by the side lengths of the formed triangle. In the implementation of [39], minutiae are ordered in counter-clockwise according to the right-hand rule of two vectors $\overrightarrow{m_i n_0}$ and $\overrightarrow{m_i n_1}$. Furthermore, ridge counts and minutiae types information are not utilized because it is not reliable. Bifurcation minutia and ending minutia might exchange under the varied impression pressure and dirt on the scanner surface.

In [39], both matching algorithms utilize the same triplet local structure information as input. There are three stages, namely local matching stage, validation stage and similarity score calculation stages, as indicated by the multi-path algorithm. An additional stage called extended matching in localized size-specific matching algorithm have been inserted between the validation stage and the similarity score calculation stage in the multi-path matching algorithm. We will present the multi-path matching method in the following section [39].

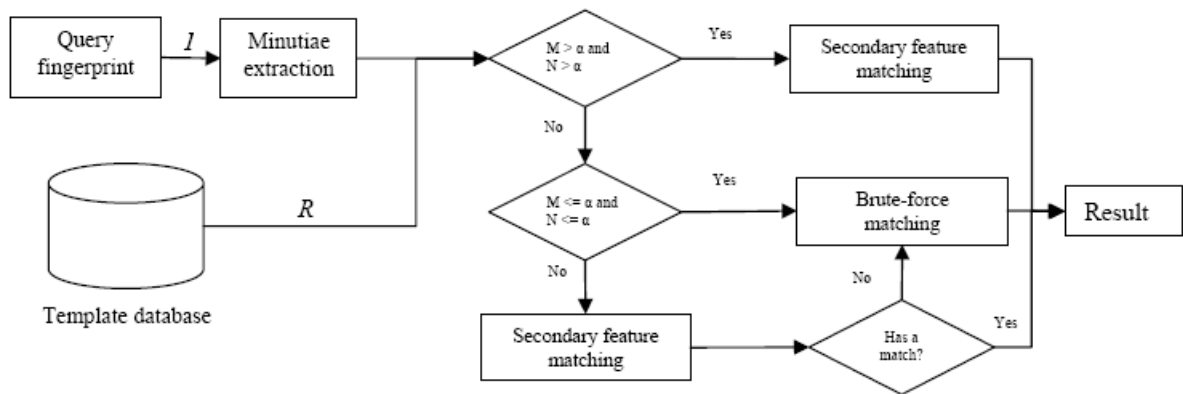


Figure 2.1.2: Multi-path Matching Schematic Flow.

2.1.2 Multi-path Matching Algorithm

A multi-path matching algorithm includes two matching methods: (i) brute-force matching for small number of minutiae query and reference partial fingerprints; (ii) secondary-feature matching for the relative larger number of minutiae in query and reference fingerprints. Minimum cost maximum flow (MCF) algorithm is used by both matching paths to get the optimal pairing of features.

Brute-force matching method checks all the possible matching scenarios, and selects the match with the most number of matches as the final result. Each minutia point in R and I are used as reference points. Choosing the appropriate matching methods in terms of speed and accuracy is dependent on an empirical threshold (α) (Figure 2.1.2). I and R represent the query fingerprint and reference fingerprint, respectively. Brute-force matching is adopted in the two scenarios where either or both of the reference fingerprint and query fingerprint have the number of minutiae less than α . This is because brute-force matching is very time-consuming.

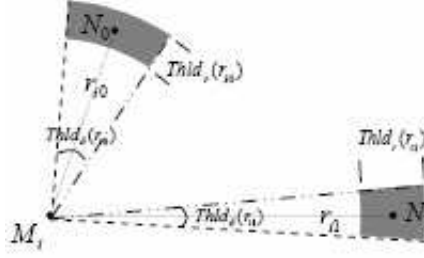


Figure 2.1.3: Dynamic tolerance bounding boxes.

Due to the possible deformation in the fingerprint image, dynamic tolerance is used to reduce the distortion effects. The tolerance area is decided by three threshold functions $Thld_r(\cdot)$, $Thld_\theta(\cdot)$, and $Thld_\phi(\cdot)$. The distance thresholds function ($Thld_r(\cdot)$) is more restrictive (smaller) when r_{i0} and r_{i1} are smaller and more flexible when r_{i0} and r_{i1} are larger. On the other hand, the thresholds on angles ($Thld_\theta(\cdot)$ and $Thld_\phi(\cdot)$) should be larger in order to allow large distortions when r_{i0} and r_{i1} are small, but smaller when r_{i0} and r_{i1} are large (Figure 2.1.3). The following empirical functions are used to get the thresholds:

$$(2.1.2) \quad Thld_r(r) = D_{max} \cdot \max\{5, r \cdot D_{ratio}\}$$

$$(2.1.3) \quad Thld_\theta(r) = \begin{cases} A1_{max} \cdot C_{lb} & \text{if } r \geq R_{max} \\ A1_{max} \cdot C_{ub} & \text{if } r \leq R_{min} \\ A1_{max} \cdot \left(C_{ub} - \frac{(r-R_{min})(C_{ub}-C_{lb})}{(R_{max}-R_{min})}\right) & \text{otherwise} \end{cases}$$

$$(2.1.4) \quad Thld_\phi(r) = \begin{cases} A2_{max} \cdot C_{lb} & \text{if } r \geq R_{max} \\ A2_{max} \cdot C_{ub} & \text{if } r \leq R_{min} \\ A2_{max} \cdot \left(C_{ub} - \frac{(r-R_{min})(C_{ub}-C_{lb})}{(R_{max}-R_{min})}\right) & \text{otherwise} \end{cases}$$

where D_{max} , D_{ratio} , $A1_{max}$, $A2_{max}$, C_{lb} , C_{ub} , R_{max} , and R_{min} are predefined constants. These values are chosen differently in the local matching stage and validation stage,

since stricter constraints are desired in the latter case.

2.1.2.1 Local Matching Stage

This stage results in an initial registration, namely, highly-feasible corresponding local triplet pairs between R and I .

2.1.2.2 Validation Stage

The candidate list, which is obtained in the initial registration stage, can only provide local alignments. However, not all well-matched local structures are reliable, Jiang and Yau [94] utilize the best fit local structure as reference points. In [39], a heuristic validation procedure is used to check all the matched triplet pairs. First, orientation differences between the two fingerprints are collected into bins of size of 10° . One dominant bin and its neighbors are obtained to filter out the matched pairs which are in the other trace bins. The top C best matched pairs as reference points instead of first one [94]. The MCF algorithm with dynamic tolerance strategy is used again to obtain the number of matched minutiae. The largest matched minutiae is taken as the final result of this stage, and is used to calculate the similarity score detailed in the following section.

2.1.2.3 Similarity Score Computation Stage

The result of this stage is used directly by the automatic fingerprint recognition system to measure how close the two fingerprints are and perform authentication. The most popular way to compute the similarity score is $\frac{n^2}{size_I \times size_R}$, where $size_I$ and

$size_R$ are the numbers of minutiae in the query fingerprint and reference fingerprint, and n is the number of matched minutiae. In [10], $\frac{2n}{size_I+size_R}$ is claimed to generate more consistent similarity scores. However, both methods are not reliable enough when the fingerprints are of different sizes. In [39], the overlapping regions and the average feature distances are integrated into a single reliable score calculation. The overlapping areas are defined as convex hulls which enclose all the matched minutiae in the query fingerprint and reference fingerprint.

The following information is needed to compute the similarity scores.

- n : the number of matched feature points;
- $size_I$: the number of feature points on the query fingerprint (I);
- $size_R$: the number of feature points on the reference fingerprint (R);
- O_I : the number of feature points in the overlapping area of query fingerprint (I);
- O_R : the number of feature points in the overlapping area of reference fingerprint (R);
- S_{avg} : the average feature distance of all the matched features.

The details of scoring function are shown in Figure 2.1.4.

2.1.3 Localized Size-specific Matching Algorithm

In the multi-path matching strategy, matching of small partial fingerprints is performed by an expansive brute-force matching when the number of feature points

```

Let  $S$  as the similarity score; Let  $height_c$  as the height of combined fingerprint;
Let  $width_c$  as the width of combined fingerprint;
Let  $max_h$  as the maximum possible height;
Let  $max_w$  as the maximum possible width;
Let  $T_m$  as a integer-valued threshold;
If ( $N < 7$  And ( $height_c > max_h$  Or  $width_c > max_w$ )) then
     $S = 0$ ;
Else
    If ( $O_a < 5$ ) then
         $O_a = 5$ ;
    Endif
    If ( $O_b < 5$ ) then
         $O_b = 5$ ;
    Endif
    If ( $N > T_m$  And  $N > \frac{3}{5}O_a$  And  $N > \frac{3}{5}O_b$ ) then
         $S = S_{avg}$ ;
    Else
         $S = \frac{N^2 S_{avg}}{O_a O_b}$ ;
        If  $S > 1.0$  then
             $S = 1.0$ ;
        Endif
    Endif
Endif
Endif

```

Figure 2.1.4: A heuristic rule for generating similarity scores.

present on the fingerprints is less than a certain threshold (α). The selection of α is important to the system's performance in terms of speed and accuracy. If α is set too low, only those fingerprints which have few feature points would benefit from brute-force matching. This may result in a high false reject rate (FRR), since most of the participating fingerprints contain more feature points than α , and some of them do not have enough feature points to obtain a successful match in the first stage of secondary feature matching. On the other hand, a large α would yield most matches via brute-force matching causing low speed and high false accept rate (FAR). Furthermore, when each minutia is associated with only one triplet (secondary feature), the local structure is neither reliable nor robust due to the influence of missing and spurious minutiae (Figure 2.1.5).

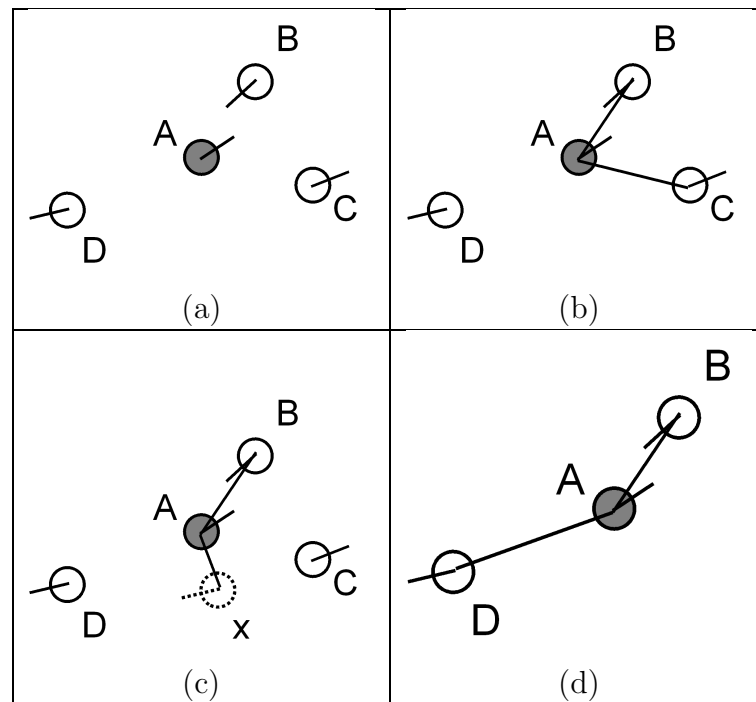


Figure 2.1.5: (a) Four synthetic minutiae. The gray-colored minutia A is used as central minutia to generate secondary features. (b) A genuine secondary feature. (c) The resulting false secondary feature if there is a spurious minutia X that is close to A . (d) The resulting false secondary feature if the minutia C is missing from the minutiae set.

The limitation of choosing an empirical threshold (α) for matching in a multi-path matching method can be solved by localized size-specific algorithm, where a central minutia is associated with many triplets formed from the k nearest neighboring minutiae instead of the first nearest two. This enhances robustness of the local structure, even though there might be missing or spurious minutiae [10] (Figure 2.1.6). The value of k is adaptively adjusted based on the size of the fingerprint image. Therefore, for a chosen k each minutiae can have

$$h = \binom{k}{2} = \frac{k!}{2! \times (k-2)!} \quad (2.1.5)$$

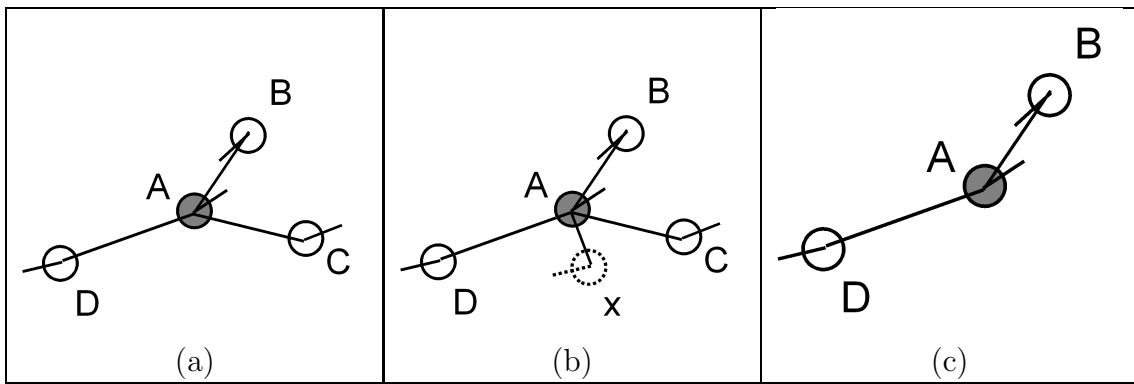


Figure 2.1.6: (a) Genuine secondary features generated from the closest three neighboring minutiae. (b) Under the influence of a spurious minutia, genuine secondary features remain intact. (c) Under the influence of a missing minutia, some of the genuine secondary features are still available for matching.

triplets. If the size of the acquired fingerprint image is sufficiently large, the value of k should be relatively small so that the total number of triplets is not too large. However, for partial fingerprints, usually there is insufficient information available in terms of the number of minutiae. Thus the small k may increase the probability of a false rejection. In [39], the value of k is decided by the detected number of minutiae on the fingerprint. The value of k is 6 if the number of minutiae is more than 30; k is 10 if the number of minutiae is less than 20; otherwise, the value of k is 7.

This heuristic rule can keep the number of triplets for every fingerprint around 600. The increased number of triplets makes the matching process time-consuming. An innovative indexing technique is used [39] to reduce computation complexity. The indexing method clusters triplets according to geometric characteristics. The central minutia is regarded as the origin point for reference. The plane is divided evenly into 8 non-overlapping quadrants, which are aligned with the orientation of the central minutia (Figure 2.1.7(a)). Two neighboring minutiae in a triplet are labeled with the quadrants which they are closest to (Figure 2.1.7(b)). This binning mechanism is invariant to rotation, translation and scaling. Each triplet is located in the 2-4 bins. Irregular triplets are removed if the angle between the central minutia and the two neighboring minutiae are abnormal (either close to 180° or close to 0°). This method can result in 92% reduction of the number of triplets.

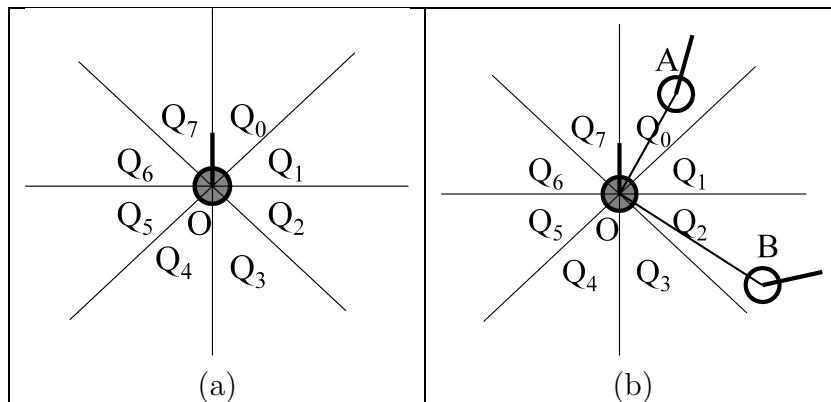


Figure 2.1.7: (a) The eight quadrants, Q_0 to Q_7 , of a central minutia. Note that the quadrants are aligned with the orientation of the central minutia. (b) An example of secondary feature and it can be labeled as Q_0Q_2 , Q_0Q_3 , Q_1Q_2 , and Q_1Q_3 .

2.1.3.1 Local Matching and validation

Each triplet in the neighboring list of a selected central minutia is matched separately. Because indexing is based on the shape of the triplet, searching of possible matches

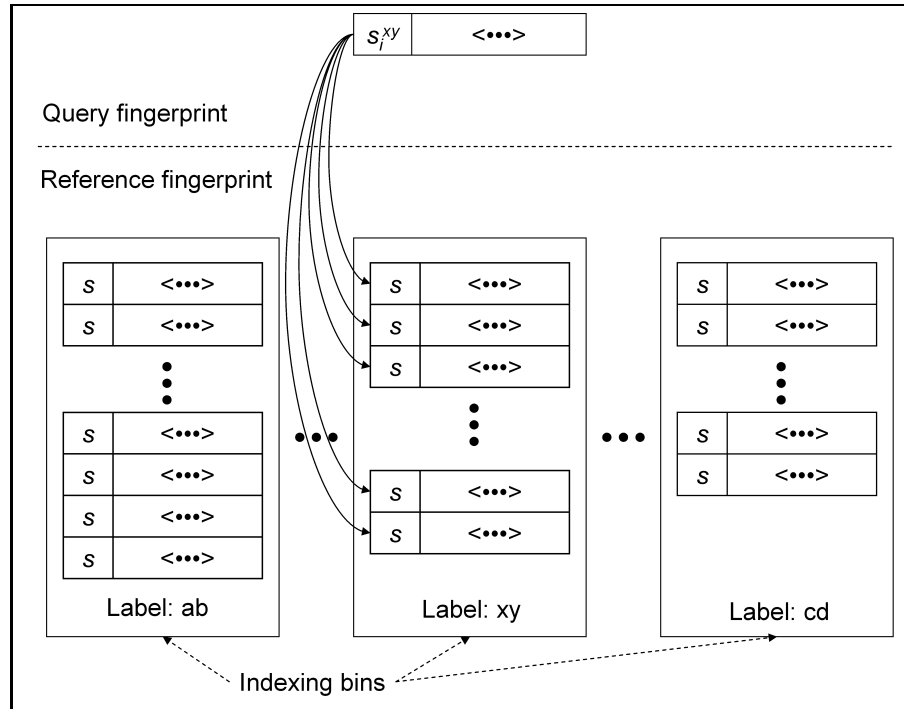


Figure 2.1.8: s_i^{xy} is a secondary feature on the query fingerprint with index label xy . When the matching is being executed, s_i^{xy} is matched against the secondary features on the reference fingerprint with the same index label.

for a given triple of a fixed index label, for example xy , need only focus on the bins with the same index label. This is illustrated in Figure 2.1.3.1. The validation phase utilize global context information to remove any incorrectly matched local structures. The surviving candidate pairs in the validation stage are referred to as *seeds* for subsequent extended matching.

2.1.3.2 Extended Matching

The approach proposed in [39] does not involve any global alignment to obtain the extended matching of minutia points, and all the matchings are performed locally. Since local distortion is easier to handle, the approach has a better chance of dealing with the effect of fingerprint deformation. Moreover, the *neighborhood list* of a triplet contains all the information needed for the extended match without a need for recalculation. The information is generated only once during the feature extraction process. The extended match extends the searching to possible matches from the immediate neighborhood around the previously matched minutiae. However, two issues need to be addressed:

1. If the minutiae are densely clustered, the extended match can be restricted to a small portion of the fingerprint, and may not propagate the match globally;
2. Since the extended match can start from any pair of matched feature points, the selection of the best result is challenging. One solution is to use every pair of *seeds* that are returned from the validation stage as starting points, and chose the extended matching result with the largest number of matched feature points as the final outcome. Another approach is to combine the extended matching results with different starting points, since each extended matching

result represents the correspondence of a local portion of a fingerprint.

These two issues are solved by adding the *seeds* into each other's *neighborhood list*. This gives a better chance of propagating the match throughout the fingerprint. The combination problem is automatically solved because each pair of matched *seeds* represents a different region of the participating fingerprints. The results have no conflicts if the matching extends from one pair of *seeds* to another pair. Many methods can be applied to find the optimal matching between the minutiae in the *neighborhood list* of two matched *seeds*.

The extended matching chooses the starting points from the set of *seeds*, which are the final result of the validation stage. This approach is more efficient than using all the possible correspondence pairs as starting points. Given a pair of starting *seeds* on the query (I) and the reference (R) fingerprints, a breadth first search is simultaneously executed on both fingerprints. Details of the extended matching is outlined in Figure 2.1.9.

```

Algorithm: ExtendedMatch
Inputs   :  $NL_q$ , the array of neighborhood lists of query fingerprint ( $I$ )
              $NL_r$ , the array of neighborhood lists of reference fingerprint ( $R$ )
              $SL$ , the array of seed pairs  $\langle s_q, s_r \rangle$ 
Outputs :  $M$ , the array of matched minutiae

Let  $M_{local}$  be an array for matched minutia pairs;
Let  $SL_{flag}$  be a boolean array to indicate if a pair of seeds has been used;
Let  $Mask_q$  be a boolean array to indicate if a minutia on  $I$  has found a match;
Let  $Mask_r$  be a boolean array to indicate if a minutia on  $R$  has found a match;
Let  $Q_q$  be a queue of minutiae on  $I$  that has found matched minutiae on  $R$ ;
Let  $Q_r$  be a queue of minutiae on  $R$  that has found matched minutiae on  $I$ ;
Initialize all elements in  $SL_{flag}$ ,  $Mask_q$ , and  $Mask_r$  to false;
FOR each seed pair,  $\langle s_q, s_r \rangle$ , in  $SL$ 
    Insert  $s_q$  into  $NL_q[s_{q'}]$ ,  $\forall s_{q'} \in SL$ , and  $s_{q'} \neq s_q$ ;
    Insert  $s_r$  into  $NL_r[s_{r'}]$ ,  $\forall s_{r'} \in SL$ , and  $s_{r'} \neq s_r$ ;
ENDFOR
FOR  $\langle s_q, s_r \rangle$  in  $SL$ 
    IF ( $SL_{flag}[\langle s_q, s_r \rangle] == \text{true}$ )
        CONTINUE;
    ENDIF
     $SL_{flag}[\langle s_q, s_r \rangle] = \text{true}$ ;
     $Q_q = \{s_q\}$ ;
     $Mask_q[s_q] = \text{true}$ ;
     $Mask_r[s_r] = \text{true}$ ;
     $M_{local} = \{\}$ ;
    WHILE ( $Q_q$  is not empty and  $Q_r$  is not empty)
         $m_q = \text{DEQUEUE}(Q_q)$ ;
         $m_r = \text{DEQUEUE}(Q_r)$ ;
        Find matched neighbors in  $NL_q[m_q]$  and  $NL_r[m_r]$ ;
        FOR each matched neighbor pair  $\langle m_{q_i}, m_{r_j} \rangle$ 
            IF ( $Mask_q[m_{q_i}] == \text{false}$  and  $Mask_r[m_{r_j}] == \text{false}$ )
                ENQUEUE( $m_{q_i}$ );
                ENQUEUE( $m_{r_j}$ );
                 $Mask_q[m_{q_i}] = \text{true}$ ;
                 $Mask_r[m_{r_j}] = \text{true}$ ;
                Add  $\langle m_{q_i}, m_{r_j} \rangle$  into  $M_{local}$ ;
            ENDIF
        ENDFOR
    ENDWHILE
    IF ( $\text{SIZEOF}(M_{local}) > \text{SIZEOF}(M)$ )
         $M = M_{local}$ ;
    ENDIF
ENDFOR
RETURN  $M$ ;

```

Figure 2.1.9: Outlines of proposed extended matching.

Chapter 3

Objective Fingerprint Image Quality Modeling

3.1 Background

Real-time image quality assessment can greatly improve the accuracy of an AFIS. The idea is to classify fingerprint images based on their quality and appropriately select image enhancement parameters for different quality of images. Good quality images require minor preprocessing and enhancement. Parameters for dry images (low quality) and wet images (low quality) should be automatically determined. We propose a methodology of fingerprint image quality classification and automatic parameter selection for fingerprint enhancement procedures.

Fingerprint image quality is utilized to evaluate the system performance [18, 48, 78, 82], assess enrollment acceptability [83] and improve the quality of databases, and

evaluate the performance of fingerprint sensors. Uchida [83] described a method for fingerprint acceptability evaluation. It computes a spatially changing pattern of gray level profile along with the frequency pattern of the images. The method uses only a part of the image - "observation lines" for feature extraction. It can classify fingerprint images into two categories. Chen et al. [18] used fingerprint quality indices in both the frequency domain and spatial domain to predict image enhancement, feature extraction and matching. They used the FFT power spectrum based on global features but do not compensate for the effect of image-to-image brightness variations. Based on the assumption that good quality image blocks possess clear ridge-valley clarity and have strong Gabor filters responses, Shen et al. [78] computed a bank of Gabor filter responses for each image block and determined the image quality with the standard deviations of all the Gabor responses. Hong et al. [32] applied a sinusoidal wave model to dichotomize fingerprint image blocks into recoverable and unrecoverable regions. Lim et al. [48] computed the local orientation certainty level using the ratio of the maximum and minimum eigen values of gradient covariance matrix and the orientation quality using the orientation flow.

In this chapter, we propose a limited ring-wedge spectral measure to estimate the global fingerprint image features. We use the inhomogeneity and directional contrast to estimate local fingerprint image features. Five quality levels of fingerprint images are defined. The enhancement parameter selection is based on the quality classification. Significant improvement in system performance is achieved by using the proposed methodology. Equal error rate(EER) was observed to drop from 1.82% to 1.22%.

3.2 Proposed Quality Classification Features

In Figure 3.2.1, sample fingerprint images of different qualities are taken from the DB1 database of FVC 2002. The dry image blocks with light ridge pixels in fingerprints are due to either slight pressure or dry skin surface. Smudge image blocks in the fingerprints are due to wet skin environment, unclean skin surface or heavy pressure.(Figure 1(c)). Other noise is caused by dirty sensors or damaged fingers. The following five categories have been defined:

- Level 1- (good) clear ridge/valley contrast; easily-detected ridges; precisely-located minutiae; easily-segmented.
- Level 2- (normal) Most of the ridges can be detected; ridge and valley contrast is medium; fair amount of minutiae; possesses some poor quality blocks (dry or smudge).
- Level 3- (Smudge/Wet) not well-separated ridges.
- Level 4- (Dry/lightly inked) broken ridges; only small part of ridges can be separated.
- Level 5- (Spoiled) totally corrupted ridges.

3.2.1 Global Quality Measure: Limited Ring-Wedge Spectral Energy

The images with the directionality pattern of periodic or almost periodic wave can be represented by the Fourier spectrum [18, 27]. A fingerprint image is a good example

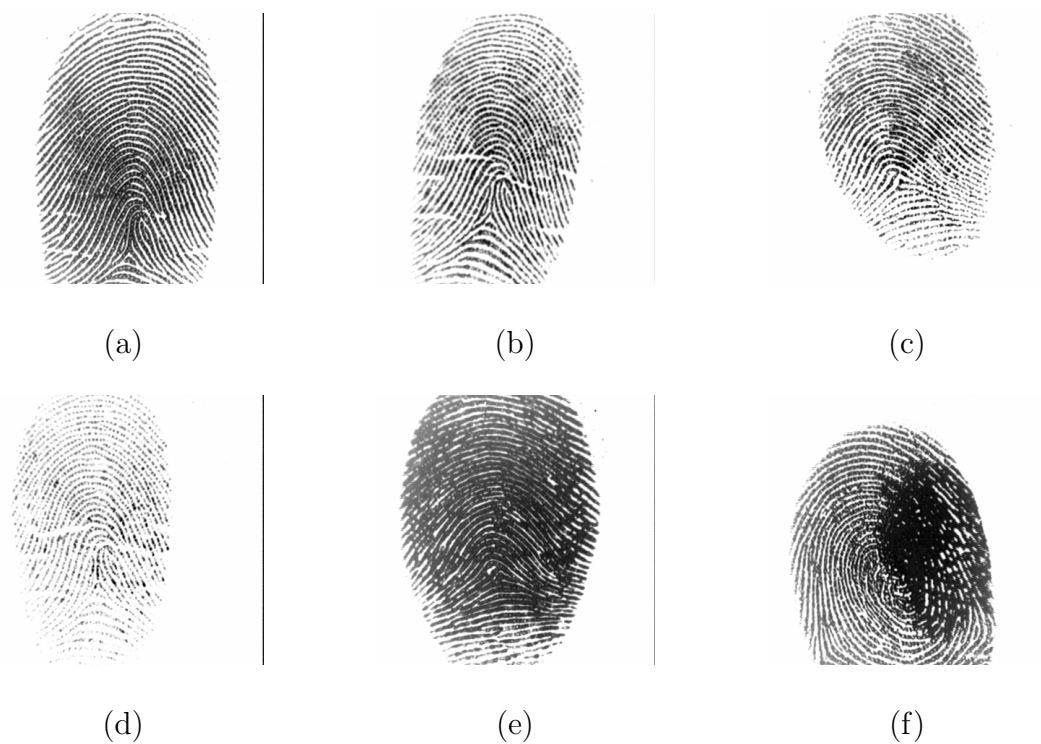


Figure 3.2.1: Typical sample images of different image qualities in DB1 of FVC2002. (a) and (b) Good quality, (c) Normal, (c) Dry, (d) wet and (e) Spoiled

of such types of texture. We represented the spectrum with the function $S(r, \theta)$, where r is the radial distance from the origin and θ is the angular variable. Given a digital image $f(x, y)$, its Fourier transform $F(u, v)$ is defined as:

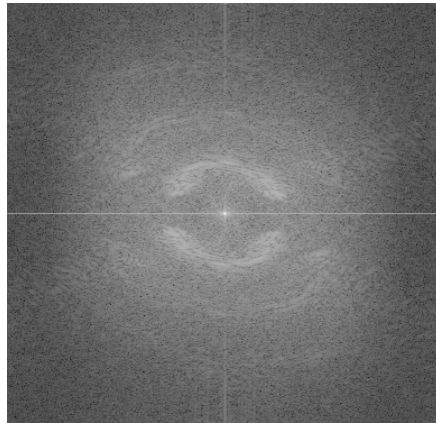
$$(3.2.1) \quad F(u, v) = \int_{-\infty}^{\infty} \int_{-\infty}^{\infty} f(x, y) e^{-j2\pi(ux+vy)} dx dy$$

$|F(u, v)|$ represents the spectrum of the Fourier transform, and it can be simplified by expressing in polar coordinates.

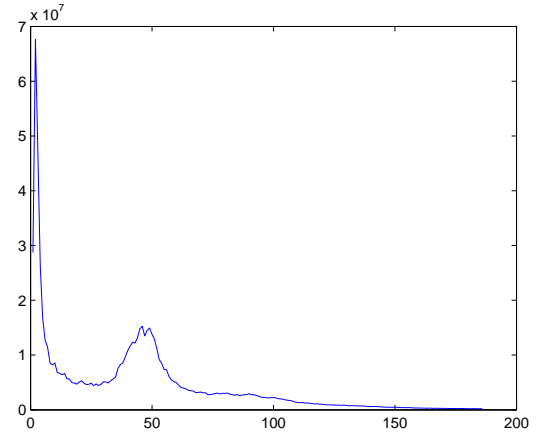
In [18], the FFT power spectrum based global feature does not compensate for the effect of image-to-image brightness variations. It measures the entropy of the energy distribution of 15 ring features, which are extracted using Butterworth low-pass filters. We convert $S(r, \theta)$ to 1-D function $S_{\theta}(r)$ for each direction, and analyze $S_{\theta}(r)$ for a fixed angle. Therefore, we can obtain the spectrum profile along a radial direction from the origin. A global descriptor can be achieved by summing the discrete variables:

$$(3.2.2) \quad S(r) = \sum_{\theta=0}^{\pi} S_{\theta}(r)$$

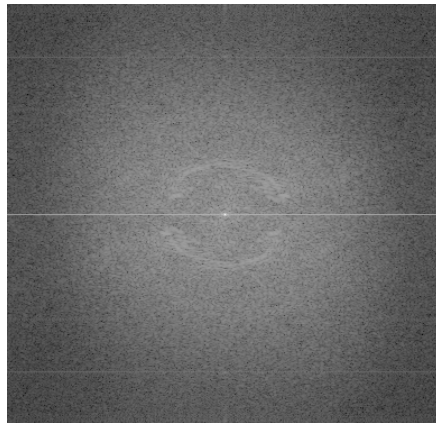
Figure 3.2.2 shows the spectra for a pair of fingerprint images (one has good quality, the other has low quality) from the same finger. We observe that there exists a characteristic principal peak around the frequency of 40. Based on actual computations and analysis of sample patterns, we compute the band energy between frequency 30 and frequency 60, which we will call the “limited ring-wedge spectral measure”. The difference between good quality and low quality images is significant as indicated by the existence of strong principal feature peak (the highest spectrum close to the origin is the DC response) and major energy distribution. The new global feature described above effectively indicates the clear layout of alternate ridge and valley patterns. However, it still can not classify fingerprint images, which are of predominantly good quality but contains occasional low quality blocks or those which are of



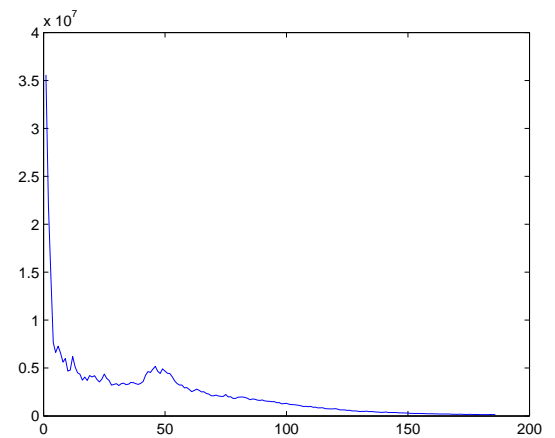
(a)



(b)



(c)



(d)

Figure 3.2.2: Spectral measures of texture for good impression and dry impression for the same finger. (a) and (b) are the corresponding spectra and the limit ring-wedge spectra for Figure 3.2.1(a), respectively; (c) and (d) are the corresponding spectra and the limit ring-wedge spectra for Figure 3.2.1(d), respectively.

predominantly low quality but contain occasional good quality blocks. A statistical descriptor of the local texture is necessary for such classification of fingerprint images.

3.2.2 Local Quality Measure: Inhomogeneity and directional contrast

To quantify the local texture of the fingerprint images, statistical properties of the intensity histogram [27] are well suited. Let I_i , L , and $h(I)$ represent gray level intensity, the number of possible gray level intensities and the histogram of the intensity levels, respectively. Mean(m), standard deviation(σ), smoothness(R) and uniformity(U) can be expressed as in equations 3-6. We define the block *Inhomogeneity*(inH) as the ratio of the product between mean and *Uniformity* and the product between standard deviation and smoothness.

$$(3.2.3) \quad m = \sum_{i=0}^{L-1} I_i h(I_i)$$

$$(3.2.4) \quad \sigma = \sqrt{\sum_{i=0}^{L-1} (I_i - m)^2 h(I_i)}$$

$$(3.2.5) \quad R = 1 - \frac{1}{1 + \sigma^2}$$

$$(3.2.6) \quad U = \sum_{i=0}^{L-1} h(I_i)^2$$

$$(3.2.7) \quad inH = \frac{m \times U}{\sigma \times R}$$

In [14], low contrast regions map out smudges and lightly-inked areas of the fingerprint. There is very narrow distribution of pixel intensities in a low contrast area. Thus the low flow maps flags blocks where the DFT analysis could not determine

a significant ridge flow. We used modified the ridge-valley orientation detector [14] as a measure of local directional contrast. Directional contrast reflects the certainty of local ridge flow orientation, and identifies damaged regions (Figure 3.2.1(d)). According to [14], for each pixel we calculate the sum of pixel values for 8 directions in 9×9 neighborhood, s_i . The values of s_{max} and s_{min} correspond to the most probable directions of white pixels in valleys and black pixels in ridges. We average the values of ratios s_{min}/s_{max} for block pixels to obtain the measure of directional contrast. By visual examination we determined the threshold for this average. If the average is bigger than threshold then the block does not have good directional contrast. The minutiae, which are detected in these invalid flow areas or those that are located near the invalid flow areas, are removed as false minutiae.

3.3 Adaptive Preprocessing Method

Fingerprint preprocessing is performed based on the frequency and statistical texture features described above. In the low quality fingerprint images, the contrast is relatively low, especially for light ridges with broken flows, smudge ridges/valleys, and noisy background regions. A high peak in the histogram is usually generated for those areas. Traditional histogram equalization can not perform well in this case. Good quality originals might even be degraded. An alternative to global histogram equalization is local adaptive histogram equalization(AHE) [27]. Local histogram is generated only at a rectangular grid of points and the mappings for each pixel are generated by interpolating mappings of the four nearest grid points. AHE, although acceptable in some cases, tends to amplify the noise in poor contrast areas. This problem can be reduced effectively by limiting the contrast enhancement to homogeneous areas. The implementation of contrast limited adaptive histogram equalization(CLAHE) has

been described in [102]. Contrast enhancement is defined as the slope of the function mapping input intensity to output intensity. CLAHE is performed by restricting the slope of the mapping function, which is equivalent to clipping the height of the histogram. We associate the clip levels of contrast enhancement with the image quality levels, which are classified using the proposed global and local image characteristic features. We define a block as a good block when the *Inhomogeneity*(inH) is less than 10 and average contrast(σ) is greater than 50 (See Fig 3.3.1). A block is defined as wet block if the product of its mean(m) and standard deviation(σ) is less than a threshold. A block is defined as dry block if its mean greater than a threshold, its average contrast is between 20 and 50, and the ratio of its mean and average contrast is greater than 5, and the ratio of its uniformity(U) and smoothness(R) is greater than 20.

- If the percentage of the blocks with very low directional contrast is above 30%, the image is classified as level 5. The margin of background can be excluded for consideration because the average gray level of blocks in the background is higher.
- If the limited ring-wedge spectral energy is below a threshold S_l , and the percentage of the good blocks, which are classified using *Inhomogeneity* and directional contrast, is below 30%, the image is classified as level 4. If the percentage of dry blocks is above 30% then it is level 3 if the percentage of wet blocks is above 30%;
- The images of level 1 possess high limited ring-wedge spectral energy and more than 75% good blocks. The images of level 2 have medium limited ring-wedge spectral energy and less than 75% good blocks.

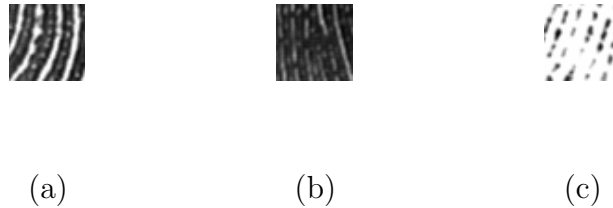


Figure 3.3.1: *Inhomogeneity*(inH) values for different quality fingerprint blocks, (a) good block sample with inH of 0.1769 and standard deviation(σ) of 71.4442, (b) wet block sample with inH of 2.0275 and standard deviation(σ) of 29.0199, and (c) dry block sample with inH of 47.1083 and standard deviation(σ) of 49.8631.

Based on our experiments, exponential distribution is used as the desired histogram shape (see equation (8)). Assume that f and g are input and output variables, respectively, g_{min} is minimum pixel value, $P_f(f)$ is the cumulative probability distribution, and $H_f(m)$ represents the histogram for the m level.

$$(3.3.1) \quad g = g_{min} - \frac{1}{\alpha} \ln(1 - P_f(f))$$

$$(3.3.2) \quad P_f(f) = \sum_{m=0}^f H_f(m)$$

3.4 Experiments

Our methodology has been tested on FVC2002 DB1, which consists of 800 fingerprint images (100 distinct fingers, 8 impressions each). Image size is 374×388 and the resolution is 500 dpi. To evaluate the methodology of correlating preprocessing parameter selections to the fingerprint image characteristic features, we modified the Gabor-based fingerprint enhancement algorithm [32] with adaptive enhancement of high-curvature regions. Minutiae are detected using chaincode-based contour tracing. In Figure 3.4, enhanced image of low quality image shown in Figure 3.2.1(d)

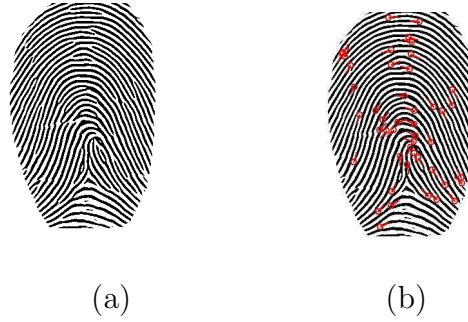


Figure 3.4.1: Enhancement and feature detection for the fingerprint of Figure 3.2.1(d)

shows that the proposed method can enhance fingerprint ridges and reduce block and boundary artifacts simultaneously.

Figure 3.4 shows results of utilizing the selective method of image enhancement on the fingerprint verification. We used the fingerprint matcher developed at the Center for Unified Biometrics and Sensors(CUBS)[39]. The automatic method selects clip limit in CLAHE algorithm depending on the image quality level in section 3.2. The non-automatic method uses the same clip limit for all images. The minimum total error rate (TER) of 2.29% (with FAR at 0.79% and FRR at 1.5%) and the equal error rate (EER) of 1.22% are achieved for the automatic method, compared with TER of 3.23% (with FAR at 1.05% and FRR at 2.18%) and ERR of 1.82% for the non-automatic enhancement parameter selection system. Note that the improvement is caused by only applying 5 different clip limit parameters to predetermined 5 image quality classes. The results confirm that image quality classification as described is indeed useful in image quality enhancement.

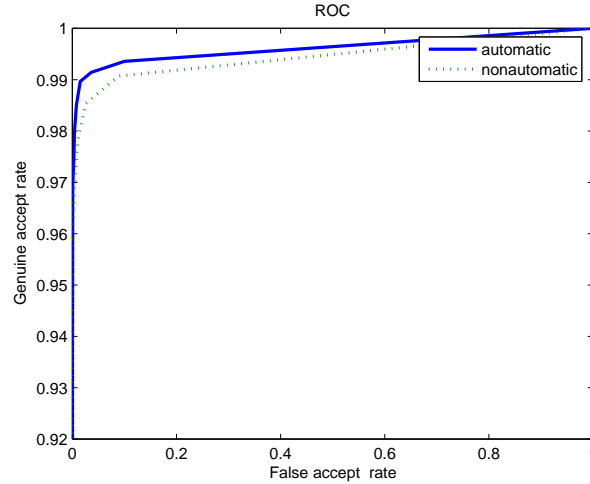


Figure 3.4.2: A comparison of ROC curves for system testings on DB1 of FVC2002.

3.5 Summary

We have presented a novel methodology of fingerprint image quality classification for automatic parameter selection in fingerprint image preprocessing. We have developed the limited ring-wedge spectral measure to estimate the global fingerprint image features, and inhomogeneity with directional contrast to estimate local fingerprint image features. Experiment results demonstrate that the proposed feature extraction methods are accurate, and the methodology of automatic parameter selection (clip level in CLAHE for contrast enhancement) for fingerprint enhancement is effective.

Chapter 4

Robust Fingerprint Segmentation

A critical step in automatic fingerprint recognition is the accurate segmentation of fingerprint images. The objective of fingerprint segmentation is to decide which part of the image belongs to the foreground, which is of our interest for extracting features for recognition and identification, and which part belongs to the background, which is the noisy area around the boundary of the image. Unsupervised algorithms extract blockwise features. Supervised methods usually first extract point features like coherence, average gray level, variance and Gabor response, then a simple linear classifier is chosen for classification. This method provides accurate results, but its computational complexity is higher than most unsupervised methods. We propose using Harris corner point features to discriminate foreground and background. Around a corner point, shifting a window in any direction should give a large change in intensity. We found that the strength of the Harris point in the fingerprint area is much higher than that of Harris point in background area. Some Harris points in noisy blobs might have higher strength, but it can be filtered as outliers using the corresponding Gabor response. The experimental results prove the efficiency and

accuracy of this new method.

Segmentation in low quality images is challenging. The first problem is the presence of noise that results from dust and grease on the surface of live-scan fingerprint scanners. The second problem is false traces which remain in the previous image acquisition. The third problem is low contrast fingerprint ridges generated through inconsistent contact, dry/wet finger surface. The fourth problem is the presence of an indistinct boundary if the features in the fixed size of window are used. Finally, that is the problem of segmentation features being sensitive to the quality of image.

Accurate segmentation of fingerprint images influences directly the performance of minutiae extraction. If more background areas are included in the segmented fingerprint of interest, more false features are introduced; If some parts of the foreground are excluded, useful feature points may be missed. We have developed a new unsupervised segmentation method.

4.1 Features for Fingerprint Segmentation

Feature selection is the first step in designing the fingerprint segmentation algorithm. There are two types of features used for fingerprint segmentation, i.e., block features and pointwise features. In [8, 44], selected point features include local mean, local variance, standard deviation, and Gabor response of the fingerprint image. Local mean is calculated as $Mean = \sum_w I$, local variance is calculated as $Var = \sum_w (I - Mean)^2$, where w is the window size centered on the processed pixel. The Gabor response is the smoothed sum of Gabor energies for eight Gabor filter responses. Usually the Gabor response is higher in the foreground region than that in

the background region. The coherence feature indicates the strength of the local window gradients centered on the processed point along the same dominant orientation. Usually the coherence is also higher in the foreground than in the background, but it may be influenced significantly by boundary signal and noise. Therefore, a single coherence feature is not sufficient for robust segmentation. Systematic combination of those features is necessary.

$$Coh = \frac{|\sum_w(G_{s,x}, G_{s,y})|}{|\sum_w(G_{s,x}, G_{s,y})|} = \frac{\sqrt{(G_{xx} - G_{yy})^2 + 4G_{xy}^2}}{G_{xx} + G_{yy}} \quad (4.1.1)$$

Because pointwise-based segmentation method is time consuming, blockwise features are usually used in the commercial automatic fingerprint recognition systems. Block mean, block standard deviation, block gradient histogram [53, 52], block average magnitude of the gradient [49] are some common features used for fingerprint segmentation. In [17], gray-level pixel intensity-derived feature called block clusters degree(Clud) has been introduced. *CluD* measures how well the ridge pixels are clustered.

$$CluD = \sum_{i,j \in block} sign(I_{ij}, Img_{mean}) sign(D_{ij}, Thre_{CluD}) \quad (4.1.2)$$

Where,

$$D_{ij} = \sum_{m=i-2}^{i+2} \sum_{n=j-2}^{j+2} sign(I_{mn}, Img_{mean}) \quad (4.1.3)$$

$$sign(x, y) = \begin{cases} 1 & \text{if } x < y; \\ 0 & \text{otherwise.} \end{cases} \quad (4.1.4)$$

Img_{mean} is the gray-level intensity mean of the whole image, and $Thre_{CluD}$ is an empirical parameter.

Texture features, such as Fourier spectrum energy [61], Gabor feature [78, 4] and Gaussian-Hermite Moments [86], have been also applied to fingerprint segmentation. Ridges and valleys in a fingerprint image are generally observed to possess

a sinusoidal-shaped plane wave with a well-defined frequency and orientation [32], whereas non-ridge regions does not conform to this surface wave model. In the areas of background and noise, it is assumed that there is very little structure and hence very little energy content in the Fourier spectrum. Each value of the energy image $E(x,y)$ indicates the energy content of the corresponding block. The fingerprint region may be differentiated from the background by thresholding the energy image. The logarithm values of the energy are used to convert the large dynamic range to a linear scale(Equation 4.1.5). A region mask is obtained by thresholding $E(x, y)$. However, uncleaned trace finger ridges and straight stripes are often get in the regions of interest (Figure 4.1.1(c)).

$$E(x, y) = \log \left\{ \int_r \int_\theta |F(r, \theta)|^2 \right\} \quad (4.1.5)$$

Gabor filter-based segmentation algorithm is a popularly used method [4, 78]. An even symmetric Gabor filter has the following spatial form:

$$g(x, y, \theta, f, \sigma_x, \sigma_y) = \exp\left\{-\frac{1}{2}\left[\frac{x_\theta^2}{\sigma_x^2} + \frac{y_\theta^2}{\sigma_y^2}\right]\right\} \cos(2\pi f x_\theta) \quad (4.1.6)$$

For each block of size $W \times W$ centered at (x,y) , 8 directional Gabor features are computed for each block, and the standard deviation of the 8 Gabor features is used for segmentation. The formula for calculating the magnitude of the Gabor feature is defined as,

$$G(X, Y, \theta, f, \sigma_x, \sigma_y) = \left| \sum_{x_0=-w/2}^{(w/2)-1} \sum_{y_0=-w/2}^{(w/2)-1} I(X + x_0, Y + y_0) g(x_0, y_0, \theta, f, \sigma_x, \sigma_y) \right| \quad (4.1.7)$$

However, fingerprint images with low contrast, false traces, and noisy complex background can not be segmented correctly by the Gabor filter-based method(Figure

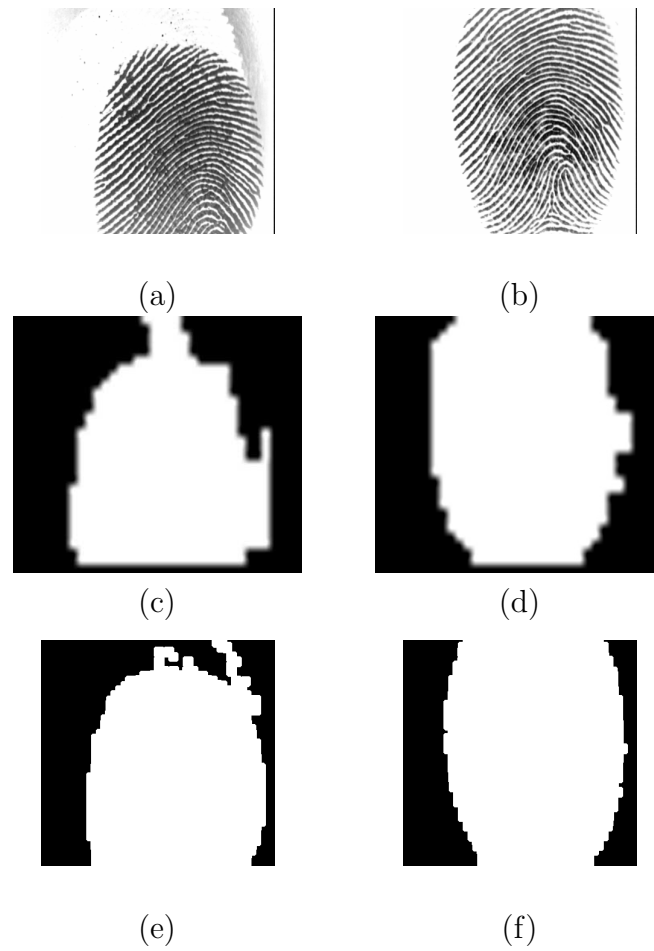


Figure 4.1.1: (a) and (b) are two original images, (c) and (d) are FFT energy maps for images (a) and (b), (e) and (f) are Gabor energy maps for images (a) and (b), respectively

4.1.1(e)).

In [71], similarity is found between Hermite moments and Gabor filter. Gaussian-Hermite Moments have been successfully used to segment fingerprint image in [86]. Orthogonal moments use orthogonal polynomials as transform kernels and produce minimal information redundancy, Gaussian Hermite Moments(GHM) can represent local texture features with minimal noise effect. The nth order Gaussian-filter smoothed Hermite moments of one-dimension signal $S(x)$ is defined as:

$$H_n(x, S(x)) = \int_{-\infty}^{+\infty} B_n(t)S(x+t) dt \quad (4.1.8)$$

Where

$$B_n(t) = g(t, \sigma)P_n(t/\sigma) \quad (4.1.9)$$

Where $P_n(t/\sigma)$ is scaled Hermite polynomial function of order n, defined as

$$P_n(t) = (-1)^n e^{t^2} \left(\frac{d^n}{dt^n} \right) e^{-t^2} \quad (4.1.10)$$

$$g(x, \sigma) = (2\pi\sigma^2)^{-\frac{1}{2}} e^{-\frac{x^2}{2\sigma^2}} \quad (4.1.11)$$

Similarly, 2D orthogonal GHM with order(p,q) can be defined as follows,

$$H_n(x, y, I(x, y)) = \int_{-\infty}^{+\infty} \int_{-\infty}^{+\infty} g(t, v, \sigma) H_{p,q} \left(\frac{t}{\sigma}, \frac{v}{\sigma} \right) I(x+t, y+v) dt dv \quad (4.1.12)$$

Where $g(t, v, \sigma)$ is 2D Gaussian filter, $H_{p,q}(\frac{t}{\sigma}, \frac{v}{\sigma})$ is the scaled 2D Hermite polynomial of order (p, q).

4.2 Unsupervised Methods

Unsupervised algorithms extract blockwise features such as local histogram of ridge orientation [52, 53], gray-level variance, magnitude of the gradient in each image

block [70], Gabor feature [4, 8]. In practice, the presence of noise, low contrast area, and inconsistent contact of a fingertip with the sensor may result in loss of minutiae or more spurious minutiae.

4.3 Supervised Methods

Supervised method usually first extract several features like coherence, average gray level, variance and Gabor response [8, 44, 61, 101], then a supervised machine learning algorithm, such as a simple linear classifier [8], Hidden Markov Model(HMM) [44], Neural Network [61, 101], is chosen for classification. This method provides accurate results, but its computational complexity is higher than most unsupervised methods, and needs time-intensive training, and possibly faces overfitting problems due to presence of various noises.

4.4 Evaluation Metrics

Visual inspection can provide qualitative evaluation of fingerprint segmentation result. More strict objective evaluation method is indispensable to assess quantitatively segmentation algorithms. Let R_1 represents standard segmentation pattern by a fingerprint expert. Let R_2 represent segmentation results by proposed automatic segmentation algorithms. In pixel levels, two metrics: correct percentage(CP) and mistaken percentage(MP) can be defined as follows:

$$CP = \frac{Region(R_1 \cap R_2)}{Region(R_1)} \quad (4.4.1)$$

$$MP = \frac{Region(R_1 - R_2)}{Region(R_1)} \quad (4.4.2)$$

Another quantitative evaluation method is based on minutiae extraction accuracy [8]. Our proposed minutiae extraction is applied to a fingerprint image segmented by a human fingerprint expert and to that segmented by our algorithm. The number of false and missed minutiae are counted for comparison.

4.5 Proposed Segmentation Methods

We propose using Harris corner point features [29, 54] to discriminate between foreground and background. The Harris corner detector was developed originally as features for motion tracking. It can reduce significantly the amount of computation compared to the processing of tracking every pixel. It is translation and rotation invariant but not scale invariant. Around the corner, shifting a window in any direction should give a large change in intensity. We also found that the strength of a Harris point in the fingerprint area is much higher than that of a Harris point in the background area. Some Harris points in noisy blobs might have higher strength, but can be filtered as outliers using corresponding Gabor response. Our experimental results prove the efficiency and accuracy of this new method with markedly higher performance than those of previously described methods. Corner points provide repeatable points for matching, so some efficient methods have been designed [29, 54]. At a corner, gradient is ill defined, so edge detectors perform poorly. In the region around a corner, gradient has two or more different values. The corner point can be easily recognized by examng a small window. Shifting the window around the corner point in any direction should give a large change in gray-level intensity, and no obvious change can be detected in “flat” regions and along the edge direction.

Given a point $I(x,y)$, and a shift $(\Delta x, \Delta y)$, the auto-correlation function E is defined

as:

$$E(x, y) = \sum_{w(x,y)} [I(x_i, y_i) - I(x_i + \Delta x, y_i + \Delta y)]^2 \quad (4.5.1)$$

and $w(x,y)$ is window function centered on image point (x,y) . For a small shift $[\Delta x, \Delta y]$, the shifted image is approximated by a *Taylor expansion* truncated to the first order terms,

$$I(x_i + \Delta x, y_i + \Delta y) \approx I(x_i, y_i) + [I_x(x_i, y_i)I_y(x_i, y_i)] \begin{bmatrix} \Delta x \\ \Delta y \end{bmatrix} \quad (4.5.2)$$

where $I_x(x_i, y_i)$ and $I_y(x_i, y_i)$ denote the partial derivatives w.r.t x and y , respectively. Substituting approximation Equation 4.5.2 into Equation 4.5.1 yields,

$$\begin{aligned} E(x, y) &= \sum_{w(x,y)} [I(x_i, y_i) - I(x_i + \Delta x, y_i + \Delta y)]^2 \\ &= \sum_{w(x,y)} \left(I(x_i, y_i) - I(x_i, y_i) - [I_x(x_i, y_i)I_y(x_i, y_i)] \begin{bmatrix} \Delta x \\ \Delta y \end{bmatrix} \right)^2 \\ &= \sum_{w(x,y)} \left(-[I_x(x_i, y_i)I_y(x_i, y_i)] \begin{bmatrix} \Delta x \\ \Delta y \end{bmatrix} \right)^2 \\ &= \sum_{w(x,y)} \left([I_x(x_i, y_i)I_y(x_i, y_i)] \begin{bmatrix} \Delta x \\ \Delta y \end{bmatrix} \right)^2 \\ &= [\Delta x, \Delta y] \begin{bmatrix} \sum_w (I_x(x_i, y_i))^2 & \sum_w I_x(x_i, y_i)I_y(x_i, y_i) \\ \sum_w I_x(x_i, y_i)I_y(x_i, y_i) & \sum_w (I_y(x_i, y_i))^2 \end{bmatrix} \begin{bmatrix} \Delta x \\ \Delta y \end{bmatrix} \\ &= [\Delta x, \Delta y] M(x, y) \begin{bmatrix} \Delta x \\ \Delta y \end{bmatrix} \end{aligned} \quad (4.5.3)$$

That is,

$$E(\Delta x, \Delta y) = [\Delta x, \Delta y] M(x, y) \begin{bmatrix} \Delta x \\ \Delta y \end{bmatrix} \quad (4.5.4)$$

where $M(x,y)$ is a 2×2 matrix computed from image derivatives, called auto-correlation

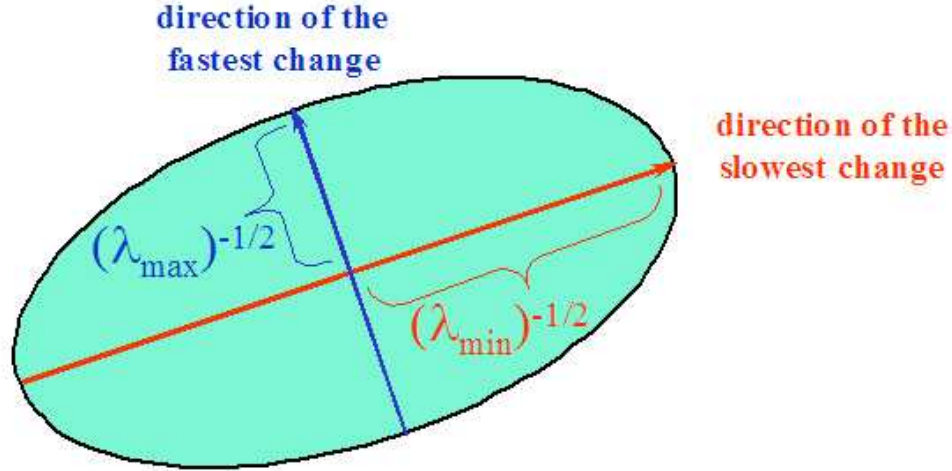


Figure 4.5.1: Eigenvalues analysis of autocorrelation matrix.

matrix which captures the intensity structure of the local neighborhood.

$$M = \sum_{x,y} w(x,y) \begin{bmatrix} (I_x(x_i, y_i))^2 & I_x(x_i, y_i)I_y(x_i, y_i) \\ I_x(x_i, y_i)I_y(x_i, y_i) & (I_y(x_i, y_i))^2 \end{bmatrix} \quad (4.5.5)$$

4.5.1 Strength of Harris-corner points of a Fingerprint Image

In order to detect intensity change in shift window, eigen value analysis of autocorrelation matrix M can classify image points. Let $\lambda_1 \lambda_2$ be the eigenvalues of autocorrelation matrix M , and autocorrelation function $E(\Delta x, \Delta y)$ with the ellipse shape constant. Figure 4.5.1 shows the local analysis.

In order to detect interest points, the original measure of corner response in [29] is :

$$R = \frac{\det(M)}{\text{Trace}(M)} = \frac{\lambda_1 \lambda_2}{\lambda_1 + \lambda_2} \quad (4.5.6)$$

The auto-correlation matrix (M) captures the structure of the local neighborhood. Based on eigenvalues(λ_1, λ_2) of M , interest points are located where there are two

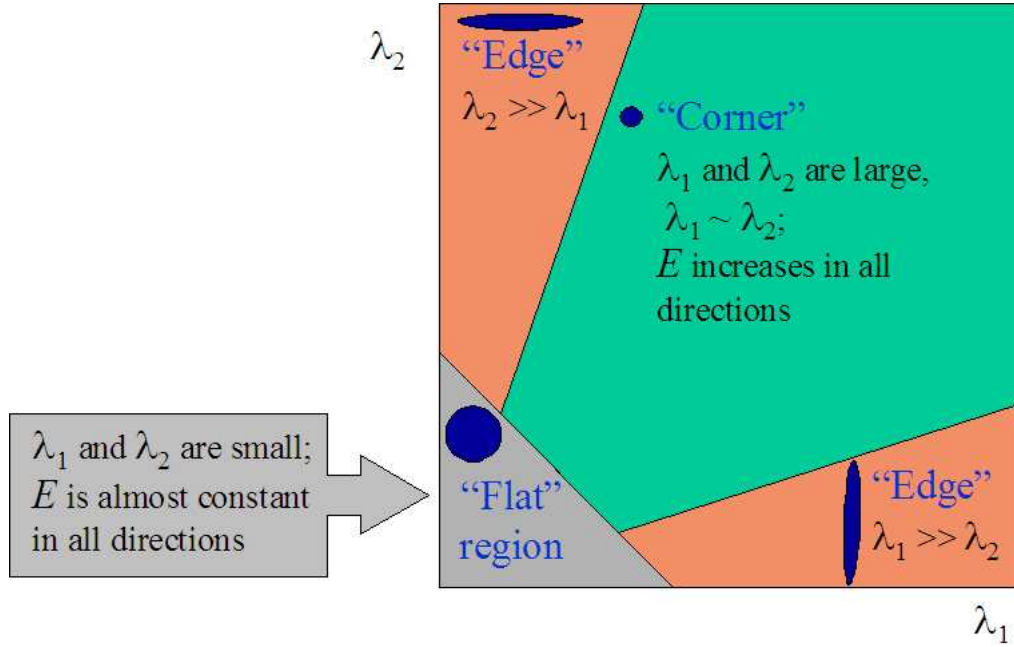


Figure 4.5.2: Eigenvalues distribution for corner points, edges and flat regions.

strong eigen values and the corner strength is a local maximum in a 3×3 neighborhood (Figure 4.5.2). To avoid the explicit eigenvalue decomposition of M , $Trace(M)$ is calculated as $I_x^2 + I_y^2$; $Det(m)$ is calculated as $I_x^2 I_y^2 - (I_x I_y)^2$. Corner measure for edges, flat regions and corner points are illustrated in Figure 4.5.3. The corner strength is defined as,

$$R = Det(m) - k \times Trace(M)^2 \quad (4.5.7)$$

We found that the strength of a Harris point in the fingerprint area is much higher than that of a Harris point in background area, because boundary ridge endings inherently possess higher corner strength. Most high quality fingerprint images can be easily segmented by choosing an appropriate threshold value. To segment the fingerprint area (foreground) from the background, the following “corner strength”

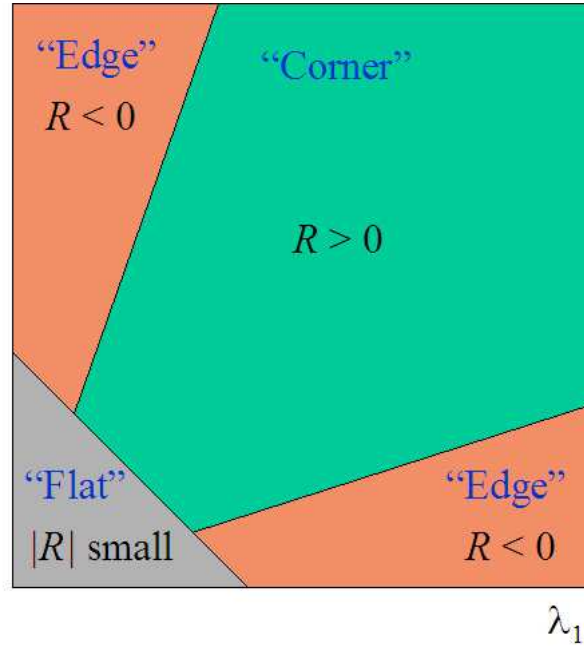


Figure 4.5.3: Corner measure for corner points, edges and flat regions.

measure is used, because there is one undecided parameter k in equation(5).

$$R = \frac{I_x^2 I_y^2 - I_{xy}^2}{I_x^2 + I_y^2} \quad (4.5.8)$$

In Figure 4.5.4, a corner strength of 300 is selected to distinguish corner points in the foreground from those in the background. Convex hull algorithm is used to connect Harris corner points located in the foreground boundary.

It is relatively easy for us to segment fingerprint images for the purpose of image enhancement, feature detection and matching. However, two technical problems need to be solved. First, different "corner strength" thresholds are necessary to achieve good segmentation results for images with varying quality. Second, some Harris points in noisy blobs might have higher strength, and therefore can not be segmented by choosing just one threshold. When a single threshold is applied to all the fingerprint images in the whole database, not all the corner points in the background are removed. Also

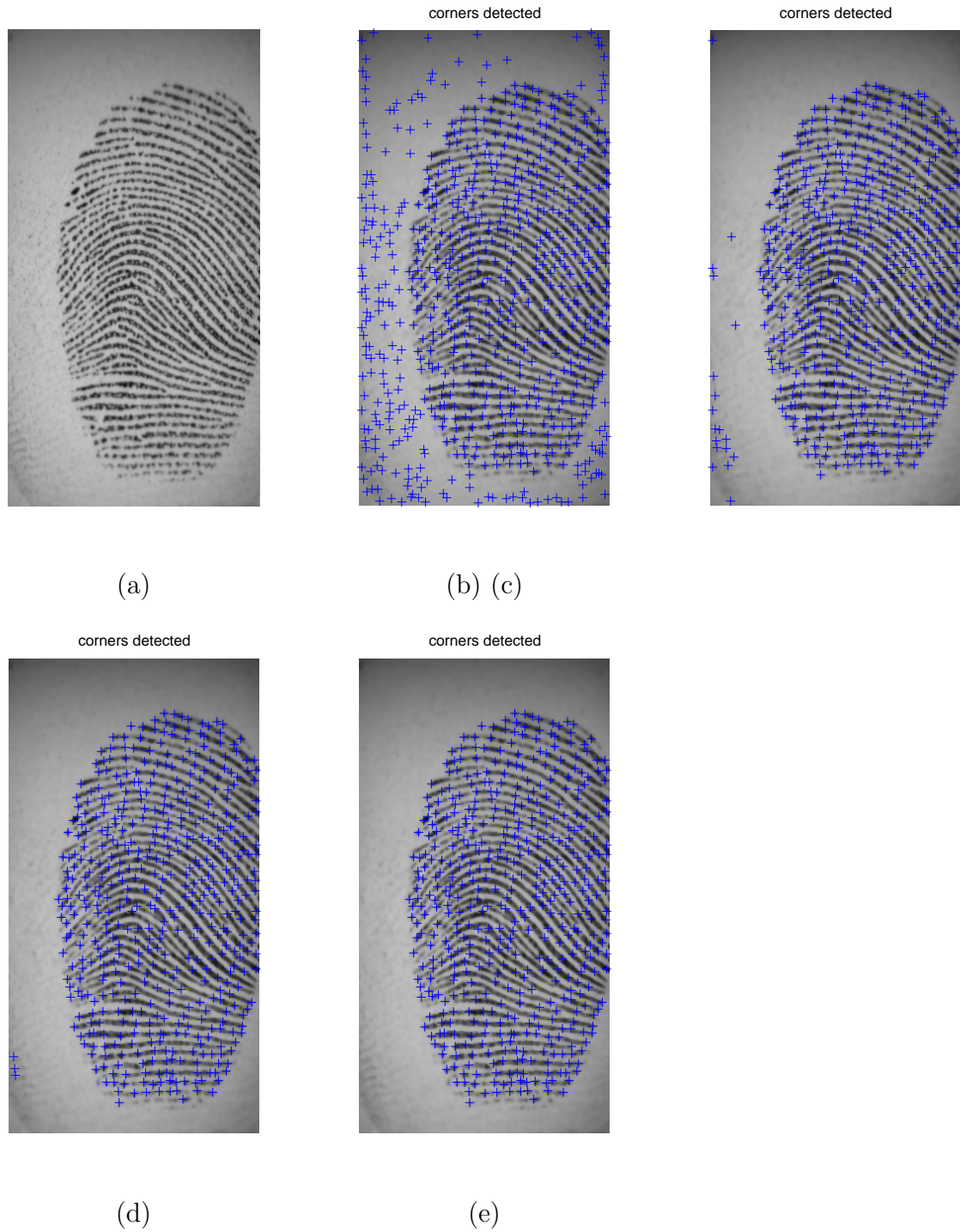


Figure 4.5.4: a good quality fingerprint with harris corner strength of (b)10, (c)60, (d)200, and (e)300. This fingerprint can be successfully segmented using corner response threshold of 300.

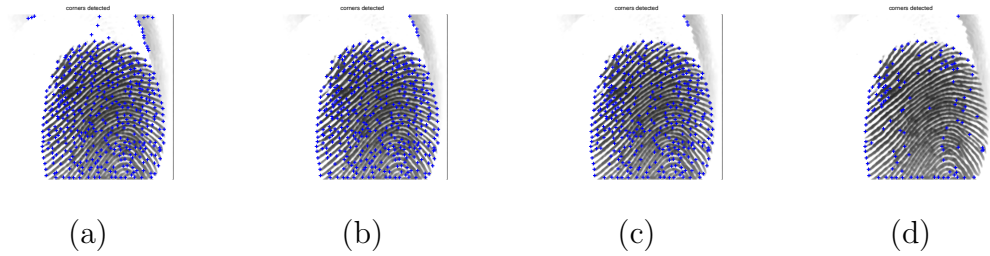


Figure 4.6.1: a fingerprint with harris corner strength of (a)100, (b)500, (c)1000, (d) 1500 and (e)3000. Some noisy corner points can not be filtered completely even using corner response threshold of 3000.

some corner points in noisy regions can not be thresholded even by using a high threshold value (Figure 4.6.1). In order to deal with such situations, we have implemented a heuristic algorithm based on the corresponding Gabor response (Figure 4.6.2). We have tested our segmentation algorithm on all the FVC2002 databases. Some test results are shown in Figure 4.6.3, 4.6.4, 4.6.5, and 4.6.6.

4.6 Summary

A robust interest point based fingerprint segmentation is proposed for fingerprints of varying image qualities. The experimental results compared with those of previous methods validate our algorithm. It has better performance even for low quality images, by including less background and excluding less foreground. In addition, this robust segmentation algorithm is capable of efficiently filtering spurious boundary minutiae.

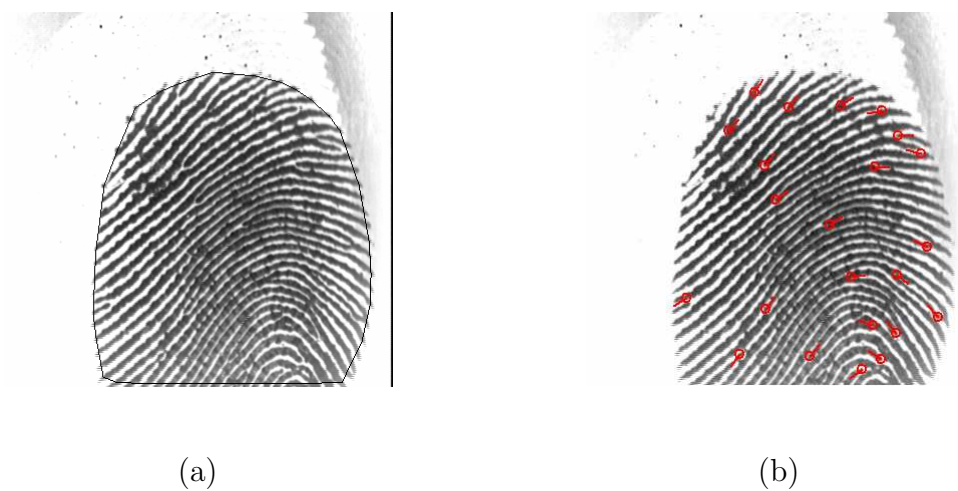


Figure 4.6.2: Segmentation result and final feature detection result for the image shown in the Figure 4.1.1(a). (a) Segmented fingerprint marked with boundary line, (b) final detected minutiae.



Figure 4.6.3: (a), (c) and (e) are original images from FVC DB1, (b), (d) and (f) show segmentation results with black closed boundary line



(a)



(b)



(c)



(d)



(e)

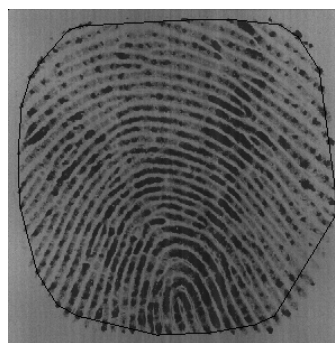


(f)

Figure 4.6.4: (a), (c) and (e) are original images from FVC DB2, (b), (d) and (f) show segmentation results with black closed boundary line



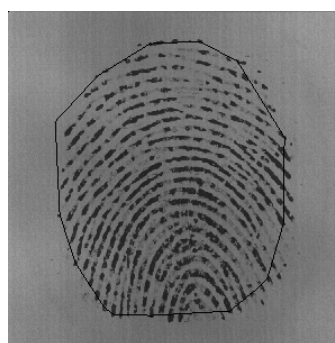
(a)



(b)



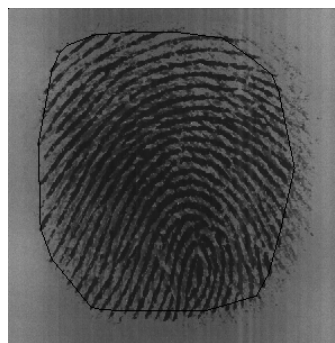
(c)



(d)



(e)



(f)

Figure 4.6.5: (a), (c) and (e) are original images from FVC DB3, (b), (d) and (f) show segmentation results with black closed boundary line



(a)



(b)



(c)



(d)



(e)



(f)

Figure 4.6.6: (a), (c) and (e) are original images from FVC DB4, (b), (d) and (f) show segmentation results with black closed boundary line

Chapter 5

Adaptive Fingerprint Image Enhancement

5.1 Introduction

The performance of any fingerprint recognizer depends heavily on the fingerprint image quality. Different types of noise in the fingerprint images pose difficulty for recognizers. Most Automatic Fingerprint Identification Systems (AFIS) use some form of image enhancement. Although several methods have been described in the literature, there is still scope for improvement. In particular, effective methodology of cleaning the valleys between the ridge contours are lacking. Fingerprint image enhancement needs to perform the following tasks [60]:

1. Increase the contrast between the ridges and valleys.
2. Enhance locally ridges along the ridge orientation. The filter window size should

be adapted to the local ridge curvature [90]. It should be large enough to increase the signal-to-noise ratio and complete the broken ridges in cuts and creases, and average out noise such as artifacts in valleys. However, it should not be too large to change the local ridge shape in the high-curvature regions (around core and delta points).

3. Facilitate feature points detection, and the number of genuine minutiae should be retained be the same as before enhancement.
4. Not change the ridge and valley structure and not flip minutiae type.
5. Improve the ridge clarity in the *recoverable regions* [32], and detect the unrecoverable regions as useless regions for spurious minutiae filtering.

In order to facilitate: (i) minutiae point detection and spurious minutiae filtering, and (ii) generation of less artifacts and smooth noise, accurate estimation of local image parameters is important. Filter window size, local ridge orientation, local ridge frequency and scale, ridge curvature as well as block image quality in terms of ridge flow and contrast entropy must be estimated and/or modeled from the original acquired image. The following section will review the methods for orientation field estimation.

5.2 Local ridge orientation field Estimation

Orientation fields are very useful in image segmentation [52] and enhancement [91, 32], classification and ridge detection [15], coherence calculation and singular points detection [9], and spurious minutiae filtering [92]. There are several techniques to compute local ridge orientation fields. In [96], Wang, Hu and Phillips proposed a

orientation model using 2-D Fourier expansions in the phase plane. The method had a low-computational cost, and worked well even for noisy fingerprints. In [80], Stock and Swonger used ridge-valley mask with a fixed number of reference templates (8 slits) to calculate the orientation field. The variation of the gray-scale pixels should be smaller along the local ridge direction and larger in the direction perpendicular. This method is simple and easy to compute, but it considers only 8 limited directions, and does not provide sufficient accuracy. The most common and accurate method is based on gradient. The ridge direction can be obtained by averaging of gradients of pixels in some neighborhood (blockwise). The gradient $\nabla(x_i, y_i)$ at point $[x_i, y_i]$ of image I is a two-dimensional vector $[G_x(x, y), G_y(x, y)]^T$. It can be defined as follows:

$$\begin{pmatrix} G_x(x, y) \\ G_y(x, y) \end{pmatrix} = \text{sign}(G_x(x, y))\nabla I(x, y) = \text{sign}\left(\frac{\partial I(x, y)}{\partial x}\right) \begin{pmatrix} \frac{\partial I(x, y)}{\partial x} \\ \frac{\partial I(x, y)}{\partial y} \end{pmatrix} \quad (5.2.1)$$

One limitation of gradient-based direction estimation is the cancellation problem when the gradients of two ridge sides represent the same ridge direction with opposite directions. Kass and Witkin [43] solved this problem by doubling the angles of the gradient vectors before averaging.

Block-level direction field is more often used for high-performance computation. Even though overlapping blocks are used for noise suppression, aliasing artifacts are generated due to fixed subsampling size and uniform averaging-filter shape. Scale-space theory [3, 81] can be used to smooth the orientation field by adapting to the ridge shape. The Gaussian window size can be chosen based on the scale-space theory. In [60], O’Gorman and Nickerson proposed a consistency-based orientation smoothing method. The smoothing was performed from low to high resolution in the same manner as in multi-scale-space theory [81]. Inconsistent blocks are split into four subsquares of sizes $3W/4 \times 3W/4$ (i.e each was overlapped by 50%) till the required consistency is achieved. Jain, Hong and Bolle [37] suggest an adaptive coarse to fine

smoothing of gradient tensor or angular data. It stopped when desired consistency level was achieved. If the consistency level was above the threshold, then the local orientation around the region was re-computed at a lower resolution level. The final effect was that less smoothing was done for high-curvature regions around cores and deltas. Donahue and Rokhlin [55] proposed an orientation smoothing method which was based on a least-square minimization. Nakamura, Nagaoka and Minami [59] proposed a stochastic relaxation technique for smoothing the orientation field which discriminates the high-curved regions from the rest of the image. Bergengruen [58] used the directional filters at a discrete number(3) of different scales, and selected the scale which gave the highest gray-scale variance along the direction perpendicular to the selected ridge direction.

5.3 Review of fingerprint image enhancement methods

Directional image enhancement can be performed in both spatial and frequency domains. The constraints of a problem dictates which domain is suitable. Filtering can be performed as a convolution task in the spatial domain, executed as multiplication in the frequency domain. Background patterns which are often indiscernible in the spatial domain are easily removed in the frequency domain. Similarly, a sinusoidal signal in broadband noise might be difficult to see in the time domain but is readily visible in the frequency domain. The following two sections review image enhancement techniques in the spatial domain and frequency domain, respectively.

5.3.1 Spatial Domain

Contextual filters with tuned local ridge orientation and frequency are averaged along the ridge direction to link ridge gaps, fill pores, filter noise, and improve the clarity between ridges and valleys. O’Gorman and Nickerson [60] designed a bell-shaped filter elongated along the ridge direction and cosine tapered in the direction perpendicular to the ridge direction. The filter design needs four main parameters: minimum and maximum ridge width, and minimum and maximum valley width. A set of 16 rotated versions of the mother filter with a step of 22.5° are obtained for image enhancement. However, the parameters for the filter are not determined empirically, rather they are estimated from the image. This makes it difficult to apply in large-scale real-time automatic fingerprint authentication systems. In [91], a non-linear filter is proposed with local ridge direction tuned and dynamic filter window size adapted to the local ridge curvature. The technical details of the method are described in the section 5.4.

5.3.2 Frequency Domain

Sherlock, Monroe, and Millard [79] designed the following contextual filter in the Fourier domain:

$$H(\rho, \theta) = H_{radial}(\rho) \cdot H_{direction}(\theta) \quad (5.3.1)$$

Here (ρ, θ) shows the polar co-ordinates in the Fourier domain, it can be separated into ρ and θ components. Both $H_{radial}(\rho)$ and $H_{direction}(\theta)$ are defined as bandpass filters. It assumes that the frequency is stable in the processed block, so only the direction determines the shape of filter. A set of prefiltered images (8 or 16) are calculated by convolving a set of prefilters with the image. The prefiltered image with the orientation closest to the local ridge orientation is selected as the enhancement result.

Prefiltered images are combined to improve the enhancement accuracy in the high-curvature regions when the pixel is close to singular points. Angular bandwidth of $\pi/8$ is selected for points away from singular points. The angular bandwidth π is selected for points close to singular points. An empirical piecewise linear equation defines angular bandwidth as a function of distance from the nearest singular point. However, there is no discussion about singular point detection. Kamei and Mizoguchi [42] designed a similar filter with the separable $H_{radial}(\rho)$ and $H_{direction}(\theta)$. $H_{radial}(\rho)$ defines the frequency filter, and $H_{direction}(\theta)$ defines the directional filter. An energy function is used to select the filters which match the ridge features.

Because it is time consuming to compute explicitly the local ridge orientation and frequency, Candela et al. [14] and Willis and Myers [89] propose multiplying the Fourier transform of the block by its power spectrum (of a power k):

$$I_{enh}[x, y] = F^{-1}\{F(I[x, y]) \times |F(I[x, y])|^k\} \quad (5.3.2)$$

The effect of multiplying the power spectrum (containing intrinsic major ridge orientation and frequency) can achieve enhancement of the dominant spectral components while attenuating the noisy spectral components. One limitation of this method is that it needs overlapping neighboring blocks to eliminate discontinuity artifacts. Pradenas [68] proposed directional image enhancement in the frequency domain. The local direction estimation of the method was not limited to fit one of a set of pre-defined directions. It performed better in noisy and high-curvature regions because more than one direction in the high-curvature regions was enhanced.

5.4 New Noise Model

We observe that noisy valley pixels and the pixels in the interrupted ridge flow gap are “impulse noises”. Therefore, we propose a new approach to fingerprint image enhancement, which is based on integration of the Anisotropic Filter and the Directional Median Filter(DMF). Gaussian-distributed noises are reduced effectively by Anisotropic Filter, whereas “impulse noises” are reduced efficiently by DMF. Usually, a traditional median filter is the most effective method to remove pepper-and-salt noise and other small artifacts. The proposed DMF can not only perform the original tasks, but it can also join broken fingerprint ridges, fill out the holes in fingerprint images, smooth irregular ridges, and remove some annoying small artifacts between ridges. Our enhancement algorithm has been implemented and tested on fingerprint images from FVC2002. Images of varying quality have been used to evaluate the performance of our approach. We have compared with other methods described in the literature in terms of matched minutiae, missed minutiae, spurious minutiae, and flipped minutiae (between end points and bifurcation points).

Most enhancement methods (either in frequency domain or in spatial domain) can not meet the needs of real-time AFIS in improving valley clarity and ridge flow continuity. Most enhancement techniques rely heavily on the local ridge orientation. We have developed an integrated method, which utilizes both the advantages of anisotropic filter and directional median filter. The fingerprint images are first convolved with the anisotropic filter, and are then filtered by the DMF. The pores in the fingerprint ridge are completely removed (currently, use of pore features is not practical because it requires very high quality fingerprint images), small to medium artifacts are cleared, and broken ridges in most clear regions are joined. The following two subsection will describe the two filters in detail.

5.4.1 Anisotropic Filter

Anisotropic filter reduces Gaussian-like noise similar to the Gabor filter in Hong's [32] work. Greenberg [28] modified the anisotropic filter by shaping the filter kernel to process fingerprint images. It is essentially adapting the filter shape to the local features (local intensity orientation) of the fingerprint image. The general form of the anisotropic filter can be defined as follows:

$$H(x_0, x) = V + S\rho(x - x_0)\exp\left\{-\left[\frac{((x - x_0) \cdot n)^2}{\sigma_1^2(x_0)} + \frac{((x - x_0) \cdot n_\perp)^2}{\sigma_2^2(x_0)}\right]\right\}$$

Where V and S are parameters for adjusting the phase intensity. The impact of the neighborhood, $\sigma_1^2(x_0)$ and $\sigma_2^2(x_0)$ controls the shape of the filter kernel. n and n_\perp are mutually normal unit vectors where n is along the direction of ridge line. ρ meets the condition $\rho(x) = 1$ when $|x| < r$. r is the maximum support radius. In our experiments, V and S are set to -2 and 10 respectively, $\rho_1^2(x_0) = 2$ and $\rho_2^2(x_0) = 4$ so that the Gaussian-shape is created with a $1 : 2$ ratio between the two kernel axes.

According to Gonzalez [27] and Shapiro [77], median filtering is performed by replacing a pixel with the median value of the selected neighborhood. The median filter performs well at filtering outliers points while leaving edges intact. The two-dimensional ($2D$) standard median filter is defined as follows:

Definition 5.4.1 *Given a gray-level image IM of size $M \times N$ with random impulse noise distribution n , the observation OIM of original image is defined as,*

$$OIM = IM + n$$

A median filter mask with suitably pre-selected window W of size $(2k + 1) \times (2l + 1)$

operates on the position $OIM(i, j)$, such that

$$Y(i, j; W) = \text{Median} \{OIM_{i-k, j-l}, \dots, OIM_{i, j}, \dots, OIM_{i+k, j+l}\}$$

where $i = 1, \dots, M$, $j = 1, \dots, N$, Y is the filtered output.

In fingerprint image processing, the standard median filter with rectangle topology appears to be unsuitable for achieving significant results in terms of noise reduction and image restoration. Further, filtering using the standard median filter can not only break up the bifurcation minutiae due to orientation uncertainty surrounding it, but also generate some annoying artifacts which lead to false minutiae. Actually, the ridges and valleys in a fingerprint image alternate at a relatively stable frequency, and flow in a local constant direction [70]. Assume that the pixels in the broken ridge gap are in a rectangle with width of about 3 pixels and length of about 5-7 pixels, and the long side of the rectangle is in parallel to the local ridge direction. Clearly, the broken ridge gap pixels can be considered as “impulse noise” in this rectangular region. Similarly, noise, which is in the rectangle region of the valleys with the long side parallel to the local ridge direction, can also be regarded as “impulse noise”. Therefore, the adaptive median filter with the same direction as local ridge can effectively reduce these “impulse noises”. Before the DMF is defined, the eight orientations of the fingerprint ridge flow structure are defined as shown in Figure 5.4.1. The corresponding directional templates are described in Figure 5.4.2.

Based on the eight directions, the shapes of the directional median filters are determined accordingly. The optimum window size of the median filter is set to 9 based on empirical data. The DMFs can hold more details by adding filters which are locally adaptive to the coherent flow fields. Therefore, the proposed directional median filter(DMF) is defined as follows:

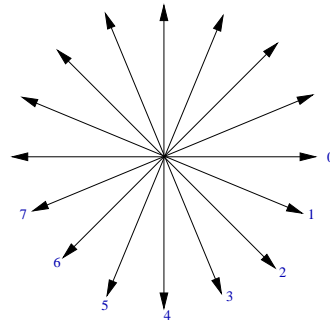


Figure 5.4.1: Orientation of Fingerprint Ridge Flow

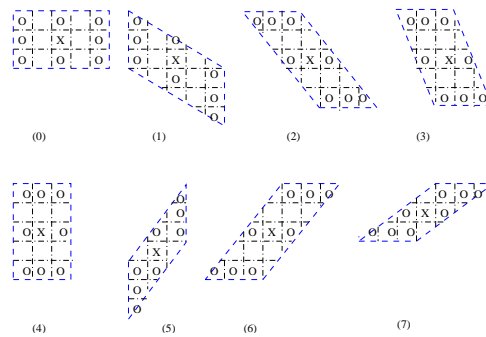


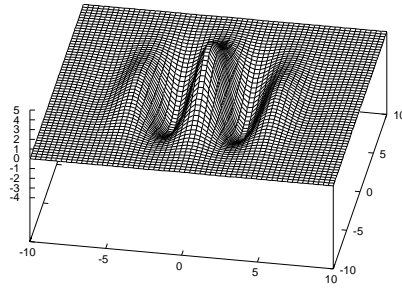
Figure 5.4.2: Eight directional templates, following orientation definitions

Definition 5.4.2 *Eight Directional median filter templates with suitably pre-selected window size W adopt different flow-like topological shapes, based on the orientations. When a point in the image is overlapping the focus point of the template kernel of the same orientation, then the chosen median filter is convolved with the current point. This generates W input samples, i.e., IM_1, \dots, IM_W in the specified window. Thus, the output of the median filter is given by*

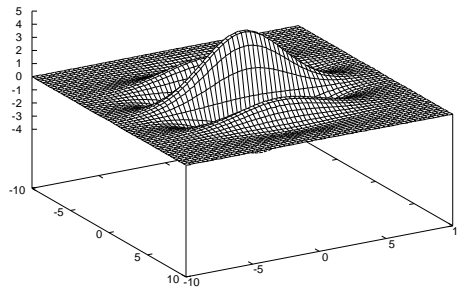
$$Y(i, j; W) = \text{Median} \{IM_1, \dots, IM_W\}$$

The length of filter windows must be carefully chosen so that filtering can achieve optimal results. Too small a window might fail to reduce the noise adequately, while too large a window might produce unnecessary distortions or artifacts. Also directional median filter shapes must follow local orientations appropriately, and select more relative points to enhance the ridge-flow continuity. Obviously, the window size should be selected based on the image features. DMF possesses a recursive property. The DMF window of size W replaces some of the old input samples with previously derived output samples. With the same amount of operations, the DMFs with recursive feature usually provide better smoothing capability and of interrupted ridges.

The properties of DMFs are illustrated in Figures 5.4.3, 5.4.4 and 5.4.5. Figure 5.4.3 shows the three-dimension shapes of the Gabor filter. Gabor filters consider the frequency and orientation of the images simultaneously [32], Gabor function is a Gaussian modulated sinusoid. Gabor filter is essentially a bandpass filter with a calculable frequency and bandwidth determined by the standard deviations of the Gaussian envelope. The coefficient weights of the Gabor filter place greater emphasis on the orientation flow of the fingerprint image, thereby filtering efficiently the noises with Gaussian distribution. However, the Gaussian-distributed noise model is not a



(a)



(b)

Figure 5.4.3: View of Gabor filter from (a)front and (b)side

good noise model for fingerprints. Pepper-salt noise, smudge in the valleys, interrupted ridge lines can not explained by the Gaussian model. In fact, any single noise model is too simple to explain the fingerprint image noise. Our proposed adaptive median filter eliminate efficiently noises in the valleys. Figure 5.4.4 demonstrates how the noise of medium size between the adjacent ridge lines can be removed. In Figure 5.4.5, one hole with the size of four pixels can be filled out completely, this saving a lot of post-processing steps in removing false minutiae. Repairing of broken fingerprint ridge flow lines using DMFs can be illustrated similarly.

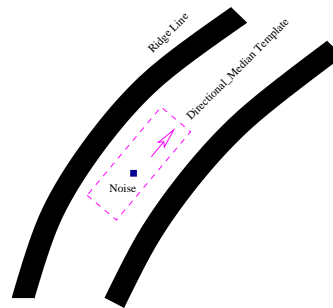


Figure 5.4.4: Noises between the ridgelines

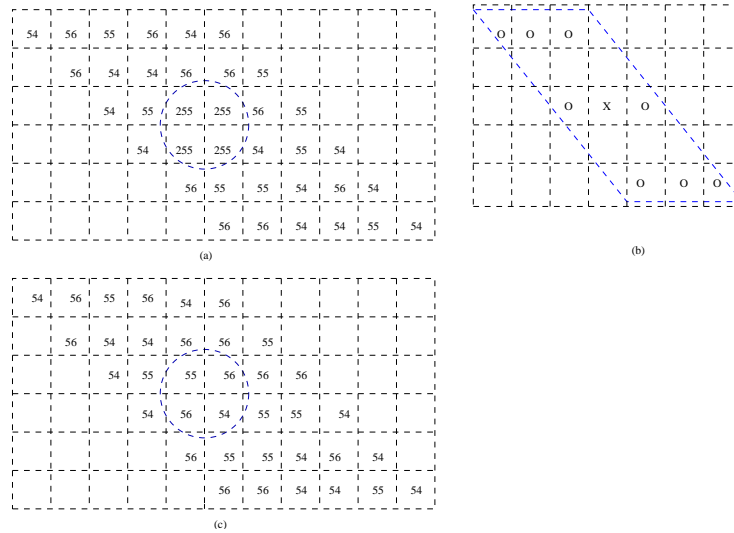


Figure 5.4.5: Filling out the hole in fingerprint image. (a) image with one hole, (b) Median template with the same direction as the ridge, (c) filtered image

5.4.2 Orientation estimation

Orientation calculation is critical for fingerprint image enhancement and restoration in both frequency and spatial domain. Without exception, the computation of the orientation image in the proposed algorithm directly affect the enhancement efficiency. In the literature, most of the fingerprint classification and identification processes calculate the local ridge orientation of the fixed-size block instead of each pixel. The most popular approach is based on binary image gradients [70, 32]. Other approaches have been proposed by different research groups [3, 60]. An innovative computational method, based on chaincode, was proposed in [91]. Chaincode is a lossless representation of gray-level image in terms of image recovery. The chaincode representation of fingerprint image edges captures not only the boundary pixel information, but also the *counter-clockwise ordering* of those pixels in the edge contours. Therefore, it is convenient to calculate the direction for each boundary pixel. End points and singular points, which are detected by the ridge flow following method (rest section), are not used for computation of ridge flow orientation in the fingerprint images. Also the components with chaincode elements less than 20 are regarded as noises and excluded from orientation computations. The computation procedure is as follows,

1. Each image is divided into 15×15 pixel blocks.
2. In each block, frequencies $F[i], i = 0..7$ for eight directions are calculated. Average frequency is computed. Then the difference between the frequency for each direction and average frequency is calculated.
3. Standard Deviation for the eight directions is calculated. If Standard Deviation is larger than a threshold, then the direction with the *maximum frequency* is regarded as the dominant direction. Otherwise, weighted average direction is

computed as the dominant direction.

The standard deviation of the orientation distribution in a block is used to determine the quality of the ridges in that block, and the quality measure of the whole fingerprint image can also be determined and classified into several classes. Each block direction is smoothed based on the surrounding blocks. Directional inconsistencies of some of the blocks is corrected by simple rules. For example, if for the block of interest, the directions of its left and right block are the same, then the current block takes the direction of its left block. This method can get correct ridge orientations even for very noisy images.

The enhancement algorithm described above has been implemented and tested on fingerprint images from FVC2002. Images of varying quality are used to evaluate the performance of our algorithm. For a typical fingerprint, the results of the orientation field, the binary fingerprint images filtered by an anisotropic filter and the proposed filter and the detected minutiae features are shown in Figures 5.4.6 and Figure 5.4.7, respectively. In the circle-marked regions in Figure 5.4.6(c) the broken ridge gaps can be seen clearly, and in the corresponding circle-marked regions of Figure 5.4.6(d) those gaps are filled completely. The filtering performance improvement by DMF is easily observed. It is verified further in Figure 5.4.7 with the minutiae detected by the ridge contour following algorithm.

The algorithm parameters such as the length of the DMFs' window, the number of directions in the orientation field, and the block size of adaptive binarization processing were empirically determined by running the algorithm on a set of test images from FVC2002. After a careful review of the results, we observe that each block direction can reflect the local ridge flow pattern with high accuracy, and the locations and types of detected minutiae can also be determined correctly. This also demonstrates



Figure 5.4.6: (a)Original Fingerprint image. (b)orientation field. (c)The binarization of filtered image by Anisotropic filter. (d)The binarization of filtered image by the proposed filter.

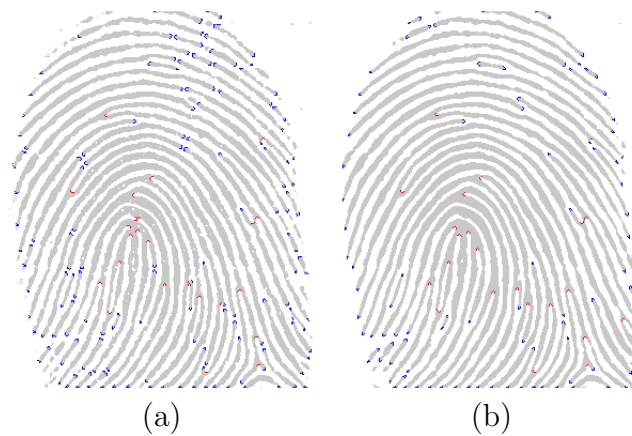


Figure 5.4.7: (a) minutiae for the image filtered by Anisotropic filter. (b)minutiae for the image filtered by the proposed filter.

the robustness of the ridge contour following evaluation measure. To quantitatively assess the performance of the fingerprint enhancement algorithm, and evaluate the quality of extracted minutiae features, the following terms are defined [28, 70]:

Matched minutiae: A minutiae detected by the algorithm can match with the ground truth minutiae with reasonable accuracy.

Missed minutiae: Minutiae that were not found within the tolerance distance of the true minutiae

Spurious minutiae: Minutiae that were found in the region not containing true minutiae, i.e., the minutiae were created during enhancement, binarization, or feature extraction.

Flipped minutiae: Detected minutiae type is different from the true minutiae type in the same image region.

In Table 5.4.1, the comparison results for a representative subset of 8 fingerprint images by anisotropic filter and proposed filter are shown in terms of matched minutiae(Ma), missed minutiae(Mi), spurious minutiae(S) and flipped minutiae(F). Clearly, the proposed image enhancement algorithm has outperformed the anisotropic filter in feature extraction accuracy. It should be noted that most minutiae classified as spurious minutiae after filtering can be eliminated because they are generated by a long gap of broken ridges. After enhancement, the number of flipped or missed minutiae is relatively low. Experimental results show our method to be superior to those described in the literature for local image enhancement.

Database	Number	Filter	Ma	Mi	S	F
FVC2002 db1	1_8	Anisotropic	41	0	31	3
		Proposed	41	0	8	2
FVC2002 db1	15_8	Anisotropic	36	8	65	4
		Proposed	37	6	14	2
FVC2002 db1	20_6	Anisotropic	36	8	65	4
		Proposed	37	6	14	2
FVC2002 db1	72_8	Anisotropic	30	10	115	2
		Proposed	37	6	23	1
FVC2002 db1	59_6	Anisotropic	20	8	83	1
		Proposed	29	3	20	1
FVC2002 db1	89_1	Anisotropic	16	9	97	2
		Proposed	24	4	16	1
FVC2002 db1	96_5	Anisotropic	16	8	107	4
		Proposed	25	3	28	3
FVC2002 db1	102_6	Anisotropic	33	1	41	0
		Proposed	40	0	11	0

Table 5.4.1: Performance comparison on testing set.

5.5 Singularity preserving fingerprint adaptive filtering

Most AFISs can accurately extract minutiae in the well defined ridge-valley regions of a fingerprint image where the ridge orientation changes slowly but cannot obtain satisfactory results in the high-curvature regions [3, 87]. In [32], the Gabor filter was used to enhance fingerprint images, and local ridge orientation and ridge frequency were critical parameters for high performance. However, it may be insufficient that only single low-pass filter with the size of 5×5 was adopted with the assumption that there is slow orientation change in local ridges. Noisy regions like creases cannot be smoothed successfully with such a size of Gaussian kernel.

Curvature estimation directly from ridge orientation fields has attracted a lot of research effort [38, 88]. The coherence map reflects the local strength of the directional field. It is computed based on the principal component analysis of local gradients in [5]. We calculate an orientation coherence map and determine the minimum coherence regions as high-curvature areas.

The basic idea of singularity-preserving fingerprint image filtering is that adaptive Gaussian filter kernels are adapted directly to smooth local orientation map in terms of ridge curvature. Because the smoothing operation is applied to the local ridge shape structures, it joins efficiently the broken ridges without destroying essential singularities and enforces continuity of directional fields even in creases.

5.5.1 Computation of Ridge Orientation and High-Curvature Map

5.5.1.1 Gaussian Filtering

In a fingerprint image, additive noise in the orientation smoothing is correlated with the local ridge curvature. The high-curvature regions centered around the delta and core points need to be filtered by relatively small Gaussian kernel size σ , compared to clear regions with almost parallel ridges. Because the Fourier transform of a Gaussian is also a Gaussian, a Gaussian filter in the spatial domain performs like a low-pass filter in the frequency domain [32].

5.5.1.2 Computation of Ridge Orientation and High-Curvature Map

The Gradient Square Tensor (GST) is the most commonly used robust flow pattern orientation estimator. The direction of the gradient is an estimator of the local orientation and is very sensitive to noise. Therefore, Gaussian filter regularization is needed. Let $G_x(i, j)$ and $G_y(i, j)$ be the x and y components of the gradient vector at point (i, j) . To solve the cancellation problem of the gradient vector and its opposite correspondence, the following tensor T is used to calculate the gradient direction:

$$(5.5.1) \quad T = \nabla I \nabla I^T = \begin{pmatrix} G_x(i, j)^2 & G_x(i, j)G_y(i, j) \\ G_x(i, j)G_y(i, j) & G_y(i, j)^2 \end{pmatrix}$$

The final orientation estimate is obtained by an eigenvalue analysis of the smoothed tensor.

Curvature at any point along a 2D curve is the change rate in the tangent direction of the contour. The local orientation in a fingerprint image is computed by the GST,

and we define curvature as the ridge orientation change rate. In NFIS2 software [88], high-curvature areas of the fingerprint are marked using two different measures: *vorticity* (the cumulative change in ridge flow direction around all the neighbors of a block) and *curvature* (the largest orientation change between a block's ridge flow and the ridge flow of each of its neighbors). In [87], singular points are determined first, and the high-curvature areas are defined as squares of 100 side length, centered around the core and delta points. In [3], a measure called "ridgeness" is defined, and points of a fingerprint image are assigned "1" in areas with clear parallel ridges, and "0" in areas with unclear ridges such as creases, fragmented ridges, blurred and over-inked areas. Unfortunately, points in high curvature areas are assigned very small values. In [38], Jain integrated the sine component of the orientation field in two regions which were geometrically designed to capture the maximum curvature in the concave ridges. However, it can not achieve precise and consistent reference points for the arch type fingerprints, nor accurately locate the reference points in noisy images. Instead of identifying the singular points, we calculate the orientation coherence map and determine the minimum coherence regions as high-curvature areas. The coherence map reflects the local strength of the directional field. It can be represented as the ratio of the difference of the sum of two eigenvalues [5] and can be computed as follows:

$$(5.5.2) \quad coh = \frac{\sqrt{((G_{xx} - G_{yy})^2 + 4G_{xy}^2)}}{G_{xx} + G_{yy}}$$

where G_{xx} , G_{yy} and G_{xy} represent the variances and cross-variance of G_x and G_y .

5.5.2 Experiments

The proposed methodology is tested on FVC2002 DB1, which consists of 800 fingerprint images (100 distinct fingers, 8 impressions each). Image size is 374×388 and

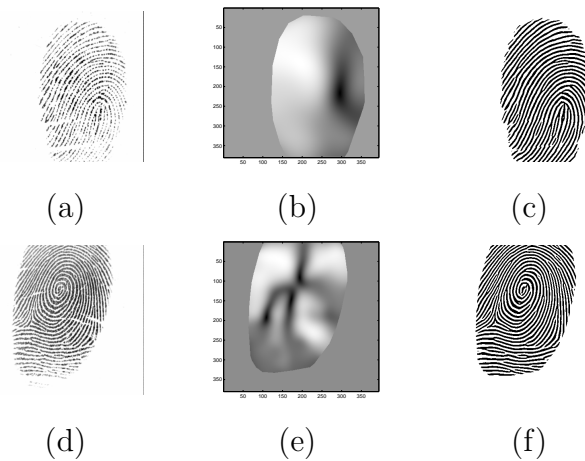


Figure 5.5.1: Coherence-map based curvature estimation. (a) and (d) Original Images. (b) and (e) corresponding coherence maps. (c) and (f) corresponding enhanced images.

the resolution is 500dpi. To evaluate the methodology of adapting a Gaussian kernel to the local ridge curvature of a fingerprint image, we have modified the Gabor-based fingerprint enhancement algorithm [32] with two kernel sizes: the smaller one in high-curvature regions and the larger one in ridge parallel regions. Minutiae is detected using chaincode-based contour tracing [91]. We first utilize image quality features to adaptively preprocess images and segment fingerprint foreground from background. The gradient map of segmented images is computed, followed by the coherence map. The coherence map is binarized by the threshold, and the high-curvature regions are detected as the regions with lower coherence value in the coherence map. The centroid and bounding-box of the high-curvature region can be used to dichotomize image blocks into two regions, where different Gaussian kernels are utilized to smooth the orientation map. The four sides for the bounding-box of the high-curvature region are extended by about 16 pixels in this paper. This parameter is changed with the different image size and resolution.

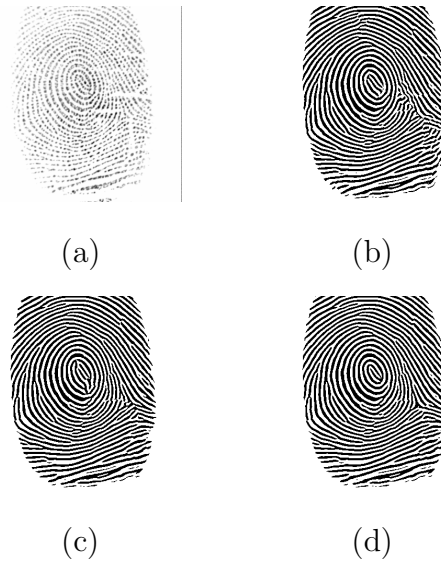


Figure 5.5.2: Gaussian kernel effects on the enhancement performance. (a)Original image, (b) single kernel of $\sigma = 5$, (c) single kernel of $\sigma = 15$ and (d) Dual kernels of $\sigma = 5$ and $\sigma = 15$.

In Figures 5.5.1 (a) and (d) two images of different quality, and corresponding coherence maps are shown. In Figure 5.5.1 (b) and (e), the final enhanced images are shown for Figure 5.5.1 (c) and (f). Adaptive Gaussian filter window sizes are used to smooth the local orientation map. One dry fingerprint with several creases is shown in Figure 5.5.2(a). In Figure 5.5.2(b) and (c), a single Gaussian kernel is used in orientation filtering. If a single large kernel is used to smooth orientation in high-curvature regions, ridges with pseudo-parallel patterns can be enhanced perfectly, but undesired artifacts are generated in high-curvature regions. Some parallel ridges are bridged, and some continue ridges with high-curvature are disconnected (Figure 5.5.2(c)). If only a single small kernel is adopted to smooth orientation, ridges in the noisy areas like creases are not enhanced properly (Figure 5.5.1(b)). Figure 5.5.2(d) shows a satisfactory enhancement result with dual kernels.

Table 5.5.1: Minutiae detection accuracy with different kernels

		N_T	N_M	N_F	N_{total}	Accuracy
σ_5	im1	44	4	5	46	76.09%
	im2	42	3	2	41	90.24%
	im3	21	1	11	31	29.03%
σ_{15}	im1	44	2	6	52	69.23%
	im2	42	3	13	52	50.00%
	im3	21	0	5	26	61.54%
σ_{5-15}	im1	44	2	3	48	81.25%
	im2	42	3	2	41	90.24%
	im3	21	0	2	23	82.61

Table 5.5.1 shows the effect of the Gaussian kernel on the minutiae detection accuracy. We define minutiae detection accuracy as $\frac{N_T - N_M - N_F}{N_{total}}$, where N_T represents the number of the true minutiae, N_M represents missed minutiae, N_F represents false minutiae, and N_{total} represents the total number of detected minutia. Experimental results show that adaptive orientation smoothing in high-curvature regions and regions of pseudo-parallel ridges achieves superior results than smoothing using a single Gaussian kernel. Isotropic filter near high-curvature areas is used in [87], and an accuracy of 81.67% is obtained. In comparison, we achieve 84.65%, because isotropic filter tends to blur pseudo-parallel ridge lines.

Chapter 6

Feature Detection

6.1 Introduction

An accurate representation of the fingerprint image is critical to automatic fingerprint identification systems, because most deployed commercial large-scale systems are dependent on feature-based matching, even though correlation-based matching methods may have high performance when additional computation time is available. Among all the fingerprint features, minutia point features with corresponding orientation maps are unique enough to provide robust discriminative capacity [62], the minutiae feature representation reduces the complex fingerprint recognition problem to a point pattern matching problem. In order to achieve high-accuracy minutiae with varied quality fingerprint images, segmentation algorithm needs to separate foreground from noisy background without excluding any ridge-valley regions and not include meaningless background. Image enhancement algorithm needs to keep the original ridge

flow pattern without altering the singularity, join broken ridges, clean artifacts between pseudo-parallel ridges, and not introduce false information. Finally minutiae detection algorithm needs to locate efficiently and accurately the minutiae points.

There are a lot of minutiae extraction methods available in the literature. Based on image detection domain, there are roughly four categories of detection algorithms. First category of methods extract minutiae directly from the gray-level image [30, 40, 47, 49, 57, 75, 76] without using binarization and thinning processes. Second category of methods extract minutiae from binary image profile patterns [12, 25, 91, 88]. Third category of methods extract minutiae via machine learning methods [6, 12, 47, 66, 75, 76]. The final category of methods extract minutiae from binary skeletons [5, 36].

Section 6.2 will review four types of minutiae extraction algorithms. Section 6.3 presents chain-coded contour tracing algorithm developed in this thesis. Section 6.4 introduces run-length scanning method for minutiae detection and efficient thinning. Section 6.5 provides details of minutiae verification and filtering rules for chain-coded contour tracing minutiae detection method. The experimental results are shown in Section 6.6.

6.2 Previous Methods

6.2.1 Skeletonization-based Minutiae Extraction

Traditional minutiae detection from a gray-level fingerprint image involves a series of steps. Most implementations include fingerprint segmentation, orientation field computation, enhancement, binarization, thinning and minutiae detection (Figure

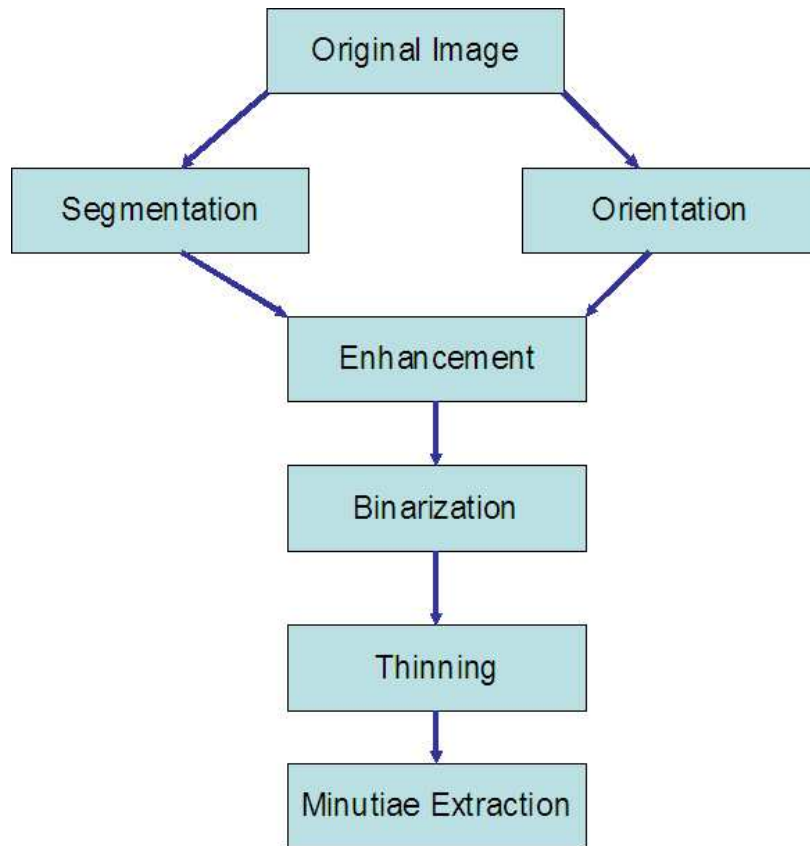


Figure 6.2.1: Typical pixel pattern for ridge ending

6.2.1).

The purpose of the binarization process is to transform the enhanced gray-level image into a binary image for subsequent feature detection. Good binarization algorithms should minimize information loss and provide efficient computational complexity. Due to the complexity of raw fingerprint images, global threshold methods fail to be effective [51]. A dynamic threshold has to be adopted, which requires that the threshold is adjusted to the local characteristics of the image, thus compensating for gray-scale intensity variations caused either by noises or by inconsistent contact

pressure during image acquisition.

The available fingerprint binarization methods are heavily dependent on the ridge flow pattern characteristics of fingerprint images. Stock and Swonger [80] designed a ridge valley filter mask (Figure 6.2.2), which is comprised of 8 slits along the eight discrete directions and was first convolved with the image. There must exist a maximum average local gray-level intensity along the local ridge line orientation, if the pixel is on a ridge line. Moayer and Fu [56] proposed an iterative algorithm using repeated convolution by a *Laplacian operator* and a pair of dynamic thresholds which are progressively moved towards an unique value. The pair of dynamic thresholds change with each iteration and control the convergence rate to the binary pattern. Xiao and Raafat [93] improved the method in [56] by incorporating a local threshold method which takes into account of the contrast difference in local regions. Both methods require repeated convolution operations and thus are time consuming. The final binarization result relies on the choice of two dynamic thresholds. Coetzee and Botha [21] first calculate the two binary images which are based on edge information and gray-scale image profile respectively. Edge-based binary image is obtained by filling in the area delimited by the edges. Gray-image based binary image is obtained by the local threshold. The final binary image is the logical *OR* of two binary images. The efficiency of this algorithm relies mainly on the efficiency of the edge detection algorithm. Ratha et al. [70] proposed a binarization approach based on the peak detection in the cross section gray-level profiles orthogonal to the local ridge orientation. The profiles are obtained by projecting pixel intensities onto the central section. This method can not keep full width of the ridges, and tends to lose some information because the resulting binary image can not truly reflect the original fingerprint image.

Domeniconi, Tari and Liang [22] observed that ridge pixels are local maxima along the direction of one of the principal curvature where the other principal curvature is

7		8		1		2		3
6		7	8	1	2	3		4
		6				4		
5		5		C		5		5
		4				6		
4		3	2	1	8	7		6
3		2		1		8		7

Figure 6.2.2: Binarization mask according to ridge valley pattern

zero. Ridges and valleys are sequences of local maxima and saddle points, which can be detected by calculating the gradient and the Hessian matrix H at each point. The Hessian H is a symmetric matrix whose elements are the second-order derivatives. Its mathematical form is $\begin{pmatrix} \frac{\partial^2 I}{\partial x^2} & \frac{\partial^2 I}{\partial x \partial y} \\ \frac{\partial^2 I}{\partial x \partial y} & \frac{\partial^2 I}{\partial y^2} \end{pmatrix}$. The maximum absolute eigenvalue of H is the direction along which gray-level intensities change significantly. A pixel is a ridge point iff $\lambda_1 \leq \lambda_2 < 0$; a pixel is a saddle point iff $\lambda_1 \lambda_2 < 0$.

Liang et al. [95] proposed using Euclidean distance transform method to obtain a near-linear time binarization of fingerprint images. Two types of distance transforms $DT_{1,0}$ and $DT_{0,1}$ are defined. $DT_{1,0}$ assigns a 1-pixel a value equal to the Euclidean distance to the nearest 0-pixel. $DT_{0,1}$ assigns a 0-pixel a value equal to the Euclidean distance to the nearest 1-pixel. The optimal threshold can be two values: t_1 and t_2 such that $t_2 - t_1 = 1$ and the sum total of $DT_{1,0} > DT_{0,1}$ at t_1 and $DT_{0,1} > DT_{1,0}$ at t_2 .

Zhang and Xiao [99] divided the image into regions with similar mean gray-scale

value for each block, and performed binarization with local threshold for each region separately. they proposed robust uniform region generation scheme with well-designed data structure which can be extended to image normalization.

Fingerprint thinning is usually implemented via morphological operation which reduces the width of ridges to a single pixel while preserving the extent and connectivity of the original shape. Templates of 3×3 and/or 3×4 , and 4×3 windows are usually utilized. Good fingerprint thinning algorithms should preserve the topology of the object, keep the original connectivity, and generate few artifacts. A hole in ridge will result in a skeleton with two spurious bifurcations, and a noise speckle will create two spurious ridge endings. Therefore, it is critical to utilize regularization techniques, which usually fill holes, remove small breaks, and eliminate ridge bridges [51]. Bazen and Gerez [5] encode each 3×3 pixel neighborhood in a 9-bit integer. This number is used as an index into a lookup table which contains the binary value after the current thinning step. Two different lookup tables which both take care of a different thinning direction are used iteratively, till the final skeleton is obtained.

An innovative rotation invariant thinning algorithm was proposed by Ahmed and Ward in [2]. The method is iterative, but well-designed 20 rules can be applied simultaneously to each pixel in the image, the system guarantees symmetrical thinning, rotation invariance and high speed. The algorithm uses a set of rules over 8-neighbors of the pixel to be considered for deletion, but it can not properly handle 2-pixel wide lines. Authors extended the window to 20 pixels in all, and required a set of rules to handle the 20 pixel set (around 2^{20} possible configurations). Rockett [72] improved the method of handling the case of the 2-pixel wide lines in [2] by using two steps. Algorithm in [2] trims the image down to a skeleton which includes 2-pixel wide lines. A graph-based method determines whether a pixel in a two-pixel wide line can be deleted without compromising the connectivity of the skeleton. This

rotation-invariant thinning algorithm was utilized in [64].

You et al. [98, 97] proposed a multiscale fingerprint thinning algorithm, which is based on calculating the modulus minima of the wavelet transform. A random scale of wavelet transform is first chosen to compute all wavelet minima. The obtained skeleton ribbons of the underlying ridge (with the topologies of the ridge kept) are thinner than the original shapes. A much smaller scale than the previous one is selected to perform second wavelet transform. This procedure is repeated till one-pixel wide ridge central line is eventually obtained. Experimental results showed that relatively low computational time (than previous thinning methods) was achieved. Run-length scanning with vertical and horizontal passes can improve the speed of the fingerprint thinning task (Section 6.4).

After a skeleton of the fingerprint image is computed, extracting the minutiae from the one-pixel wide ridge map is a trivial task. In the context of eight-connected neighbor connectivity, a ridge ending point has only one neighbor. A bifurcation point possesses more than two neighbors, and a normal ridge pixel has two neighbors. Minutiae detection in a fingerprint skeleton is implemented by scanning thinned fingerprint and counting the *crossing number*(cn) [51]. Therefore, the cn of the ridge ending point, intermediate ridge point, and bifurcation point should be 1, 2 and more than 3, respectively. The cn can be defined as follows:

$$cn(p) = \frac{1}{2} \sum_{i=1..8} |val(p_{i \bmod 8}) - val(p_{i-1})| \quad (6.2.1)$$

Where $p_0, p_1..p_7$ are neighbors of p , $val(p) \in (0, 1)$. Due to the limitations of the skeletonization-based Minutiae Extraction, false minutiae caused by undesired spikes and broken ridges need to be filtered by some heuristics [23, 70, 93].

6.2.2 Gray-Level Minutiae Extraction

Because the fingerprint image binarization might lead to information loss, and the aberrations and irregularity of the binary fingerprint image adversely affect the fingerprint thinning procedure, a relatively large number of spurious minutiae are introduced by the binarization-thinning operations. Minutiae detection directly from gray-level fingerprint images is a topic of research.

Based on the observation that a ridge line is composed of a set of pixels with local maxima along one direction, Maio and Maltoni [49] proposed extracting the minutiae directly from the gray-level image by following the ridge flow lines with the aid of the local orientation field. This method attempts to find a local maximum relative to the cross-section orthogonal to the ridge direction. From any starting point $Pt_s(x_c, y_c)$ with local direction θ_c in the fingerprint image, a new candidate point $Pt_n(x_n, y_n)$ is obtained by tracing the ridge flow along the θ_c with fixed step of μ pixels from $Pt_s(x_c, y_c)$. A new section Ω containing the point $Pt_n(x_n, y_n)$ is orthogonal to θ_c . The gray-level intensity maxima of Ω becomes $Pt_s(x_c, y_c)$ to initiate another tracing step. This procedure is iterated till all the minutiae are found. The optimal value for the tracing step μ and section length σ are chosen based on the average width of ridge lines. Jiang et al. [40] improved the method of Maio and Maltoni by choosing dynamically the tracing step μ according to the change of ridge contrast and bending level. A large step μ is used when the bending level of the local ridge is low and intensity variations along the ridge direction is small. Otherwise a small step μ value is used. Instead of tracing a single ridge, Liu et al. [41] proposed tracking a central ridge and the two surrounding valleys simultaneously. In each cross section Ω , a central maximum and two adjacent minima are located at each step, and the ridge following step μ is dynamically determined based on the distance between the

lateral minima from the central maximum. Minutiae are extracted where the relation ⟨minimum, maximum, minimum⟩ is changed.

Linear Symmetry (LS) filter in [30, 57] is used to extract the minutiae based on the concept that minutiae are local discontinuities of the LS vector field. Two types of symmetries - parabolic symmetry and linear symmetry are adopted to model and locate the points in the gray-scale image where there is lack of symmetry (Figure 6.2.3). If D_x and D_y represent the derivatives in x and y directions respectively, the orientation tensor can be expressed as:

$$z = (D_x + iD_y)^2 \quad (6.2.2)$$

The tensor Z can be implemented by convolving the gray-scale image with separable Gaussians and their derivatives. A symmetry filter can be modeled by $exp(im\phi)$, where m is its order. The following polynomial incorporated with a Gaussian window function is utilized to approximate the symmetry filter:

$$h_m = (x + iy)^m exp(-\frac{x^2 + y^2}{2\sigma^2}) \quad (6.2.3)$$

In the fingerprint image, parabolic symmetry of order $m = 1$ is most similar to a minutia point pattern. The following complex filtering can be applied to minutiae detection:

$$PS = \langle z, h_1 \rangle = \langle (D_x + iD_y)^2, (x + iy).g(x, y) \rangle \quad (6.2.4)$$

Where ⟨,⟩ and g(x,y) represent 2D scalar product and Gaussian window, respectively. Linear symmetry occurs at the points of coherent ridge flow. To detect linear symmetry reliably, second order complex moments $I_{20} = \langle z, h_0 \rangle$ and $I_{11} = \langle |z|, h_0 \rangle$ are computed. The measure of LS is calculated as follows:

$$LS = \frac{I_{20}}{I_{11}} = \frac{\langle z, h_0 \rangle}{\langle |z|, h_0 \rangle} \quad (6.2.5)$$



Figure 6.2.3: Symmetry filter response in the minutia point. Left-ridge bifurcation, Right-ridge ending. Adopted from [30].

where I_{11} represents an upper bound for the linear symmetry certainty. Finally, reliable minutiae detection can be implemented via the following inhibition scheme:

$$PSi = PS(1 - |LS|) \quad (6.2.6)$$

A window size of 9×9 is used to calculate the symmetry filter response. Candidate minutiae points are selected if their responses are above a threshold.

6.2.3 Binary-image based Minutiae Extraction

6.2.3.1 Pixel Pattern Profile

NIST [88] designed and implemented binary image based minutiae detection method by inspecting the localized pixel patterns. In Figure 6.2.4 the right-most pattern represents the family of ridge ending patterns which are scanned vertically. Ridge ending candidates are determined by scanning the consecutive pairs of pixels in the fingerprint searching for pattern-matched sequences. Figure 6.2.5(a) and (b) represent possible ridge ending patterns in the binary fingerprint images. Potential bifurcation patterns are shown in Figure 6.2.5(c-j). Because the mechanism of this minutiae detection

method is totally different from that of skeletonization-based Minutiae Extraction method, specific minutiae filtering methods are also designed.

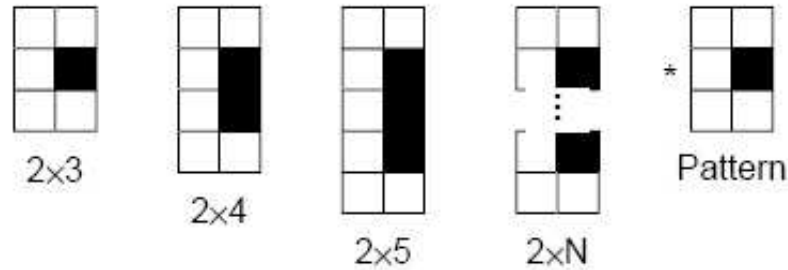


Figure 6.2.4: Typical pixel pattern for ridge ending

Minutiae extraction in [25] is based on fingerprint local analysis of squared path centered on the processed pixel. The extracted intensity patterns in a true minutia point along the squared path possess a fixed number of transitions between the mean dark and white level (Figure 6.2.6). A minutia candidate needs to meet the following criteria:

- Pre-screen Average pixel value for the preliminary ending point is ≤ 0.25 , and the average pixel value for the preliminary bifurcation point ≥ 0.75 in the 3×3 mask surrounding the pixel of interest.
- Filtering a square path P with size of $W \times W$ (W is twice the mean ridge size in the point) is created to count the number of transitions. Isolated pixels are shown in Figure 6.2.7 and are excluded from consideration. Minutiae points usually have two logical transitions.
- Verification for ending minutia: the pixel average in path P is greater than the threshold K , then the pixel average in path P is lesser than the threshold $1 - K$ for bifurcation points.

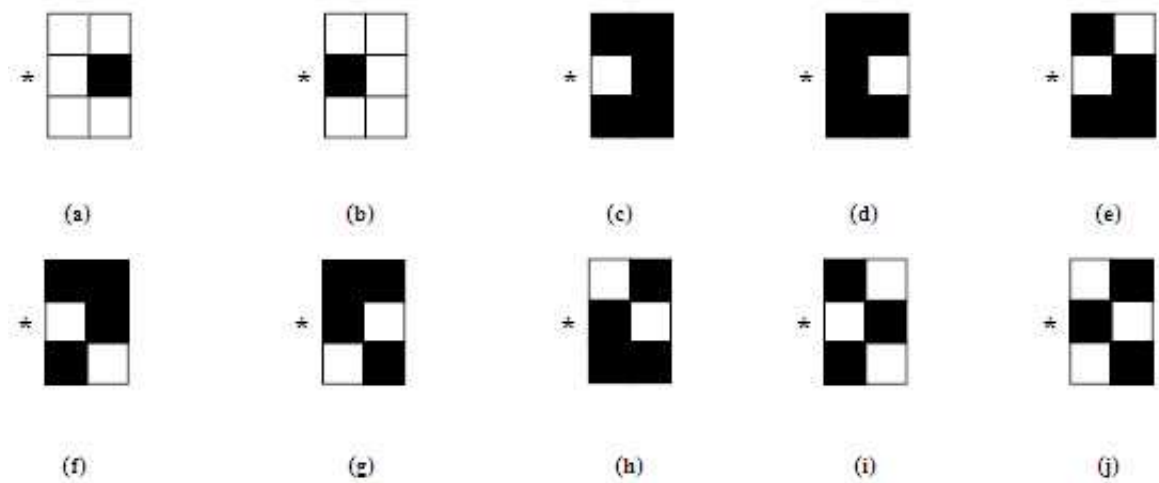


Figure 6.2.5: Typical pixel pattern profiles for ridge ending minutiae and bifurcation minutiae. (a) and (b) are ridge ending pixel profiles; the rest represent different ridge bifurcation profiles.

The orientation computation for ending point is illustrated in Figure 6.2.8. Some false minutiae can be eliminated by creating a square path $P2$ which is twice larger than the path P . If $P2$ doesn't intersect another ridge at an angle of $\alpha + \pi$ (α is the minutia direction), then it is verified as genuine minutia; otherwise is rejected as spurious (Figure 6.2.9).

In [12], minutiae are extracted from the learned templates. An ideal endpoint template T is shown in Figure 6.2.10. Template learning is optimized using the Lagrange's Method.

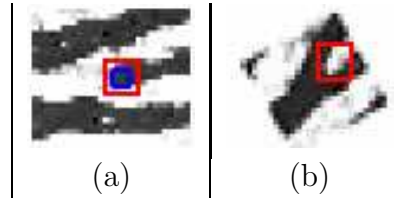


Figure 6.2.6: Typical pixel patterns for minutiae. (a) Ending point profile, (b) Bifurcation point profile. Adopted from [25]

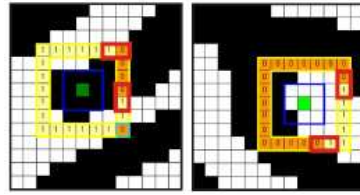


Figure 6.2.7: Compute the number of logic communications. Adopted from [25]

6.2.4 Machine Learning

Conventional machine learning methods have been used by several research groups to extract minutiae from the fingerprint image [6, 47, 66, 75, 76]. Leung et al. [47] first convolve the gray-level fingerprint image with a bank of complex Gabor filters. The resulting phase and magnitude of signal components are subsampled and input to a 3-layer back-propagation neural network composed of six sub-networks. Each sub-network is used to detect minutiae at a particular orientation. The goal is to identify the presence of minutiae. Reinforcement learning is adopted in [6] to learn how to follow the ridges in the fingerprint and how to recognize minutiae points. Genetic programming (GP) is utilized in [66] to extract minutiae. However, they concluded that the traditional binarization-thinning approach achieves more satisfactory results than Genetic Programming and Reinforcement. Sagar et al. [75, 76] have integrated

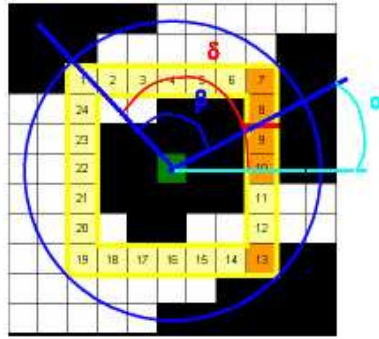


Figure 6.2.8: Estimating the orientation for the ending minutia. Adopted from [25]

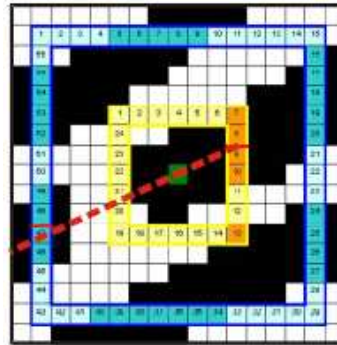


Figure 6.2.9: Removal of spurious ending minutia. Adopted from [25]

a Fuzzy logic approach with Neural Network to extract minutiae from the gray-level fingerprint images.

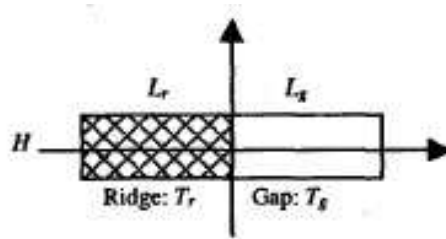


Figure 6.2.10: Typical template T for an ending minutia point. Adopted from [12]

6.3 Proposed Chain-code Contour Tracing Algorithm

Commonly used minutiae extraction algorithms that are based on thinning are iterative. They are computationally expensive and produce artifacts such as spurs and bridges. We propose a chain coded contour tracing method to avoid these problems. Chain codes yield a wide range of information about the contour such as curvature, direction, length, etc. As the contour of the ridges is traced consistently in a counter-clockwise direction, the minutiae points are encountered as locations where the contour has a *significant* turn. Specifically, the *ridge ending* occurs as a significant *left turn* and the *bifurcation*, as a significant *right turn* in the contour. Analytically, the turning direction may be determined by considering the sign of the cross product of the incoming and outgoing vectors at each point. The product is right handed if the sign of the following equation is positive and left handed if the sign is negative (Figure 6.3.1(b)&(c)). If we assume that the two normalized vectors are $P_{in} = (x_1, y_1)$ and $P_{out} = (x_2, y_2)$, then the turn corner is the ending candidate if $sign(\vec{P}_{in} \times \vec{P}_{out}) > 0$; the turn corner is the bifurcation candidate if $sign(\vec{P}_{in} \times \vec{P}_{out}) < 0$ (see Figure 6.3.2).

The angle θ between the normalized vectors P_{in} and P_{out} is critical in locating the

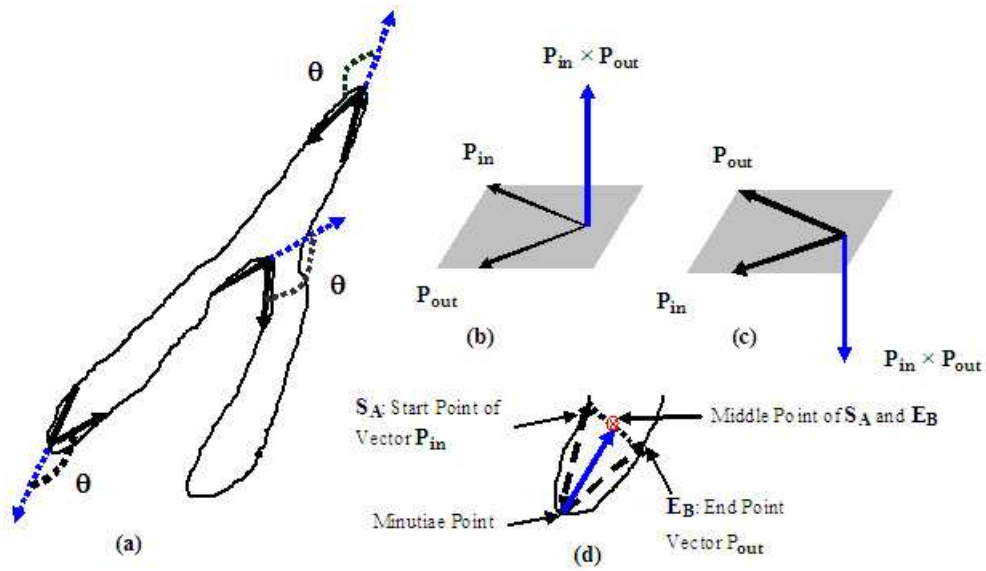


Figure 6.3.1: Minutiae Detection (a) Detection of turning points, (b) & (c) Vector cross product for determining the turning type during counter-clockwise contour following tracing, (d) Determining minutiae direction

turning point group (Figure 6.3.1 (a)). The turn is termed *significant* only if the angle between the two vectors is \leq a threshold T . No matter what type of turning points are detected, if the angle between the leading in and out vectors for the interested point is greater than 90° , then, the threshold T is chosen to have a small value. It can be calculated by using dot product of the two vectors.

$$\theta = \arccos \frac{\vec{P}_{in} \cdot \vec{P}_{out}}{\left| \vec{P}_{in} \right| \left| \vec{P}_{out} \right|} \quad (6.3.1)$$

In practice, a group of points along the turn corner satisfies this condition. We define the minutia point as the center of this group (Figure 6.3.1 (d)).

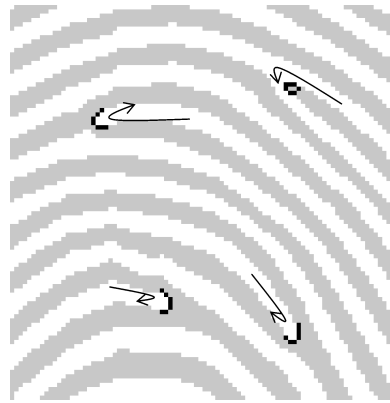


Figure 6.3.2: Minutiae are located in the contours by looking for *significant* turns. A ridge ending is detected when there is a sharp left turn; whereas the ridge bifurcation is detected by a sharp right turn.

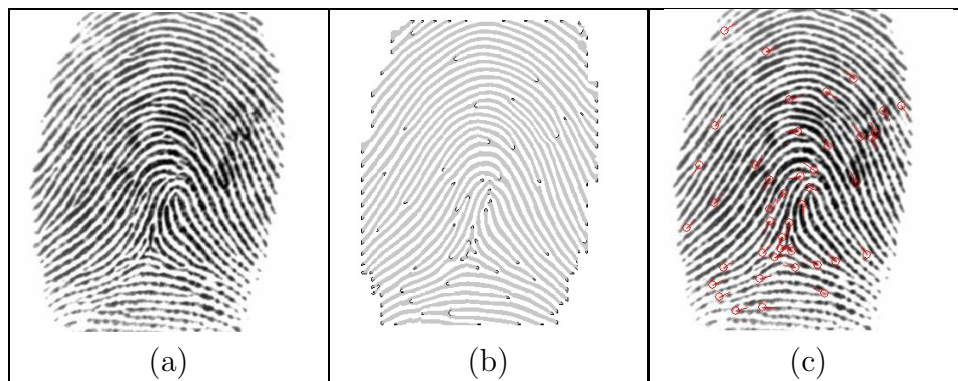


Figure 6.3.3: (a) Original image; (b) detected turn groups superimposed on the contour image; (c) detected minutiae superimposed on the original image.

6.4 Proposed Run-length Scanning Algorithm

A good fingerprint image thinning algorithm should possess the following characteristics: fast computation, convergence to skeleton of unit width, work well on varying ridge width, generate less spikes, preserve connectivity of skeleton, prevent excessive erosion. The run-length-coding based method can speed up the thinning process because it does not need to go through multiple passes to get a thinned image of unit width. It retains continuity because it calculates the medial point for each run, and adjusts locally and adaptively the connectivities of consecutive runs in the same ridge with the same labels. It reduces distortion in the junction area (singular points and bifurcation points) by a new merging algorithm.

From the frequency map, the median frequency is used to calculate the threshold of the run length. If the length of the horizontal run is greater than a threshold, it is not used to calculate the medial point. Instead, the vertical run should be used to calculate the medial point. Similarly, if the length of the vertical run is greater than the threshold, this run should not be used to calculate the medial point. Instead the horizontal run should be used.

6.4.1 Definitions

Two 2-dimensional arrays, f and t , are used to represent the original fingerprint image and its skeleton, respectively. The pixel with the value of one and the pixel with the value of zero represent objects and the background, respectively. Some definitions are needed to describe the thinning method and feature detection algorithm. The mask in Figure 6.4.1(a) is used for region labeling in the horizontal scan, and the mask in Figure 6.4.1(b) is used for region labeling in the vertical scan. A simple modification

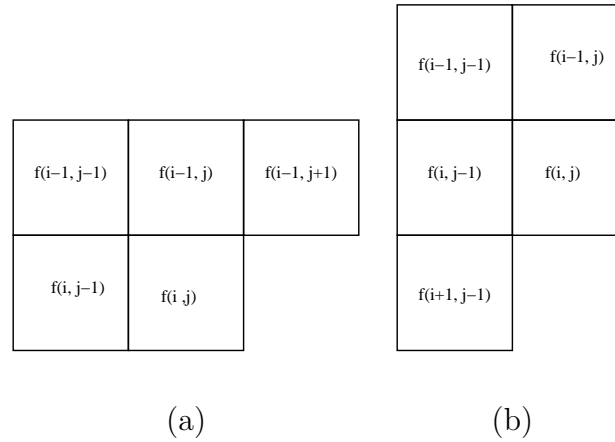


Figure 6.4.1: Masks for region identification (a)Horizontal scan and (b)Vertical scan needs to be made for column-runs.

Definition 6.4.1 *Scanline* – a one-pixel-wide horizontal (or vertical) line that crosses the fingerprint image from left to right (or from up to down), is used to find the horizontal runs (or vertical runs).

Definition 6.4.2 *Horizontal runs* – this deals with vertical or slanted ridges with an angle greater than 45° and less than 135° . Find the pair of points (Point L and R) in each horizontal run, i.e., $L(i, j) = 0$, $L(i, j - 1) = 1$, and $L(i, j + 1) = 0$; $R(i, j) = 0$, $R(i, j - 1) = 0$, and $R(i, j + 1) = 1$. If the length of run is less than or equal to a threshold, calculate the medial point of this run.

In order to reduce the computational complexity, a simple threshold, instead of the calculation of the run histogram, is used to find the runs for skeletonization.

Definition 6.4.3 *Vertical runs* – this deals with horizontal or slanted ridges with an angle less than 45° or greater than 135° . Find the pair of points (Point U and D) in

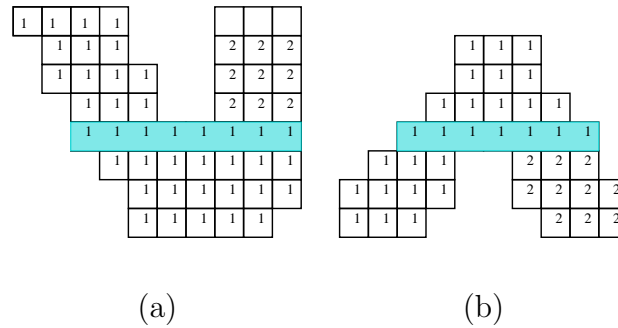


Figure 6.4.2: Illustration of junction runs. (a)Convergence run and (b)Divergence run

each vertical run, i.e., $U(i, j) = 0$, $U(i - 1, j) = 1$, and $U(i + 1, j) = 0$; $D(i, j) = 0$, $R(i - 1, j) = 0$, and $R(i + 1, j) = 1$. If the length of run is less than or equal to a threshold, calculate the medial point of this run.

Definition 6.4.4 *Convergence run* – one relatively longer horizontal (vertical) run that overlaps with two consecutive horizontal (vertical) runs in the previous scanline. Refer to the filled run in Figure 6.4.2(a).

Definition 6.4.5 *Divergence run* – one relatively long horizontal (vertical) run overlaps with two consecutive horizontal (vertical) runs in the next scanline. Refer to the filled run in Figure 6.4.2(b).

Definition 6.4.6 *Ending run* – first run or last run for one fingerprint ridge. The middle point of each ending run is the ending minutia candidate point.

Label collision appears to be very common occurrences in the bifurcation point regions and singular point regions. The mask shape for horizontal scans is used to define the label collision pixel (with question mark). $L(i, j)$ is used to express the label of pixel(i, j).

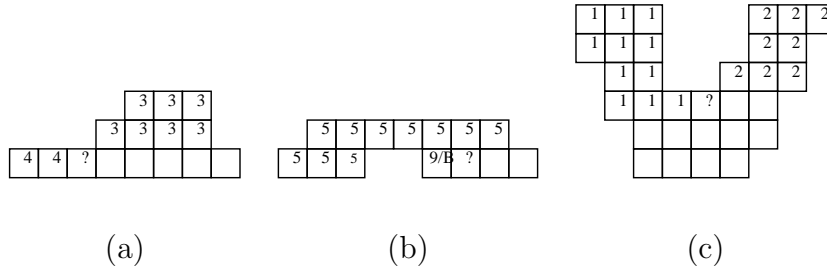


Figure 6.4.3: Illustration of label collision types. (a)Label collision type A, (b) Label collision type B, and (c)Label collision type C

Definition 6.4.7 *Label collision type A – it usually appears in the protrusive parts of the ridge. It meets the following two constraints: (1) $L(i, j - 1) > L(i - 1, j + 1)$; (2) $L(i - 1, j - 1) \neq L(i, j - 1)$ (Figure 6.4.3(a)).*

Definition 6.4.8 *Label collision type B – it usually appears in the middle pixels of the second run which overlaps with divergence run. It meets the following two constraints: (1) $L(i, j - 1) > L(i - 1, j + 1)$; (2) $L(i - 1, j - 1) = 0$ (Figure 6.4.3(b)).*

Definition 6.4.9 *Label collision type C – it usually appears in the convergence run, i.e., cross section in the ridge line of “Y” shape. It meets the following two conditions: (1) $L(i, j - 1) < L(i - 1, j + 1)$; (2) $L(i - 1, j) = 0$ (Figure 6.4.3(c)).*

6.4.2 One-pass embedding labeling run-length-wise thinning and minutiae detection algorithm

We need only one pass to get runs for fingerprint images, and simultaneously label according to the order of the masks described in Figure 2. The runs, which contain bifurcation point, will be detected when label collisions occur. For the case of horizontal scan, we start scanning from left to right, and up to down. For vertical scan,

we start scanning from up to down, left to right. If one relatively longer run overlaps with below two consecutive runs, one run has the same label with the longer run, and the other has a different label, the phenomenon of label collision type type A will occur, so the longer run will be a divergence run. If one relatively long run overlaps with above two consecutive runs, one run has the same label with the longer run, and the other has different label. The phenomenon of label collision type type C will occur, so the longer run will be the convergence run. The data structure for the run is: start point, end point, medial point coordinates, label and parent run. For each label, the standard depth-first graph traversal algorithm is used to track consecutive runs and make a minor local adjustment to maintain local connectivity. We have modified the line adjacency graph data structure [65], because there are more ridges (strokes in character recognition) in the fingerprint image. The stack data structure for each label is: label, top run, number counter, runs (record of each run order number). For the divergence runs and convergence runs, the data structure is coordinates, junction type, label, run and index. The details for the algorithm are as follows (This is for horizontal scans. Similar method exists for vertical scans):

1. Initialize $L(nr, nc)$, nr and nc —row and column number of the fingerprint image respectively. set the run length threshold value.
2. for each scanline
3. for each pixel
4. if the start point for one run is found
5. check $L(i-1, j-1)$, $L(i-1, j+1)$ and $L(i, j-1)$
6. case 1: if $L(i-1, j-1) \neq 0$, and the label of previous run equals to $L(i-1, j-1)$, and the row coordinate equal to current scanline, record it in the bifurcation point array

7. increase bifurcation run counter
8. record index, run number, medial point coordinates
9. increase label value by 1, record junction type
to divergence
10. case 2: if either of $L(i-1, j)$ and $L(i-1, j+1)$
is not equal to zero,
11. set $L(i, j) = L(i-1, j)$ or $L(i-1, j+1)$
12. set the label of current run to $L(i, j)$
13. case 3: Otherwise, set the new label for current run, and
increase the label value by 1
14. check the ending point for the run, two cases
15. if current pixel is the last element for this scanline
16. record the ending point, run length, medial point coordinates
17. if there is label collision type C in current run,
record it in the bifurcation point array
18. increase bifurcation run counter
19. record index, type, run number, medial point coordinates
20. increase label value by 1
21. if current pixel is the last element for current run
22. record the ending point, run length, medial point coordinate
23. check whether label collision type B occurs
24. decrease label number by 1 to compensate wrong label
started from the starting point of current run
25. set $L(i, j) = L(i-1, j+1)$
26. check whether label collision type A occur and
27. if $L(i-1, j-1) = 0$ and the y coordinate of the
top element for $L(i, j-1)$ equals to that of

- the top element for $L(i-1,j+1)$
- 28. record bifurcation point as step 7–9
- 29. check whether label collision type C occurs
- 30. if yes, record bifurcation point as step 7–9
- 31. if current pixel is the middle element of one run.
- 32. repeat step 22-28

6.5 Minutiae Verification and Filtering

Although there are a lot of minutiae detection algorithms available in the literature, minutiae detection accuracy can not reach 100%. Before minutiae filtering and verification, minutiae detection accuracy could be relatively low because there are always some missing minutiae and/or spurious minutiae in the extracted minutiae set. There are some common spurious minutiae filtering techniques such as removal of islands (ridge ending fragments and spurious ink marks) and lakes (interior voids in ridges), and boundary minutiae filtering. Each detection algorithm needs ad hoc spurious filtering methods.

6.5.1 Structural Methods

Xiao and Faafat [93] combined statistical and structural approaches to post-process detected minutiae (Figure 6.5.1). The minutiae were associated with the length of corresponding ridges, the angle, and the number of *facing* minutiae in a neighborhood. This rule-based algorithm connected ending minutiae (Figure 6.5.1 (a) and (b)) that

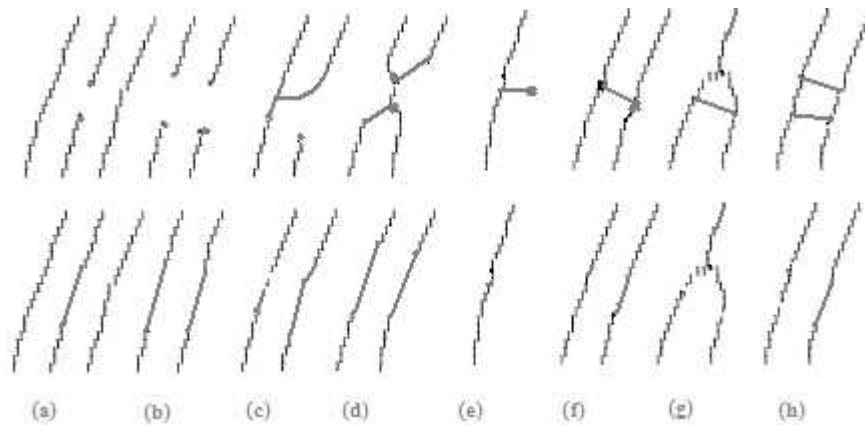


Figure 6.5.1: Removal of the most common false minutiae structures. Adopted from [93].

face each other, and removed bifurcation minutiae facing the ending minutiae (Figure 6.5.1(c)) or with other bifurcation minutiae (Figure 6.5.1(d)). It removes spurs, bridges, triangles and ladder structures (see Figure 6.5.1(e), (f), (g), and (h), respectively). Chen and Guo [19] proposed a three-step false minutiae filtering method, which dropped minutiae with short ridges, minutiae in noise regions, and minutiae in ridge breaks using ridge direction information. Ratha, Chen and Jain [70] proposed an adaptive morphological filter to remove spikes, and utilized foreground boundary information to eliminate boundary minutiae. Zhao and Tang [100] proposed a method for removing all the bug pixels generated at the thinning stage, which facilitated subsequent minutiae filtering. In addition to elimination of close minutiae in noisy regions, bridges, spurs, adjacent bifurcations, Farina et al. [23] designed a novel topological validation algorithm for ending and bifurcation minutiae. This method can not only remove spurious ending and bifurcation minutiae, but also eliminate spurious minutiae in the fingerprint borders.

6.5.2 Learning Methods

Based on gray-scale profile of detected minutiae, several methods utilize machine learning techniques to validate and verify reliability of minutiae. Bhanu, Boshra and Tan [11] verify each minutia through correlation with logical templates along the local ridge direction. Maio and Maltoni [50] propose a shared-weights neural network verifier for their gray-scale minutiae detection algorithm [49]. The original gray-level image is first normalized with respect to their angle and the local ridge frequency, and the dimensionality of the normalized neighborhoods is reduced through Karhunen-Loeve transform [33]. Based on the ending/bifurcation duality characteristics, both the original neighborhood and its negative version are used to train and classify. Their experimental results demonstrate that the filtering method offers significant reduction in spurious minutiae and flipped minutiae, even though there is some increase in the number of missed minutiae.

Chikkerur et al. [20] propose a minutiae verifier based on Gabor texture information surrounding the minutiae. Prabhakar et al. [67] verify minutiae based on the gray-scale neighborhoods extracted from normalized and enhanced original image. A Learning Vector Quantizer [45] is used to classify the resulting gray-level patterns so that genuine minutiae and spurious minutiae are discriminated in a supervised manner.

6.5.3 Minutiae verification and filtering rules for chain-coded contour tracing method

The feature extraction process is inexact and results in the two forms of errors outlined below.

1. Missing minutiae: The feature extraction algorithm fails to detect existing minutia when the minutiae is obscured by surrounding noise or poor ridge structures.
2. Spurious minutia: The feature extraction algorithm falsely identifies a noisy ridge structure such as a crease, ridge break or gaps as minutiae.

The causes for the spurious minutiae are very particular to the feature extraction process. In our approach, spurious minutiae are generated mostly by irregular or discontinuous contours. Therefore, minutiae extraction is usually followed by a post-processing step that tries to eliminate the false positives. It has been shown that this refinement can result in considerable improvement in the accuracy of a minutia based matching algorithm.

We use a set of simple heuristic rules to eliminate false minutiae (See Figure 6.5.2)

1. We merge the minutiae that are within a certain distance of each other and have similar angles. This is to merge the false positives that arise out of discontinuities along the significant turn of the contour.
2. If the direction of the minutiae is not consistent with the local ridge orientation, then it is discarded. This removes minutiae that arise out of noise in the contour.
3. We remove the pair of opposing minutiae that are within a certain distance of each other. This rule removes the minutiae that occur at either ends of a ridge break.
4. If the local structure of a ridge or valley ending is not Y-shaped and too wide, then it is removed because it lies on a malformed ridge and valley structure.

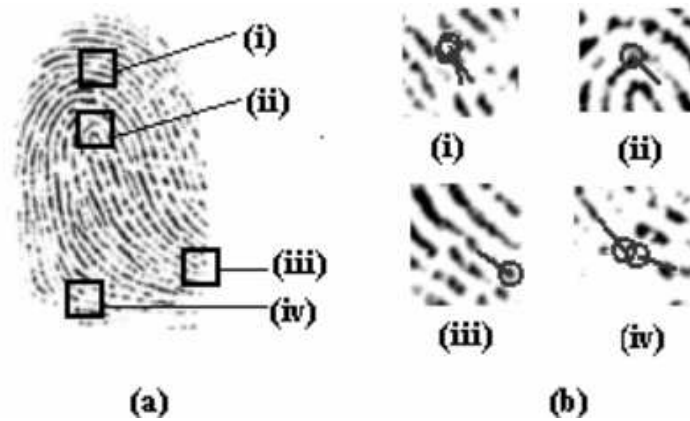


Figure 6.5.2: Post processing rules, (a) Fingerprint image with locations of spurious minutiae marked (b) Types of spurious minutiae removed by applying heuristic rules (i-iv)

The spurious minutiae in the foreground boundary of a fingerprint image can be removed by gray-level profile and local ridge direction. But this method is not robust and affected easily by noise. This type of spurious minutiae can be removed by our developed segmentation algorithm (Refer to Chapter 4).

6.6 Experiments

Our methodology is tested on FVC2002 DB1 and DB4. In each database consists of 800 fingerprint images (100 distinct fingers, 8 impressions each). The image size is 374×388 and the resolution is 500dpi. To evaluate the methodology of adapting a Gaussian kernel to the local ridge curvature of a fingerprint image. We have modified the Gabor-based fingerprint enhancement algorithm [32, 90] with two kernel sizes: the smaller one in high-curvature regions and the larger one in pseudo-parallel ridge regions. Minutiae are detected using chaincode-based contour tracing [91]. The fingerprint matcher developed by Jea et al. [39] is used for performance evaluation.

Our methodology has been tested on low quality images from FVC2002. To validate the efficiency of the proposed segmentation method, the widely-used Gabor filter-based segmentation algorithm [4, 78] and NIST segmentation [14] are utilized for comparison.

Our segmentation method has an advantage over other methods in terms of boundary spurious minutiae filtering. Figure 6.6.1 (a) and (b) show unsuccessful boundary minutiae filtering using the NIST method [14]. It removes spurious minutiae pointing to invalid blocks and removes spurious minutiae near invalid blocks. Invalid blocks are defined as blocks with no detectable ridge flow. However, boundary blocks are more complicated. So the method in [14] fails to remove most of the boundary minutiae. Figures 6.6.1 (c) and (d) show the filtering results of our method. In Comparing Figure 6.6.1(a) against (c) and (b) and (d), 30 and 17 boundary minutiae are filtered, respectively. Performance evaluations for FVC2002 DB1 and DB4 are shown in Figure 6.6.2. For DB1, ERR for false boundary minutiae filtering using our proposed segmented mask is 0.0106 and EER while for NIST boundary filtering is 0.0125. For DB4, ERR for false boundary minutiae filtering using our proposed segmented mask is 0.0453 and EER while for NIST boundary filtering is 0.0720.

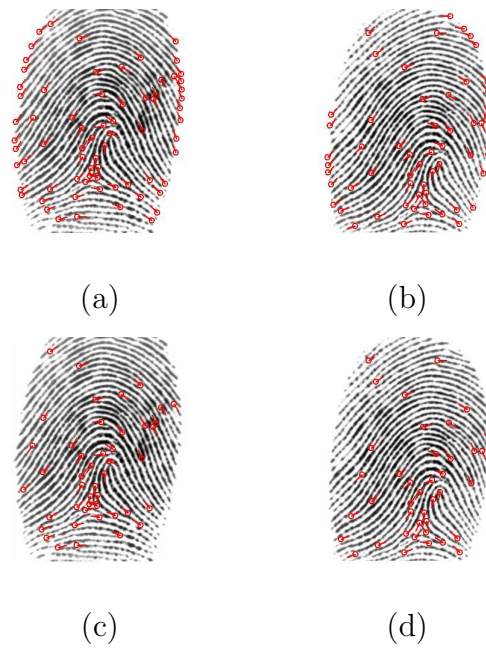


Figure 6.6.1: Boundary spurious minutiae filtering. (a) and (b) incomplete filtering using NIST method, (c) and (d) proposed boundary filtering.

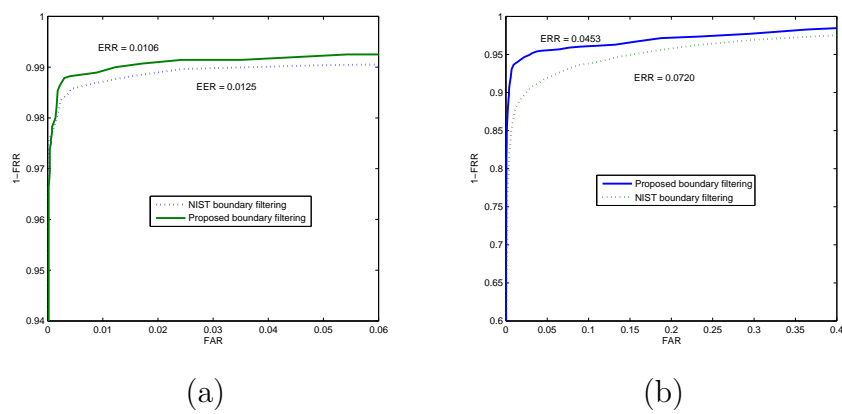


Figure 6.6.2: ROC curves for (a) FVC2002 DB1 and (b) FVC2002 DB4.

Chapter 7

Conclusions

The contributions of this thesis are:

- Novel fingerprint image quality classification metrics are proposed for automatically selecting fingerprint preprocessing and enhancement parameters.
- Innovative corner point feature based segmentation method with efficient boundary spurious minutiae filtering capability. Noisy corner points are eliminated as outliers using Otsu's thresholding of Gabor features.
- Adaptive image enhancement filter design depends on the topology of the ridge pattern. Simple gradient based coherence map is used to locate high curvature regions around core and/or delta point(s). Statistical texture features are used to separate noisy regions from singular regions.
- Two thinning-free feature detection algorithms have been developed to produce high accuracy feature sets. The minutiae verification and filtering rules for chain-coded contour tracing algorithm are have been implemented.

Image quality is related directly to the final performance of automatic fingerprint authentication systems. Good quality fingerprint images need only minor preprocessing and enhancement for accurate feature detection algorithm. But low quality fingerprint images need preprocessing to increase contrast, and reduce different types of noises. An adaptive segmentation algorithm and enhancement filter must be designed. Hybrid image quality measures are proposed in this thesis to classify fingerprint images and perform corresponding automatic selection of preprocessing parameters. Band-limited ring-wedge spectrum energy of the Fourier transform is used to characterize the global ridge flow pattern. Local statistical texture features are used to characterize block-level features. Combination of image quality measure in the frequency domain and in the spatial domain can provide quantitative quality estimation. Our method considers the size of fingerprint ridge flows, partial fingerprint image information such as appearance of singularity points, the distance between singularity points and the closest foreground boundary.

When some background is included in the segmented regions of interest, noisy pixels also generate a lot of spurious minutiae because these noisy pixels are also enhanced during preprocessing and enhancement steps. It is difficult to determine the threshold value in blockwise segmentation methods, because one does not know what percentage of pixels in the boundary blocks belong to foreground. Therefore, it is impossible for blockwise segmentation to filter boundary spurious minutiae. We take advantage of the strength property of the Harris corner point, and perform statistical analysis of Harris corner points in the foreground and the background. It is found that the strength of the Harris corner points in the ridge regions is usually much higher than that in the non-ridge regions. Although some Harris points possess high strength and can not be removed by thresholding, they lie on noisy regions with low Gabor response, and so can be eliminated as outliers. The foreground boundary contour is

located among remaining Harris points by the convex hull method.

Fingerprint ridge flow patterns can be categorized into two types: pseudo-parallel ridges and high-curvature ridges surrounding singular points. Enhancement filters should follow the ridge topological patterns, and filter window size in the regions of different ridge patterns should be dynamically adjusted to local ridge flow. In order to repair broken ridges, clean noise in the valley, and retain local ridge flow shapes, accurate ridge orientation estimation is critical. In order to deal with the problem of ambiguous ridge orientations at singular points like minutiae or cores and deltas, some models have been proposed which allow the co-existence of multiple ridge orientations at a single point. However, it is then difficult to perform enhancement if there is no local dominant ridge direction. We introduce the coherence map to locate high-curvature regions. Local ridge direction is filtered with Gaussian kernel size adapted to the local ridge topology. Furthermore, local statistical texture features are used to distinguish singular regions with noisy smudge regions, even though the coherence values in the two regions are similar.

Gray-level minutiae extraction algorithm works well only for good quality fingerprint images. Thinning based minutiae detection algorithms are time-consuming, and the position of detected minutiae shifts by the ridge width. Irregularity and aberration of ridge flows produce spurious minutiae. Two thinning-free minutiae extraction methods are proposed, and the minutiae filtering algorithms for chain-coded contour tracing method have been developed.

Bibliography

- [1] M. Ahmed and R. Ward. A rotation invariant rule-based thinning algorithm for character recognition. *Pattern Analysis and Machine Intelligence, IEEE Transactions on*, 24(12):1672–1678, 2002.
- [2] A. Almansa and T. Lindeberg. Fingerprint enhancement by shape adaptation of scale-space operators with automatic scale selection. *IEEE Transactions on Image Processing*, 9(12):2027–2042, 2000.
- [3] F. Alonso-Fernandez, J. Fierrez-Aguilar, and J. Ortega-Garcia. An enhanced gabor filter-based segmentation algorithm for fingerprint recognition systems. In *Proceedings of the 4th International Symposium on Image and Signal Processing and Analysis (ISPA 2005)*, pages 239–244, 2005.
- [4] A.M.Bazen and S.H.Gerez. “Achievement and challenges in fingerprint recognition”. In *Biometric Solutions for Authentication in an e-World*, pages pp.23–57, 2002.
- [5] S. A.M.Bazen, M. Van Otterlo and M. Poel. “Areinforcement learning agent for minutiae extraction from fingerprints”. In *Proc. BNAIC*, pages pp.329–336, 2001.

- [6] American national standard for information systems, data format for the interchange of fingerprint information, 1993. Doc# ANSI/NIST-CSL 1-1993.
- [7] A. Bazen and S. Gerez. Segmentation of fingerprint images. In *Proc. Workshop on Circuits Systems and Signal Processing (ProRISC 2001)*, pages pp. 276–280, 2001.
- [8] A. M. Bazen and S. H. Gerez. Systematic methods for the computation of the directional fields and singular points of fingerprints. *Pattern Analysis and Machine Intelligence, IEEE Transactions on*, 24(7):905–919, 2002. 0162-8828.
- [9] A. M. Bazen and S. H. Gerez. “Fingerprint matching by thin-plate spline modeling of elastic deformations”. *Pattern Recognition*, 36(8):1859–1867, 2003.
- [10] B. Bhanu, M. Boshra, and T. Xuejun. Logical templates for feature extraction in fingerprint images. In *International Conference on Pattern Recognition*, volume 2, pages 846–850 vol.2, 2000.
- [11] B. Bhanu and T. Xuejun. Learned templates for feature extraction in fingerprint images. In *Computer Vision and Pattern Recognition (CVPR)*, volume 2, pages II–591–II–596 vol.2, 2001.
- [12] B. Bir and T. Xuejun. “Fingerprint indexing based on novel features of minutiae triplets”. *Pattern Analysis and Machine Intelligence, IEEE Transactions on*, 25(5):616–622, 2003.
- [13] G. T. Candela, P. J. Grother, C. I. Watson, R. A. Wilkinson, and C. L. Wilson. “PCASYS - a pattern-level classification automation system for fingerprints”. Technical Report NISTIR 5647, American National Standards Institute, 1995.

- [14] R. Cappelli, A. Lumini, D. Maio, and D. Maltoni. Fingerprint classification by directional image partitioning. *Pattern Analysis and Machine Intelligence, IEEE Transactions on*, 21(5):402–421, 1999. 0162-8828.
- [15] R. Cappelli, D. Maio, J. L. Wayman, and A. K. Jain. “Performance evaluation of fingerprint verification systems”. *IEEE Transactions on Pattern Analysis and Machine Intelligence*, 28(1):3–18, 2006.
- [16] X. Chen, J. Tian, J. Cheng, and X. Yang. Segmentation of fingerprint images using linear classifier. *EURASIP Journal on Applied Signal Processing*, 2004(4):480–494, 2004. doi:10.1155/S1110865704309194.
- [17] Y. Chen, S. Dass, and A. Jain. “Fingerprint quality indices for predicting authentication performance”. *AVBPA*, pages 160–170, 2005.
- [18] Z. Chen and C. H. Kuo. A topology-based matching algorithm for fingerprint authentication. In *IEEE International Carnahan Conference on Security Technology*, pages 84–87, 1991.
- [19] S. Chikkerur, V. Govindaraju, S. Pankanti, R. Bolle, and N. Ratha. Novel approaches for minutiae verification in fingerprint images. In *Seventh IEEE Workshops on Application of Computer Vision (WACV/MOTION’05)*, volume 1, pages 111–116, 2005.
- [20] L. Coetzee and E. C. Botha. Fingerprint recognition in low quality images. *Pattern Recognition*, 26(10):1441–1460, 1993.
- [21] C. Domeniconi, S. Tari, and P. Liang. Direct gray scale ridge reconstruction in fingerprint images. In *Proceedings of the 1998 IEEE International Conference on Acoustics, Speech, and Signal Processing(ICASSP)*, volume 5, pages 2941–2944 vol.5, 1998.

- [22] A. Farina, Z. M. Kovacs-Vajna, and A. Leone. Fingerprint minutiae extraction from skeletonized binary images. *Pattern Recognition*, 32(5):877–889, 1999.
- [23] “Fingerprint verification competition(FVC)”, available at <http://bias.csr.unibo.it>.
- [24] M. Gamassi, V. Piuri, and F. Scotti. Fingerprint local analysis for high-performance minutiae extraction. In *IEEE International Conference on Image Processing(ICIP)*, volume 3, pages III–265–8, 2005.
- [25] R. S. Germain, A. Califano, and S. Colville. “Fingerprint matching using transformation parameter clustering”. *Computational Science and Engineering, IEEE Computing in Science & Engineering*, 4(4):42–49, 1997.
- [26] R. C. Gonzalez and R. E. Woods. “*Digital Image Processing*”. Prentice Hall, Upper Saddle River, NJ, 2002.
- [27] S. Greenberg, M. Aladjem, and D. Kogan. Fingerprint image enhancement using filtering techniques. *Real-Time Imaging*, 8:227–236, 2002.
- [28] C. Harris and M. Stephens. A combined corner and edge detector. In *Proc. in Alvey Vision Conference*, pages pp. 147–151, 1988.
- [29] K. K. Hartwig Fronthaler and J. Bigun. “Local feature extraction in fingerprints by complex filtering”. In *Advances in Biometric Person Authentication, LNCS*, volume 3781, pages pp.77–84, 2005.
- [30] E. Henry. “*Classification and Uses of Finger Prints*”. Routledge, London, 1900.
- [31] L. Hong, Y. Wan, and A. K. Jain. “Fingerprint image enhancement: Algorithms and performance evaluation”. *IEEE Transactions on Pattern Analysis and Machine Intelligence*, 20(8):777–789, 1998.

- [32] J. I.T. “*Principle Component Analysis*”. Springer-Verlag, New York, 1986.
- [33] A. K. Jain, Y. Chen, and M. Demirkus. “A fingerprint recognition algorithm combining phase-based image matching and feature-based matching”. In *Proc. of International Conference on Biometrics (ICB)*, pages 316–325, 2005.
- [34] A. K. Jain, Y. Chen, and M. Demirkus. “Pores and ridges: Fingerprint matching using level 3 features”. In *Proc. of International Conference on Pattern Recognition (ICPR)*, volume 4, pages 477–480, 2006.
- [35] A. K. Jain, L. Hong, S. Pankanti, and R. Bolle. “An identity authentication system using fingerprints”. *Proc. IEEE*, 85(9):1365–1388, 1997.
- [36] A. K. Jain, L. Hong, and B. R. “On-line fingerprint verification”. *IEEE Transactions on Pattern Analysis and Machine Intelligence*, 19(4):302–314, 1997.
- [37] A. K. Jain, S. Prabhakar, L. Hong, and S. Pankanti. “Filterbank-based fingerprint matching”. *Image Processing, IEEE Transactions on*, 9(5):846–859, 2000.
- [38] T.-Y. Jea. “*Minutiae-Based Partical Fingerprint Recognition*”. PhD thesis, University at Buffalo, the State University of New York, 2005.
- [39] X. Jiang, W.-Y. Yau, and W. Ser. Detecting the fingerprint minutiae by adaptive tracing the gray-level ridge. *Pattern Recognition*, 34(5):999–1013, 2001.
- [40] L. Jinxiang, H. Zhongyang, and C. Kap Luk. Direct minutiae extraction from gray-level fingerprint image by relationship examination. In *International Conference on Image Processing(ICIP)*, volume 2, pages 427–430 vol.2, 2000.
- [41] T. Kamei and M. Mizoguchi. Image filter design for fingerprint enhancement. In *International Symposium on Computer Vision*, pages 109–114, 1995.

- [42] M. Kass and A. Witkin. Analyzing oriented patterns. *Computer Vision, Graphics, and Image Processing*, 37(3):362–385, 1987.
- [43] S. Klein, A. M. Bazen, and R. Veldhuis. “fingerprint image segmentation based on hidden markov models”. In *13th Annual workshop in Circuits, Systems and Signal Processing, in Proc. ProRISC 2002*, 2002.
- [44] T. Kohonen, J. Kangas, J. Laaksonen, and K. Torkkola. Lvqpak: A software package for the correct application of learning vector quantization algorithms. In *International Joint Conference on Neural Networks*, volume 1, pages 725–730, 1992.
- [45] N. Latta. “US VISIT: Keeping america’s doors open and our nation secure”. In *Biometric Consortium*, 2004.
- [46] M. T. Leung, W. E. Engeler, and P. Frank. Fingerprint image processing using neural networks. In *TENCON 90, IEEE Region 10 Conference on Computer and Communication Systems*, pages 582–586 vol.2, 1990.
- [47] E. Lim, X. Jiang, and W. Yau. “Fingerprint quality and validity analysis”. *ICIP*, pages 469–472, 2002.
- [48] D. Maio and D. Maltoni. Direct gray-scale minutiae detection in fingerprints. *IEEE Transactions on Pattern Analysis and Machine Intelligence*, 19(1):27–40, 1997.
- [49] D. Maio and D. Maltoni. Neural network based minutiae filtering in fingerprints. In *Fourteenth International Conference Pattern Recognition*, volume 2, pages 1654–1658, 1998.
- [50] D. Maltoni, D. Maio, A. K. Jain, and S. Prabhakar. “*Handbook of Fingerprint Recognition*”. Springer, 2003.

- [51] B. M. Mehtre and B. Chatterjee. Segmentation of fingerprint images – a composite method. *Pattern Recognition*, 22(4):381–385, 1989.
- [52] B. M. Mehtre, N. N. Murthy, S. Kapoor, and B. Chatterjee. Segmentation of fingerprint images using the directional image. *Pattern Recognition*, 20(4):429–435, 1987.
- [53] K. Mikolajczyk and C. Schmid. Scale affine invariant interest point detectors. *International Journal of Computer Vision*, 60(1):pp.63–86, 2004.
- [54] D. M.L. and R. S.I. On the use of level curves in image analysis. *CVGIP: Image Understanding*, 57(2):185–203, 1993.
- [55] B. Moayer and K. S. Fu. “a tree system approach for fingerprint pattern recognition”. *Pattern Analysis and Machine Analysis, IEEE Transactions on*, 8(3):376 – 387, 1986.
- [56] K. Nilsson and J. Bign. “Using linear symmetry features as a pre-processing step for fingerprint images”. In *AVBPA*, pages pp.247–252, 2001.
- [57] B. O. Preprocessing of poor quality fingerprint images. In *Proc. XIV Int. Conf. Chilean Computer Science Soc.*, 1994.
- [58] N. O., N. Y., and M. T. A restoration algorithm of fingerprint images. *Syst. Comput. Jpn.*, 17(6):31, 1986.
- [59] L. O’Gorman and J. V. Nickerson. An approach to fingerprint filter design. *Pattern Recognition*, 22(1):29–38, 1989.
- [60] A. C. Pais Barreto Marques and A. C. Gay Thome. A neural network fingerprint segmentation method. In *Fifth International Conference on Hybrid Intelligent Systems(HIS 05)*, page 6 pp., 2005.

- [61] S. Pankanti, S. Prabhakar, and A. K. Jain. “On the individuality of fingerprints”. *IEEE Transactions on Pattern Analysis and Machine Intelligence*, 24(8):1010–1025, 2002.
- [62] G. Parziale and E. Diaz-Santana. “The surround imager: A multi-camera touchless device to acquire 3d rolled-equivalent fingerprints”. In *Proc. of IAPR Int. Conf. on Biometrics, LNCS*, volume 3832, pages pp.244–250, 2006.
- [63] P. M. Patil, S. R. Suralkar, and F. B. Sheikh. Rotation invariant thinning algorithm to detect ridge bifurcations for fingerprint identification. In *17th IEEE International Conference on Tools with Artificial Intelligence*, page 8 pp., 2005.
- [64] T. Pavlidis. Vectorizer and feature extractor for document recognition. *Computer Vision, Graphics, and Image Processin*, 35(1):111–127, 1986.
- [65] A. B. P.G.M. Van Der Meulen, H. Shcipper and S. Gerez. “Pmdpg: A distributed object-oriented genetic programming environment”. In *Proc. ASCI conference*, pages pp.284–491, 2001.
- [66] S. Prabhakar, A. K. Jain, and S. Pankanti. Learning fingerprint minutiae location and type. *Pattern Recognition*, 36(8):1847–1857, 2003.
- [67] R. Pradenas. Directional enhancement in the frequency domain of fingerprint images. In *Human Detection and Positive Identification: Methods and Technologies, SPIE*, volume 2932, pages 150–160, 1997.
- [68] C. Qin-Sheng, M. Defrise, and F. Deconinck. “Symmetric phase-only matched filtering of fourier-mellin transforms for image registration and recognition”. *Pattern Analysis and Machine Analysis, IEEE Transactions on*, 16(12):1156–1168, 1994.

- [69] N. K. Ratha, S. Chen, and A. K. Jain. Adaptive flow orientation-based feature extraction in fingerprint images. *Pattern Recognition*, 28(11):1657–1672, 1995.
- [70] C. J. Rivero-Moreno and S. Bres. “conditions of similarity between hermite and gabor filters as models of the human visual system”. In *Computer Analysis of Images and Patterns, LNCS*, volume 2756, pages pp.762–769, 2004.
- [71] P. I. Rockett. An improved rotation-invariant thinning algorithm. *Pattern Analysis and Machine Intelligence, IEEE Transactions on*, 27(10):1671–1674, 2005.
- [72] A. Ross, A. K. Jain, and J. Reisman. “A hybrid fingerprint matcher”. *Pattern Recognition*, 36(7):1661–1673, 2003.
- [73] R. Rowe and K. A. Nixon. “Fingerprint enhancement using a multispectral sensor”. In *Biometrics Technology for Human Identification II*, volume 5779, pages pp.81–93, 2005.
- [74] V. K. Sagar and K. J. B. Alex. Hybrid fuzzy logic and neural network model for fingerprint minutiae extraction. In *Neural Networks, 1999. IJCNN '99. International Joint Conference on*, volume 5, pages 3255–3259 vol.5, 1999.
- [75] V. K. Sagar, D. B. L. Ngo, and K. C. K. Foo. Fuzzy feature selection for fingerprint identification. In *Security Technology, 1995. Proceedings. Institute of Electrical and Electronics Engineers 29th Annual 1995 International Carnahan Conference on*, pages 85–90, 1995.
- [76] L. G. Shapiro and G. C. Stockman. *Computer Vision*. Prentice Hall, Upper Saddle River, NJ, 2000.
- [77] L. Shen, A. Kot, and W. Koo. “Quality measures of fingerprint images”. *AVBPA*, pages 266–271, 2001.

- [78] B. G. Sherlock, D. M. Monro, and K. Millard. Fingerprint enhancement by directional fourier filtering. *Vision, Image and Signal Processing, IEE Proceedings-*, 141(2):87–94, 1994. 1350-245X.
- [79] R. Stock and C. Swonger. “development and evaluation of a reader of fingerprint minutiae”. Technical Report XM-2478-X1:13-17, Cornell Aeronautical Laboratory, 1969.
- [80] L. T. “*Scale Space Theory in Computer Vision*”. Kluwer Academic Publisher, Boston, 1994.
- [81] E. Tabassi and C. L. Wilson. “A new approach to fingerprint image quality”. *ICIP*, pages 37–40, 2005.
- [82] K. Uchida. “Image-based approach to fingerprint acceptability assessment”. *ICBA*, pages 294–300, 2004.
- [83] L. Wang, H. Suo, and M. Dai. Fingerprint image segmentation based on gaussian-hermite moments. In *Advanced Data Mining and Applications, LNCS3584*, pages 446–454, 2005.
- [84] S. Wang and Y. Wang. Fingerprint enhancement in the singular point area. *IEEE Signal Processing Letters*, 11(1):16–19, January 2004.
- [85] C. I. Watson, M. D. Garris, E. Tabassi, C. L. Wilson, R. M. MsCabe, and S. Janet. “*User’s Guide to NIST Fingerprint Image Software2(NFIS2)*”. NIST, 2004.
- [86] A. J. Willis and L. Myers. A cost-effective fingerprint recognition system for use with low-quality prints and damaged fingertips. *Pattern Recognition*, 34(2):255–270, 2001.

- [87] C. Wu and V. Govindaraju. Singularity preserving fingerprint image adaptive filtering. In *IEEE International Conference on Image Processing (ICIP)*, pages 313–316, 2006.
- [88] C. Wu, Z. Shi, and V. Govindaraju. Fingerprint image enhancement method using directional median filter. In *Biometric Technology for Human Identification, SPIE*, volume 5404, pages 66–75, 2004.
- [89] C. Wu, S. Tulyakov, and V. Govindaraju. Image quality measures for fingerprint image enhancement. In *International Workshop on Multimedia Content Representation, Classification and Security(MRCS)*, volume LNCS 4105, pages 215–222, 2006.
- [90] Q. Xiao and H. Raafat. Fingerprint image postprocessing: A combined statistical and structural approach. *Pattern Recognition*, 24(10):985–992, 1991.
- [91] J. Xudong and Y. Wei-Yun. “Fingerprint minutiae matching based on the local and global structures”. In *Proc. of International Conference on Pattern Recognition (ICPR)*, volume 2, pages 1038–1041 vol.2, 2000.
- [92] A. B. Xuefeng Liang and T. Asano. A near-linear time algorithm for binarization of fingerprint images using distance transform. In *Combinatorial Image Analysis*, pages 197–208, 2004.
- [93] W. Yi, H. Jiankun, and P. Damien. A fingerprint orientation model based on 2d fourier expansion (fomfe) and its application to singular-point detection and fingerprint indexing. *Pattern Analysis and Machine Intelligence, IEEE Transactions on*, 29(4):573–585, 2007. 0162-8828.
- [94] X. You, B. Fang, V. Y. Y. Tang, and J. Huang. Multiscale approach for thinning ridges of fingerprint. In *Second Iberian Conference on Pattern Recognition and Image Analysis*, volume LNCS 3523, pages 505–512, 2005.

- [95] T. Yuan Yan and Y. Xinge. Skeletonization of ribbon-like shapes based on a new wavelet function. *Pattern Analysis and Machine Intelligence, IEEE Transactions on*, 25(9):1118–1133, 2003.
- [96] Z. Yuheng and X. Qinghan. An optimized approach for fingerprint binarization. In *International Joint Conference on Neural Networks*, pages 391–395, 2006.
- [97] F. Zhao and X. Tang. Preprocessing and postprocessing for skeleton-based fingerprint minutiae extraction. *Pattern Recognition*, 40(4):1270–1281, 2007.
- [98] E. Zhu, J. Yin, C. Hu, and G. Zhang. A systematic method for fingerprint ridge orientation estimation and image segmentation. *Pattern Recognition*, 39(8):1452–1472, 2006.
- [99] K. Zuiderveld. “*Contrast Limited Adaptive Histogram Equalization*”. Academic Press, 1994.